Sensorimotor cortex plasticity in upper-limb amputees



Sanne Kikkert

Merton College & Nuffield Department of Clinical Neurosciences

University of Oxford

A thesis submitted for the degree of

Doctor of Philosophy

August 2017

Sensorimotor cortex plasticity in upper-limb amputees

Sanne Kikkert

Trinity Term 2017 Merton College

A thesis submitted in partial fulfilment of the requirements for the degree of Doctor of Philosophy in the University of Oxford.

Thesis Abstract

The current thesis was aimed at investigating how the primary sensorimotor cortex, and in particular the missing hand cortex, is affected by upper-limb amputation. This thesis further explores how activity in this region relates to phantom limb pain (PLP). As such, a series of neuroimaging experiments was designed, aimed at answering 3 main questions: 1) What happens to the neural fingerprint of a hand following its amputation? 2) What are the behavioural and neural underpinnings of PLP? 3) Can novel targets for PLP treatment be identified?

By making use of ultra-high field 7 tesla fMRI and the phenomenology of phantom limb sensations, this thesis demonstrates that the topographical representation of a missing hand's individual digits is preserved in primary somatosensory cortex, even decades after arm amputation. This finding of stable topography questions the extent to which continued sensory input is necessary to maintain organisation in sensory cortex.

Slowed phantom hand motor control was identified as a behavioural correlate of chronic PLP. Stronger maintained activity in the primary sensorimotor missing hand cortex was reaffirmed as a neural correlate of chronic PLP and was further associated with deteriorated phantom hand motor control. This thesis presents results challenging the maladaptive plasticity model and instead emphasising a likely relationship between persistent peripheral inputs pertaining to the missing hand representation and chronic PLP.

Anodal tDCS over the primary sensorimotor missing cortex during a phantom hand movement task effectively relieved PLP with effects lasting at least one week post stimulation. In accordance with above, amputees with more PLP relief showed less activity in the primary sensorimotor cortex after brain stimulation. Importantly, tDCS-concurrent neuroimaging identified the insula and secondary somatosensory cortex as neural correlates of PLP relief and subsequent sensorimotor cortex downregulation.

Together, this thesis reveals new roles of primary sensorimotor cortex following arm amputation and provides a first comprehensive overview of the neural mechanisms underlying missing hand sensations, offering novel opportunities for PLP treatment.

This thesis contains approximately 36 000 words

Acknowledgements

This thesis would not have existed without the volunteers that participated in my research. They delivered endless inspiration, never got tired of my many questions and never complained about the (boring) hours I asked them to spend in the MRI scanner. Thanks to all these volunteers, and Bruce in particular, for helping me understand the importance of my work.

My sincerest gratitude goes out to Merton College and the Medical Research Council of the United Kingdom for funding my DPhil.

Tamar Makin and Heidi Johansen-Berg, thank you to for being great co-supervisors and female role models. Thank you for all the brilliant guidance in the past years.

My special thanks go out to Tamar. I could not have wished for a more supportive supervisor. Thank you for always challenging me, pushing me to work hard, and teaching me the importance of speaking your mind. Also, thanks for all the drinks and making me feel boring when I don't party at conferences!

Melvin Mezue, thank you for being a great collaborator and for making the running of a stressful study much more fun and less stressful. Also, thanks for your lessons about the insula.

Irene Tracey, thank you for always fitting me into your busy schedule and for the invaluable feedback on my plans and manuscripts.

Christian Beckmann, thank you for hosting me in your wonderful lab of SINners in Nijmegen. I learned a lot and feel much less afraid of complicated analysis. Thanks also to all the sinners for making me feel welcome in the group, in particular Roselyn, Izabella, Marianne, and Thomas.

I wish to thank the following collaborators: James Kolasinski, for showing me how to do the travelling-wave analysis and help with data collection for the research presented in Chapter 2. Saad Jbabdi, for his analysis support (thanks for persevering at times in trying to understand what I meant). Jacinta O'Shea, for the help with the tDCS work in Chapter 4. David Henderson-Slater, for the help with patient recruitment.

Pain group members, in particular Andy Segerdahl and Falk Eippert, thank you for always taking the time to answer my many pain questions and for the peptalks before presentations in front of intimidating groups of pain experts.

Thank you to Harriet Dempsey-Jones, who proof-read my thesis and is a great friend for doing so – I owe you a drink!

Thank you to all members of the Oxford Plasticity group, for all the feedback over the past years and for not complaining about my obsession with phantom limb pain. Apologies to some of you (but mainly to Tamar and the members of the hand&brain group) for having to see the same videos over and over in my presentations… Many

thanks for all the pub visits, plasticity gone wild and other parties that made my DPhil more fun!

And of course: thanks to the full Tamarmy!!! In particular, thanks to Harriet Dempsey-Jones, Daan Wesselink, Zeena Sanders, Roni Maimon, and Fiona van den Heiligenberg for your shared love of somatosensory cortex and (anti)plasticity. You are all brilliant, awesome and hilarious scientists – thank you for being such a great group!

Thanks to Zeena Sanders, Naiara Demnitz, and Harriet Dempsey-Jones for making the thesis-writing days in the library less lonely and much more enjoyable. Thank you also for loving wine just as much as I do and for all the lovely evenings over the past years!

Alice Cheng, thank you for being great. Thank you for being (and seeing?) ghosts, lazy evenings, enjoying wine, hikes etc. I'm VERY excited to discover Zurich with you!

Thank you to all my friends at Merton College, for being a bit part of my Oxford experience.

Vanessa, Anissa, Carmen and Nikki, thank you for creating a home away from home.

Thanks to my friends afar for their support, continuing friendship and shenanigans over the past years. Including, but not limited to Nelleke, Nicole, Britt, Mireille, Wouter, Bas, and Meabhdh.

Oma, bedankt voor al uw steun de afgelopen jaren. Ik vind het super dat ik een stoere oma heb die op hoge leeftijd nog het Kanaal overkomt om mij te bezoeken in Oxford. Ondanks de taalbarriere heeft u toch nog een goed gesprek kunnen voeren met de ganzen in het park!

Hannie, Leike and Nicky thank you for being such a supporting and loving second family.

Papa, mama, Karen and Thijs (en natuurlijk de koude kant) – thank you for your endless support, listening to my joys, sadness and dealing with my craziness at times. I couldn't wish for a more loving and supportive family. Thank you also for reminding me that you will always regard me as a bit of an idiot and that having a DPhil from Oxford won't help…

Many thanks also to Yzar. Thank you for all your smelly cuddles and unwanted kisses (that I definitely always wanted).

And foremost, thanks to David for being my light. You are the most supportive partner one could hope for, without your push I would probably not have started this PhD. Thanks for putting up with me, I can't wait to start the next chapter in our lives together.

Contents

List of Acronyms **6**

List of Figures **9**

List of Tables **10**

Publications arising from this thesis **11**

1 | Introduction **12**

1.1 Maintained sensations of a missing limb 12

1.1.1 Phantom limb sensations 12

1.1.2 Phantom limb pain 14

1.2 Original theories of phantom limb pain 15

1.3 Primary sensorimotor cortex and limb loss 16

1.3.1 Organisation in primary somatosensory cortex 16

1.3.1 Reorganisation in primary somatosensory cortex 18

1.4 Referred phantom sensations 20

1.5 Maladaptive plasticity theory of PLP 23

1.6 Re-emphasising the peripheral attributes of PLP 25

1.7 Aims of this thesis 27

2 | Revealing the neural fingerprints of a missing hand **30**

Chapter abstract: 30

2.1 Introduction 31

2.2 Materials and methods 32

2.2.1 Participants 32

2.2.2 Phantom sensations testing 35

2.2.3 Brachial plexus avulsion testing 36

2.2.4 MRI tasks 37

2.2.5 MRI acquisition 41

2.2.6 MRI analysis 42

2.3 Results 54

2.3.1 Travelling wave 55

2.3.2 Preserved digit maps are independent of intact hand contributions 57

2.3.3 Inter-digit overlap patterns in amputees are similar to controls 59

2.3.3 Preserved digit topography is not dependent on peripheral inputs 61

2.4 Discussion 63

3 | Reaffirming the link between chronic phantom limb pain and maintained missing hand representation **68**

Chapter abstract: 68

3.1 Introduction 69

3.2 Materials and methods 70

3.2.1 Participants 70

3.2.2 Pain ratings 71

3.2.3 Scanning procedures 72

3.2.4 MRI data acquisition 72

3.2.5 MRI data preprocessing and analysis 73

3.2.6 Statistical analysis 75

3.3 Results 75

3.3.1 Phantom hand movements activity in amputees compared to controls 75

3.3.2 Maintained activity in S1's missing hand area associates with chronic phantom limb pain 77

3.3.3 Chronic PLP did not associate with lip or residual arm movement activity 79

3.4 Discussion 80

4 | Non-invasive brain stimulation reduces phantom limb pain: an fMRI study 83
Chapter abstract: 83
4.1 Introduction 84
4.2 Materials and methods 87
4.2.1 Participants 87
4.2.2 Experimental design 88
4.2.3 Transcranial direct current stimulation 89
4.2.4 Pain ratings 90
4.2.5 Scanning procedures 93
4.2.6 MRI data acquisition 95
4.2.7 MRI preprocessing and image registration 96
4.2.8 MRI analysis 97
4.2.9 Statistical analysis 100
4.3 Results 101
4.3.1 Non-invasive brain stimulation induces phantom limb pain relief 101
4.3.2 Phantom movement activity relates to PLP relief 109
4.4 Discussion 114

5 | Motor correlates of chronic phantom limb pain 118
Chapter abstract: 118
5.1 Introduction 119
5.2 Materials and methods 120
5.2.1 Participants 120
5.2.2 Pain ratings 121
5.2.3 Finger-tapping test 122
5.2.4 Functional MRI sensorimotor task 124
5.2.5 MRI data acquisition 125
5.2.6 MRI preprocessing and analysis 125
5.2.7 Statistical analysis 127
5.3 Results 128
5.3.1 Inter-session consistency 129
5.3.2 Intact versus phantom hand movements 129
5.3.3 Correlations with chronic phantom limb pain 130
5.3.4 Phantom hand representation 131
5.4 Discussion 132

6 | Discussion 137
6.1 Thesis overview 137
6.2 Persistent representations of a missing hand 138
6.3 The neural underpinnings of phantom limb pain 141
6.3.1 Challenging the maladaptive plasticity model 141
6.3.2 Peripheral attributes of PLP 146
6.3.3 Phantom limb pain in the absence of peripheral inputs 150
6.4 Novel targets for phantom limb pain treatment 152
6.4.1 Potential mechanisms of tDCS induced PLP relief 152
6.4.2 Task-concurrent tDCS versus tDCS at rest 155
6.5 Remaining questions and future directions 157

References 162

Appendices 175
Supplementary Materials Chapter 2 175
Supplementary Materials Chapter 4 182
Supplementary Materials Chapter 5 195

List of Acronyms

3D	3 dimensional
3T	3 tesla
7T	7 tesla
A	Anterior
AMP	Amputation
Ave	Average
BBR	Boundary Based Registration
BET	Brain Extraction Tool
BOLD	blood oxygenation level dependent
BPA	Brachial Plexus Avulsion
BPI	Brief Pain Inventory
CI	Confidence interval
cm	centimeter
CSF	cerebrospinal fluid
D1	digit 1 (thumb)
D2	digit 2 (index finger)
D3	digit 3 (middle finger)
D4	digit 4 (ring finger)
D5	digit 5 (little finger)
Diff	difficulty
DOF	degrees of freedom
EMG	Electromyography
EPI	echo planar imaging

etc	etcetera
FAST	FMRIB's Automated Segmentation Tool
FDR	false discovery rate
FEAT	fMRI Expert Analysis Tool
FILM	FMRIB's Improved Linear Model
FLAME	FMRIB's Local Analysis of Mixed Effects
FLIRT	FMRIB's Linear Image Registration Tool
fMRI	functional Magnetic Resonance Imaging
FNIRT	FMRIB's Nonlinear Image Registration Tool
FOV	field of view
FSL	FMRIB Software Library
FWHM	full-width half-maximum
GABA	gamma-aminobutyric acid
GLM	general linear model
HRF	haemodynamic response function
Hz	Hertz
ICC	Intraclass correlation coefficient
L	Left
M1	primary motor cortex
Mag	Magnitude
MCFLIRT	Motion Correction using FMRIB's Linear Image Registration Tool
min	Minutes
mm	Millimetres
mN	millinewton
MNI	Montreal Neurological Institute

MP2RAGE	magnetization prepared 2 rapid acquisition gradient echo
MPRAGE	magnetisation prepared rapid gradient echo
MRI	magnetic resonance imaging
ms	millisecond
N	No
P	Posterior
PLP	Phantom limb pain
PLS	Phantom limb sensation
PDS	Phantom digit sensation
Pros	Prosthetics
QST	Qualitative sensoric testing
R	Right
RF	radio frequency
ROI	region of interest
s	seconds
S1	Primary somatosensory cortex
S2	Secondary somatosensory cortex
s.e.m	Standard error of the mean
SNR	signal-to-noise ratio
tDCS	transcranial direct current stimulation
TE	echo delay time
TR	repetition time
Vascular D	Vascular disease
WM	white matter
Y	Yes

List of Figures

Figure 1.1: Somatotopic organisation in primary somatosensory cortex. 17
Figure 1.2: Reorganisation in area 3b following digit 3 amputation in an adult owl monkey (adapted from Merzenich et al., 1984). 19
Figure 1.3: Reorganisation in area 3b after whole hand amputation in adult macaques (adapted from Pons et al., 1991). 20
Figure 1.4: Referred sensations in upper-limb amputees (adapted from Makin & Bensmaia (2017). 22
Figure 2.1: Travelling wave task and analysis. 48
Figure 2.2: Missing hand maps revealed in amputees during phantom digits movement. 56
Figure 2.3: Missing hand maps are replicated during dissociated bimanual hand movements. 58
Figure 2.4: Amputees show characteristic inter-digit overlap patterns during phantom digit movements. 60
Figure 2.5: Topography is preserved despite the absence of peripheral input. 62
Figure 3.1: Hyperactivity during phantom hand movement in amputees. 76
Figure 3.2: Chronic phantom limb pain relates to maintained cortical phantom hand representation. 78
Figure 4.1: Non-invasive brain stimulation relieves phantom limb pain with effects lasting up to one week. 107
Figure 4.2: Downregulation of phantom hand representation activity reflects phantom limb pain relief. 111
Figure 4.3: Increased insular activity during stimulation associated with downregulation of activity in the primary sensorimotor missing hand cortex after stimulation. 113
Figure 5.1: Phantom hand motor control is impaired and relates to chronic phantom limb pain and cortical sensorimotor phantom hand representation. 130

List of Tables

Table 2.1: Demographic and clinical details (Chapter 2). 33
Table 2.2: Phantom digits' movement vividness, difficulty and quality. 34
Table 3.1: Amputee demographic and clinical details (Chapter 3).....71
Table 3.2: Functional location peak activations parameters for whole brain contrasts between amputees and controls. 77
Table 4.1: Amputee demographic and clinical details (Chapters 4 and 5). 88
Table 4.2: Non-invasive brain stimulation induced PLP relief in percentages (effect sizes). 108

Publications arising from this thesis

In preparation of this thesis, I (together with my supervisors) have prioritised the development of manuscripts for submission. As such, the experimental chapters in this thesis are adapted from manuscripts that I previously prepared or I am in the process of preparing for publication in peer-reviewed journals. The respective citations are detailed at the start of each chapter.

1 | Introduction

Picture yourself waking up in the hospital. Your whole body is hurting, but you cannot remember what happened. The doctor tells you that you had a severe accident causing you to lose your hand. You think: "I definitely don't feel well, but surely the doctors must be mistaken; I can clearly feel my hand and, in fact, it is hurting." You turn your gaze to the blanket covering your hand. You lift your hand to show the doctors, but when you do so nothing happens. After taking a closer look you realize the doctor was correct; you have indeed lost your limb. The hand you can feel and move is no longer there…

1.1 Maintained sensations of a missing limb

1.1.1 Phantom limb sensations

Following upper-limb amputation, individuals generally report experiencing vivid and continuous sensations of their missing limb. Silas Weir Mitchell first introduced the term 'phantom limb' in 1871 in a report of amputees from the American Civil war. These sensory 'ghosts' typically emerge immediately after amputation and the vividness of perception can be similar to the perception of one's intact hand. Sensations coming from the missing limb can range from pins and needles, itch, warmth, pressure, cold, tingling and pain (Ramachandran & Hirstein, 1998).

In this thesis, the classic distinction has been adopted:

1. Phantom limb sensations: any sensations of the missing limb, except pain.
2. Phantom limb pain: painful sensations of the missing limb.

3. Residual limb pain: painful sensations localised to the residual limb (or stump).

Most amputees with phantom limb sensations are able to move their phantom limb to some extent, but immobility and involuntary movements have also been reported (Weeks, Anderson-Barnes, & Tsao, 2010). When instructed to move their phantom hand, amputees generally report detailed kinaesthetic sensations regarding the degree and extent of movement. This is supported by empirical evidence demonstrating that phantom limb movements elicit both central and peripheral motor signals, that are different from those found during imagined movements (Raffin, Giraux, & Reilly, 2012; Raffin, Mattout, Reilly, & Giraux, 2012).

The posture of the phantom arm is variable. Phantom arms are commonly partially flexed at the elbow and the phantom hand is typically partially or completely clenched into a fist. Sensory memories have been proposed to play a role in creating the phantom limb position, as the position of the limb prior to amputation often resembles the position of the phantom limb (Katz & Melzack, 1990).

Phantom sensations have also been reported following the loss of teeth, breasts, internal organs and genitalia, as well as following peripheral nerve damage without limb loss (e.g. brachial plexus avulsion injury). However, phantom sensations are most commonly experienced following limb loss (Ramachandran & Hirstein, 1998).

1.1.2 Phantom limb pain

Losing a limb, and in particular an arm, has devastating effects on normal daily life. Even a task as simple as tying your shoelaces becomes a huge challenge. However, in about 80% of upper-limb amputees there is a greater challenge still: these amputees experience painful phantom limb sensations (Weeks et al., 2010). Phantom limb pain (PLP), similar to non-painful phantom limb sensations, typically onsets immediately following amputation and can disappear in the years after amputation (Knotkova, Cruciani, Tronnier, & Rasche, 2012). PLP is often described as 'shooting', 'burning', 'prickling', 'tingling', 'cramping' and 'crushing' sensations. PLP is distinct from residual limb (stump) pain, and is most probably sub-served by separate neural mechanisms.

PLP can become a chronic condition and can be hugely debilitating, with severe implications on quality of life: depression is common and suicidal rates are high (Knotkova et al., 2012). Unfortunately, PLP is a neuropathic pain syndrome that is notorious for being difficult to treat. It remains a mystery how to treat pain in a body part that is no longer physically present. Examples of available therapies range from nerve block, medication, physical treatment, and surgical interventions, to alternative therapies such as mirror box interventions. These therapies appear not to be able to cause complete relief, are often invasive and suffer from inconvenient side effects (Knotkova et al., 2012). A mechanistic understanding of the cause of PLP is lacking, and, as such, targeted treatments currently do not exist. A better understanding of the neural mechanisms of PLP may aid the development of more successful therapies.

1.2 Original theories of phantom limb pain

The neural basis of PLP remains highly debated. Early theories proposed PLP to be a consequence of peripheral nerve injury (Nystrom & Hagbarth, 1981). Post amputation, nerves re-grow, leading to terminal swelling, axonal sprouting and ultimately in the creation of a neuroma made up of a tangle of neural tissue. Early observations showed that PLP could be evoked by pressing on these neuromas at the end of the residual arm. Using microelectrode recordings of residual peripheral nerve fibers, Nystorm and Hagsbarth (1981) showed that the residual axons in a human amputee remained active, although the receptors of these nerves had been amputated. Such ectopia could be evoked by tapping on the neuroma at the end of the stump, resulting in a corresponding burst of PLP. Spontaneous ectopic discharge was also observed, potentially explaining spontaneous episodes of PLP (Fried, Govrin-Lippmann, Rosenthal, Ellisman, & Devor, 1991; Nystrom & Hagbarth, 1981).

Formation of neuromas might cause neuropathic pain through abnormal evoked activity following peripheral nerve injury, including PLP following amputation. However, clinical approaches based on this theory do not appear effective in relieving PLP. Indeed, PLP frequently persists after neuroma nerve block (Flor, Nikolajsen, & Staehelin Jensen, 2006). While anaesthetic blocking of the neuroma with lidocaine eliminated both the tap-induced ectopic discharge and the tap-induced PLP, the spontaneous discharge and spontaneous PLP were unchanged (Nystrom & Hagbarth, 1981). For this reason, factors related to the function of the central nervous system started taking a more prominent place as an explanation of PLP in the past few decades (Flor et al., 2006; Halbert, Crotty, & Cameron, 2002; Ramachandran & Altschuler, 2009). Still, as described in further detail below (section 1.6) and in

Chapter 6 (Discussion), new evidence emphasises the importance of the potential peripheral attributes of PLP. This novel evidence highlights ectopic firing in the dorsal root ganglia as the origin of PLP (Vaso et al., 2014).

1.3 Primary sensorimotor cortex and limb loss

Experience shapes the central nervous system throughout life. The ability of the brain to dynamically adapt its organisation based on new experiences allows us to develop from infants to adults, learn new skills, recover from injury and adjust to ageing. One of the most striking examples of such reorganisation is observed in primary somatosensory cortex (S1) following sensory input loss, and amputation in particular. S1 has long been used as a primary example of reorganisation, due to two phenomena. Firstly, because S1 has detailed organised representation of the body. And secondly, because following focal input loss S1 reorganises. These phenomena will be discussed in detail below.

1.3.1 Organisation in primary somatosensory cortex

S1 encompasses the postcentral gyrus and central sulcus. This area of cortex receives direct input from the ventroposterior lateral and ventroposterior medial nuclei of the thalamus, as well as a multitude of efferent information from the motor system (Kandel, Schwartz, & Jessell, 2000). The organisation of S1 was first characterised in detail by the seminal work of Penfield and colleagues (Penfield & Rasmussen, 1950; Penfield & Boldrey, 1937). They directly stimulated the cortical tissue of awake human patients undergoing brain surgery for epilepsy (carried out under local anaesthesia). Based on patients' self-reports of the induced sensations, Penfield and colleagues described a detailed body map in S1, where adjacent body parts were

represented next to each other (i.e., somatotopically; see Figure 1.1). They further found that while all body parts are represented in S1 somatotopically, they were not represented in a way that is proportional to body mass. Instead, the size of each body part's representation was relative to the density of cutaneous tactile receptors in that body part (Kaas, Nelson, Sur, Lin, & Merzenich, 1979). For example, the representation of the hands is larger than the representation of the arms or trunk.

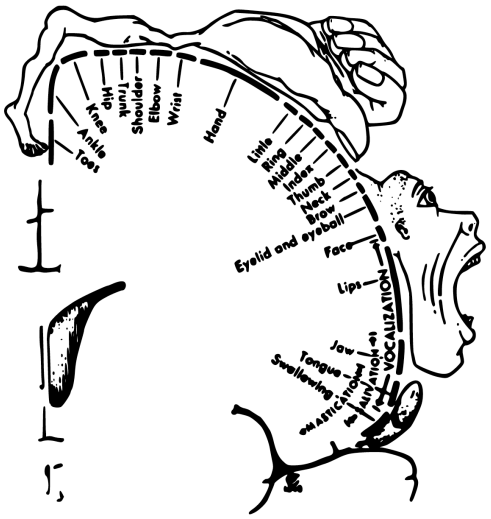


Figure 1.1: Somatotopic organisation in primary somatosensory cortex. The sensory homunculus in S1, as proposed originally by Penfield & Boldrey (1937).

Later work with electrophysiology, revealed that S1 contains four of these complete, detailed and orderly body maps. These four somatotopic maps are strip-like cortical areas running in a medio-lateral direction: Brodmann areas 3a, 3b, 1 and 2 (Brodmann, 1909). Each of these areas receives thalamocortical information of a distinct subset of somatosensory modalities. Areas 3b and 1 receive cutaneous information from the ventroposterior nucleus of the thalamus, while the ventroposterior superior nucleus feeds information regarding muscles spindle afferents to areas 3a and 2. Areas 2 and 3a contain cells that largely respond to

proprioceptive inputs (London & Miller, 2013). The four S1 areas are heavily interconnected and project to higher order cortical areas such as secondary somatosensory cortex (S2) or the parietal ventral area (Kaas, 1993).

1.3.1 Reorganisation in primary somatosensory cortex

Merzenich et al. (1983) investigated what happens to the detailed representation in S1of adult monkeys, and in areas 3b and 1 in particular, when they are deprived of sensory input. Using microelectrode recordings, they investigated the somatotopic organisation of the cutaneous hand representation following median nerve transection. They found that 2-9 months after nerve transection, the former territory of the median nerve was occupied by new and expanded representations of skin surfaces innervated by the ulnar and radial nerves. Following on this work, Merzenich et al. (1984) investigated what happened to S1, and area 3b in particular, following digit 3 amputation in adult monkeys. They mapped out the hand area in area 3b of S1 in detail prior to and 62 days post digit 3 amputation and found that the cortically adjacent body part representations (digits 2 and 4) took over the 'deprived' digit area (see Figure 1.2 for a graphical representation of results).

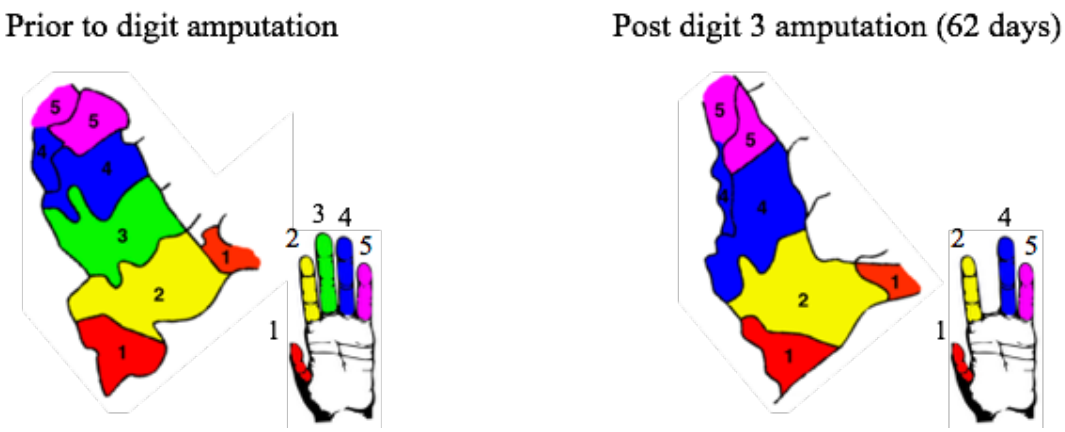


Figure 1.2: Reorganisation in area 3b following digit 3 amputation in an adult owl monkey (adapted from Merzenich et al., 1984). (Left) Prior to digit amputation, a detailed representation of all digits exists in area 3b of S1, where neighbouring digits are represented next to each other. Red = digit 1 (thumb); yellow = digit 2 (index finger); green = digit 3 (middle finger); blue = digit 4 (ring finger); pink = digit 5 (little finger). (Right) 62 days post digit 3 amputation, reorganisation can be observed in area 3b, where the neighbouring digits (2 and 4) take over the "freed-up" digit (3) area.

After long term sensory loss (i.e. 'deafferentation'), even more extensive reorganisation was observed by Pons et al. (1991). They found that 12 years post hand amputation in adult macaques, the missing hand area in area 3b became responsive to touch on the lower part of the face. Specifically, touch on the chin and lower part of the jaw activated neurons in S1's missing hand area (see Figure 1.3). Such reorganisation following major sensory input loss, where the cortical neighbours invade the 'freed-up' brain territory, has now been shown multiple times using electrophysiology in non-human primates (Florence, 1998; Jain, Florence, Qi, & Kaas, 2000; Kambi, Tandon, Mohammed, Lazar, & Jain, 2011). However, while the existence of reorganisation is well documented, the perceptual correlates of extensive S1 reorganisation remained unexplored.

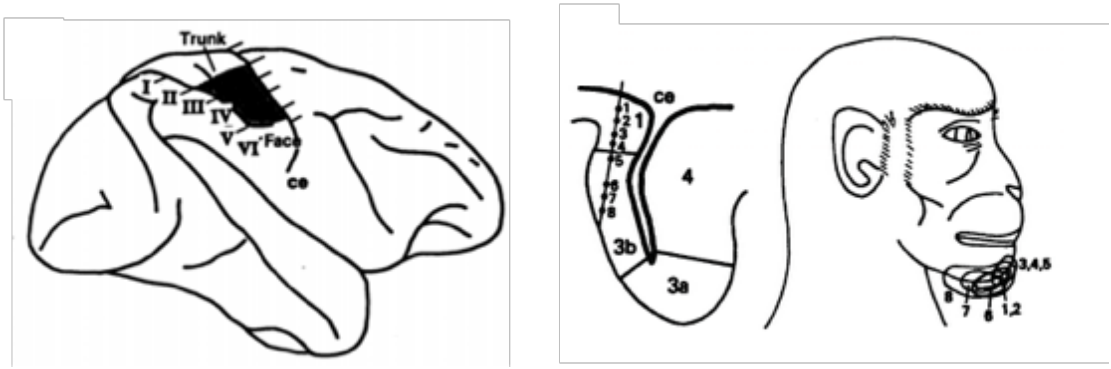


Figure 1.3: Reorganisation in area 3b after whole hand amputation in adult macaques (adapted from Pons et al., 1991). (Left) Following whole hand amputation, the S1 hand area contralateral to the amputation was deprived of its normal inputs. (Right) 12 years post hand amputation, this missing hand territory in area 3b became responsive to touch on the lower part of the chin, as found using microelectrode recordings.

1.4 Referred phantom sensations

A previously suggested perceptual correlate of S1 reorganisation, is the phenomenon of referred sensations (Ramachandran, Stewart, & Rogers-Ramachandran, 1992; 1993). Phantom hand sensations can often be elicited by touch on the residual arm (stump), which has been suggested to reflect spontaneous peripheral re-innervation. Indeed, following peripheral nerve injury, the severed nerves are thought to re-innervate the residual arm, potentially explaining why sensory stimulation in this region induces sensations referred to the missing hand's digits (Makin & Bensmaia, 2017). A more striking example of referred sensations comes from anecdotal reports that following arm amputation, shaving the face could induce tingling sensations of the phantom hand. Indeed, in a famous series of studies involving three upper-limb amputees, it was found that touch applied on the residual arm and lower part of the face elicited referred sensations of the missing hand (Ramachandran et al., 1992; Ramachandran, 1993). In one amputee, these referred sensations were modality

specific: touch on the face elicited tingling sensations in the phantom hand, warm water applied to the face elicited a warm referred phantom hand sensation, and pinprick stimuli elicited a prickling sensation. Strikingly, a one-to-one mapping existed between specific regions on the face (ipsilateral to the missing hand) and referred sensations of the individual digits of the phantom hand. That is, stimulation of neighbouring sites of the face elicited referred sensations in neighbouring digits of the missing hand, suggesting that the existence of referred sensations was topographically organised (see Figure 1.4A).

The authors suggested that these referred sensations are the perceptual consequence of S1 reorganisation, as was previously observed in non-human primates (Merzenich et al., 1984; Pons et al., 1991) where representations of cortically adjacent body parts (e.g. of the face) took over the 'freed-up' brain territory (e.g. of the missing hand; see previous section). Following such S1 reorganisation, touch of the lower part of the face would activate the missing hand representation, and brain regions receiving input from this S1 missing hand representation would interpret this sensory input signal as arising from the missing hand, resulting in both face and phantom hand sensations. S1 reorganisation is thought to occur through the sprouting of neural connections or the unmasking of existing lateral connections between the face and hand area (Florence, 1998; Jain et al., 2000). As such, if referred sensations are indeed the perceptual correlate of S1 reorganisation, then this should follow topographical principles.

However, since these influential reports, studies using more standardised approaches have showed that referred phantom hand sensations can be elicited by touching various body parts, including those that are not cortically adjacent to the missing hand

area (see Figure 1.4B; Knecht et al., 1996; Tan et al., 2014). Indeed, even touch on the trunk or shoulder contralateral to the missing hand was shown to elicit referred phantom limb sensations. This suggests that the phenomenon of referred sensations does not adhere to cortical topography, weakening the hypothesis that referred sensations are a consequence of S1 reorganisation. Furthermore, the quality of sensory experience in the phantom limb frequently differed from the stimulation modality. For example, both heat and vibration stimuli would elicit a tingling referred sensation in the phantom. Lastly, some of the key reports showing referred sensations were not conducted systematically, suffer from methodological issues, and as such, should be interpreted with caution.

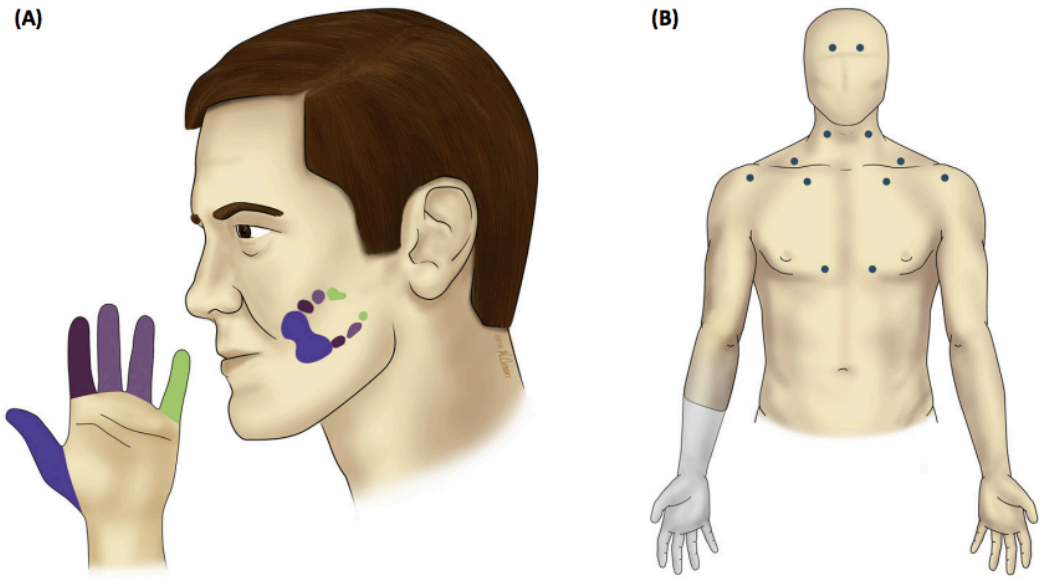


Figure 1.4: Referred sensations in upper-limb amputees (adapted from Makin & Bensmaia (2017). (A) Ramachandran et al., (1992) previously observed a systematic mapping between sensory stimulation of neighbouring sites of the face and referred sensations of neighbouring digits of the phantom hand. Following this result, the authors suggested that referred sensations of the phantom hand were the perceptual correlate of massive reorganisation in S1 (B) Knecht et al., (1996) later showed, using more systematic approaches, that referred phantom hand sensations were not restricted to the cortical neighbours of the missing limb, weakening the hypothesis that referred sensations are caused by S1 reorganisation.

1.5 Maladaptive plasticity theory of PLP

Following the suggestion that S1 reorganisation could account for the experience of non-painful phantom limb sensations in upper-limb amputees (see section 1.4), Flor et al., (1995) investigated whether a relationship may exist between PLP and S1 reorganisation. A pneumatic device was used to stimulate the lips, thumb or little finger of the intact hand of thirteen upper limb amputees with varying degrees of PLP during magnetoencephalography recording. To estimate the location of the missing hand representation, the intact hand's thumb and little finger representations were mirror reversed and the midpoint was calculated. The cortical distance between the missing hand and the lip representation was then calculated as a measure of cortical reorganisation. A positive relationship was found between cortical reorganisation and PLP magnitude, but not non-painful phantom sensation magnitude. Indeed, amputees with worse PLP had greater shifts in lip representation (i.e. towards the missing hand area). This study has now also been replicated using lip movements instead of sensory lip stimulation (Foell, Bekrater-Bodmann, Diers, & Flor, 2014; Lotze, Flor, Grodd, Larbig, & Birbaumer, 2001).

In this initial report linking PLP and cortical reorganisation, the *maladaptive plasticity model* was proposed, which remains the most commonly accepted explanation of PLP (Flor et al., 1995, 2006). This model states that PLP is caused by maladaptive reorganization in S1 (Flor et al., 1995, 2006). Following arm amputation, S1 is deprived of a major source of sensory input, leading to degradation of the missing hand representation. Because of this degradation, remapping occurs in S1, where neighbouring representations 'invade' the missing hand cortex. Such maladaptive

reorganisation causes the missing hand area to respond to inputs intended for neighbouring cortical regions. This mismatch between body part representations (e.g. the missing hand and face representation) is thought to result in an 'error' signal that is interpreted by the brain as pain arising from the missing hand (Ramachandran & Hirstein, 1998).

The influence of the maladaptive plasticity model has been vast, both on the scientific and clinical community. It has expanded in an attempt to explain other neuropathic pain syndromes, such as complex regional pain syndrome (Moseley & Flor, 2012) and neuropathic pain following spinal cord injury (Jutzeler, Freund, Huber, Curt, & Kramer, 2015). Over the past years numerous treatments have been developed that aim to target and reverse the brain changes proposed by this model (Knotkova et al., 2012). According to the model, PLP could be relieved by reversing maladaptive reorganisation or 'reinstating' the representation of the missing hand into its original territory. An example of such therapies is mirror box treatment, which uses illusory visual information of the missing hand (Ramachandran & Rogers-Ramachandran, 1996). During this treatment, a mirror is placed at the patient's midline with the phantom hand behind the mirror. Patients then move their intact hand and observe its reflection in the mirror, creating a visual illusion that one's missing hand is present and moving. This visual feedback is thought to reinstate the missing hand representation in S1.

Recently however, a number of papers have been published that challenge both the assumptions behind this maladaptive plasticity model (Blume et al., 2014; Makin, Scholz, et al., 2013; Makin, Scholz, Henderson Slater, Johansen-Berg, & Tracey,

2015; Vaso et al., 2014; Yanagisawa et al., 2016; see also Chapter 3 of this thesis) and the effectiveness of the treatments that are based on this model (Jutzeler, Curt, & Kramer, 2015; Rothgangel, Braun, Beurskens, Seitz, & Wade, 2011; Thieme, Morkisch, Rietz, Dohle, & Borgetto, 2016). A more detailed description of these criticisms will follow in the following section and Chapter 6 (Discussion) of this thesis.

1.6 Re-emphasising the peripheral attributes of PLP

The immense influence of the maladaptive plasticity model led to a disregard of the idea that PLP may be driven by aberrant inputs from the periphery. But (as mentioned in section 1.2), a recent study by Vaso et al., (2014) brought this theory back into the interest of the scientific community. Vaso and colleagues injected the dorsal root ganglion of 31 lower limb amputees with a local anaesthetic called lidocaine, and showed that this led to a rapid and reversible abolition of phantom limb sensations and phantom limb pain (Vaso et al., 2014). This research suggests that the downgrading of the peripheral attributes of PLP may have been premature. Indeed, these results suggest that PLP is caused by aberrant inputs originating in the peripheral nervous system.

A key assumption of the maladaptive plasticity model, that reorganisation is triggered by degradation of missing hand representation (i.e. through major sensory input loss) and, as such, unmasking of displaced body part inputs, was recently brought into question by Makin et al., (2013). Makin and colleagues recorded neural activity during phantom hand opening and closing movements in eighteen unilateral upper-limb amputees and 22 matched two-handed control participants. First, the authors

showed that activity elicited by phantom hand movements in the contralateral hand area of the primary sensorimotor cortex of amputees was indistinguishable from that of non-dominant hand movements in healthy two-handed control participants. This suggests that the missing hand representation may not be deteriorated in amputees. Secondly and importantly, a positive association was found between this maintained functional representation and chronic PLP. Indeed, amputees with worse chronic PLP had stronger maintained phantom hand movements activity in the primary sensorimotor missing hand cortex.

A second key assumption of the maladaptive plasticity model is that following arm amputation, the lip representation invades the cortical territory of the missing hand. Makin et al., (2015), recently provided evidence that questioned this assumption. Unlike previous studies, Makin and colleagues took into account the unique folding architecture of each participants' brain using unfolded models of the cortex. Using this approach that is arguably more suitable to study reorganisation along the sensorimotor homunculus, Makin and colleagues were unable to find a relationship between PLP and reorganisation of the lip representation. As reported previously, the lip representation in the deprived hemisphere (i.e. contralateral to the missing hand) was shifted superiorly, towards the missing hand representation. However, unlike previous reports, the magnitude of this shift was small and did not invade the missing hand representation (see Raffin, Richard, Giraux, & Reilly, 2016) for similar results). Furthermore, as reported previously (Makin, Scholz, et al., 2013), activity levels in the missing hand territory during lip movements did not differ between amputees and two-handed controls.

Instead, these results support the persistent representation model, stating that nociceptive inputs from the residual nerve form the basis of PLP. Continuous inputs from these nerves would lead to a more excitable missing hand cortex. As such, PLP would proportionately scale with brain excitability in areas normally receiving inputs from the missing hand.

1.7 Aims of this thesis

The primary aim of this thesis is to provide a better understanding of what happens to primary sensorimotor cortex following major sensory input loss, i.e. through arm amputation. I set out to investigate what mechanisms may underlie the phenomenology that is observed following arm amputation. I focus on PLP in particular, as this highly debilitating neuropathic pain syndrome remains poorly understood and novel treatment developments would benefit from a better mechanistic understanding. I will investigate both the neural and behavioural correlates of PLP and try to find a novel target for PLP treatment. I will use a range of neuroimaging techniques, as well as behavioural data and non-invasive brain stimulation, in the development of this thesis.

First, I set out to examine what happens to the representation of a missing hand following arm amputation. In Chapter 2, I will demonstrate that the topographical representation of a missing hand's individual digits is preserved in S1, even decades after arm amputation. I show that even 30 years post arm loss, the representation a missing hand is similar to that of controls. By making use of ultra-high field 7 tesla neuroimaging and the unique phenomenology of phantom sensations, I answer a

question that has remained unexplored until now: what happens to the original functional representation of S1 following major sensory input loss.

In Chapter 3, I will detail the neural correlates of PLP. I will replicate and extend the previous findings reported Makin, Scholz, et al., (2013) in a different subset of upper-limb amputees, using 3 tesla neuroimaging. We reaffirm the positive association between chronic PLP and maintained phantom hand S1 representation. We address previously raised concerns and suggest that PLP may be caused by peripheral mechanisms feeding into the S1 hand representation, rather than maladaptive plasticity in S1.

For Chapters 4 and 5, I collected data in a subset of upper-limb amputees suffering from high chronic PLP. In Chapter 4, I make use of a non-invasive brain stimulation technique, called transcranial direct current stimulation (tDCS), to try and relieve PLP as well as uncover a novel target for PLP treatment. I demonstrate that using a single 20min session of tDCS, PLP relief can be induced with effects lasting up to one week post stimulation. By combining tDCS with neuroimaging, we are able to point at the insula as a key region relating to PLP relief.

In Chapter 5, I investigate the behavioural correlates of PLP in upper-limb amputees, and demonstrate that PLP relates to worsened motor control of the phantom hand. I show that this worsened motor control relates to higher levels of maintained phantom hand representation. By further demonstrating a specific link between motor control and PLP, our findings open up new avenues for PLP management and improvement of existing PLP treatments.

Together, these studies provide the first comprehensive overview of how sensations of a missing limb, and PLP in particular, link with motor control and cortical sensorimotor mechanisms.

2 | Revealing the neural fingerprints of a missing hand

Adapted from

Kikkert, S., Kolasinski, J., Jbabdi, S., Tracey, I., Beckmann, C. F., Johansen-Berg, H., & Makin, T. R. (2016). Revealing the neural fingerprints of a missing hand. *eLife*, *5*, e15292.

Chapter abstract:

The hand area of the primary somatosensory cortex contains detailed finger topography, thought to be shaped and maintained by daily life experience. Here we utilise phantom sensations and ultra-high field neuroimaging to uncover preserved, though latent, representation of amputees' missing hand. We show that representation of the missing hand's individual fingers persists in the primary somatosensory cortex even decades after arm amputation. By demonstrating stable topography despite amputation, our finding questions the extent to which continued sensory input is necessary to maintain organisation in sensory cortex, thereby reopening the question what happens to a cortical territory once its main input is lost. The discovery of persistent digit topography of amputees' missing hand could be exploited for the development of intuitive and fine-grained control of neuroprosthetics, requiring neural signals of individual digits.

2.1 Introduction

The hand area of the primary somatosensory cortex (S1) contains detailed digit maps, with physically adjacent digits represented next to each other. Using ultra-high field neuroimaging, it is now possible to identify these characteristic digit maps in humans, with high inter- and intra-subject reliability (Ejaz, Hamada, & Diedrichsen, 2015; Kolasinski et al., 2016). Digit topography is characterised in neuroimaging by two main principles (Graziano & Aflalo, 2007): digit selectivity (Kolasinski et al., 2016) and inter-digit overlap (Ejaz et al., 2015). These maps are thought to be shaped and maintained by daily life experience: digits used more frequently together in daily life benefit from increased representational overlap (Ejaz et al., 2015), and following single digit amputation remaining digits' topography changes (Merzenich et al., 1984).

Amputees commonly experience lingering sensations from their amputated body part (Flor et al., 2006). Phantom sensations are not necessarily painful, and are best described as a vivid sensation of the missing hand as if it is still present (Flor et al., 2006). When instructed to move their phantom hand, amputees report detailed kinaesthetic sensations regarding the extent of movement afforded by different phantom digits. Phantom movements are known to evoke signals in the sensorimotor system (Makin, Scholz, et al., 2013; Raffin, Mattout, et al., 2012; Reilly, Mercier, Schieber, & Sirigu, 2006; see also Chapter 3), previously attributed to abnormal processing caused by the amputation (e.g. aberrant inputs (Makin, Scholz, et al., 2013; see also Chapter 3), peripheral reorganisation (Reilly et al., 2006)). Here we interrogate the information content underlying activity elicited by phantom hand

movements. If this information content is unchanged despite amputation, then activity patterns should show characteristic S1 digit topography.

2.2 Materials and methods

2.2.1 Participants

The main inclusion criteria for amputees in the study were: (a) unilateral upper limb amputation; (b) vivid kinaesthetic sensations during voluntary movements of each of the five digits of the phantom hand (based on self-report); (c) compatibility with magnetic resonance imaging (MRI) safety guidelines. We initially screened 63 unilateral upper-limb amputees, of which 22 met the initial criteria for MRI safety. Eight amputees met our 2nd criterion for vividness of kinaesthetic sensations while volitionally moving each of their phantom digits. Only two of these candidates were approved for undergoing ultra-high field (7 tesla) MRI, based on institute's standard operating procedures for MRI safety[1]. These amputees were invited to take part in the main study (see Table 2.1 for demographic and clinical details and Table 2.2 for details regarding the extend of movement afforded by each of the amputees' phantom digits). This involved studying movements of the phantom and intact hands, across two scanning sessions (see Appendices: Supplementary Materials Chapter 2 - Table A.2.1). Two additional inclusion criteria were used for a further investigation of peripheral contributions to the phantom digit topography: (d) brachial plexus avulsion injury; (e) abolishment of afferent inputs and efferent outputs (based on behavioural and electromyography (EMG) testing, see below for details). Three amputees who

[1] Ultra-high field (7T) imaging is a newly emerging technique, and as such most clinical implants (e.g. surgical clips) have not been approved for safety in these devices. Therefore, according to current local guidelines it is unsafe to scan individuals who have previously undergone major surgery (e.g. amputees) without a conclusive surgical history.

met criteria a, b and c also met criterion d. Only one of these candidates also met criterion e and was therefore invited to participate in the additional study. Because this individual was not approved to undergo ultra-high field MRI, he was tested in a single session at standard field (3 tesla) MRI. All three amputees included in the study were amputated on their left arm due to a trauma and were right-hand dominant prior to the amputation (based on self-report).

	Age	**Time since amp.**	**Amp. level**	**PLS mag./ scan**	**PLP mag./ scan/ ave.**	**Stump pain scan**	**Cosmetic/ functional prosthetics usage**	**Telescoping**	**Brachial plexus injury**
Above elbow	53	31	35%	100/ 100	15/0/ 20	0	2/2	Y	N
Below elbow	48	25	70%	80/20	35/0/ 30	0	3/5	N	N
Brachial plexus	50	31	30%	70/70	50/10/ 40	0	5/2	Y	Y

Table 2.1: Demographic and clinical details (Chapter 2). Amp. = amputation; Amp. level = amputation level measured in percentages: (residual arm length/intact arm length) x 100. Intact arm length is measured from shoulder to fingertips, where 41% is equivalent to the level of the elbow and 75% is equivalent to the level of the wrist; PLS = phantom limb sensations; mag. = magnitude; scan = score of phantom limb sensation vividness/pain intensity on the scanning day (scale 0 – 100); PLP = phantom limb pain; ave. = score of average phantom limb pain in a typical week (scale 0 – 100); prosthetics usage = prosthetic limb usage (frequency): 0- never, 1- rarely, 2- occasionally, 3- daily, 4- more than 4 hours a day, 5- more than 8 hours a day; Y. = yes; N. = no.

	Digit 1 PDS/diff./ quality	Digit 2 PDS/diff./ quality	Digit 3 PDS/diff./ quality	Digit 4 PDS/diff./ quality	Digit 5 PDS/diff./ quality
Above elbow	100/0/1	100/10/2	70/50/3	90/10/2	90/0/3
Below elbow	60/40/2	50/30/1	40/50/1	50/50/1	60/30/1
Brachial plexus	80/10/1	70/30/2	50/70/2	40/60/1	80/20/1

Table 2.2: Phantom digits' movement vividness, difficulty and quality. PDS = phantom digit sensation movement vividness: scale 0 – 100; ranging from unable to feel movement to movement is felt as vividly as the sensation of movement elicited by the intact hand's digits. Diff. = difficulty of the phantom sensation movement; scale 0 – 100; ranging from easy to impossible). Quality = Quality and extent of movement afforded by each phantom digit: 1 - full range of movements (i.e. equivalent to movements with the homologous digit on the intact hand). 2 – near to full range of movement (i.e. similar, though reduced, to movement of the intact hand). 3 – noticeably less range of movement compared to the intact hand (i.e. partial finger flexion and extension movement).

In addition, a group of thirteen two-handed control participants with a dominant right hand were recruited to take part in the study (mean age ± s.e.m. = 43 ± 3; three females). All control participants performed tasks with their left (non-dominant) hand as a control for the phantom digit movements, in a single session. A subset of six age- and sex-matched control participants (mean age ± s.e.m. = 50 ± 14; all male) also completed tasks involving right (dominant) hand movements. One of these participants was subsequently excluded from the study due to an atypical functional digit layout of both hands, including a reversed representation of the thumb and index finger. Another participant was excluded due to excessive head motion inside the scanner (greater than the functional voxel dimension (1.2mm) of absolute mean displacement), leading to visible spin history artefact. The resulting subset of four control participants (45 ± 13; all male: C1 – C4) also completed a standard field (3 tesla) version of the study. Participants in this group therefore completed three

sessions (two ultra-high field sessions and one standard field session; see Appendices: Supplementary Materials Chapter 2 – Table A.2.1). Ethical approval was granted by the NHS National Research Ethics service (10/H0707/29) and written informed consent was obtained from all participants prior to the study.

An additional standard field imaging dataset of 15 control participants and the three amputees specified above was also utilised in the current study. The purpose of this analysis was to explore inter-hemispheric (a)symmetry of the intact hand. The pertinent details relating to this dataset are highlighted in the Appendices: Supplementary Materials Chapter 2 – Figure A.2.3, and will not be detailed further in the materials and methods section.

2.2.2 Phantom sensations testing

To measure phantom sensations, as well as other demographic and clinical details of potential relevance to the studied missing hand representation, amputees completed a range of questionnaires (e.g., amputation details, prosthesis usage etc.; see Table 2.1). Amputees rated intensities of phantom limb pain (PLP), using a 0 – 100 scale, as follows: (i) intensity of worst PLP experienced during the last week (or in a typical week involving PLP); (ii) intensity of PLP on average over the last week (or in a typical week if last week was atypical); and (iii) current PLP intensity (i.e. on the scanning day). PLP magnitude was calculated by dividing worst pain intensity by pain frequency (1- all the time; 2- daily; 3- weekly). This approach represented the chronic aspect of the PLP as it combines frequency and intensity (Makin, Scholz, et al., 2013, 2015). Analogous measures were obtained for stump pain and vividness of non-painful phantom sensations. We also asked amputees whether they experienced

telescoping, a common phenomenon where the perceived length of the phantom limb is changed (Flor et al., 2006).

Amputees were asked to rate how vivid the phantom movement felt (scale 0 – 100; ranging from unable to feel movement to movement is felt as vividly as the sensation of movement elicited by the intact hand digits). In addition, amputees were asked to rate how difficult it was to perform each phantom digit movement (scale 0 – 100; ranging from easy to impossible). Finally, participants were asked to rate the quality and extent of movement afforded by each phantom digit. Amputees' answers were standardised as follows: 1 - full range of movements (i.e. equivalent to movements with the homologous digit on the intact hand). 2 – near to full range of movement (i.e. similar, though reduced, to movement of the intact hand). 3 – noticeably less range of movement compared to the intact hand (i.e. partial finger flexion and extension movement). See Table 2.2 for results of this measurement.

2.2.3 Brachial plexus avulsion testing

To investigate topographic mapping in the absence of peripheral inputs from the residual arm (stump), we screened participants with a brachial plexus avulsion injury. This injury involves the tearing of the nerve from its attachment at the spinal cord, abolishing afferent inputs and efferent outputs to the residual limb. To determine the extent of the brachial plexus avulsion injury, we conducted behavioural testing to measure stump sensitivity. Stimuli ranging from light touch to painful pinpricks were applied on the triceps of the residual arm (stump) and a corresponding site on the intact arm. Participants were blindfolded and asked to detect the stimuli, which were presented at varying inter-stimulus intervals in the following order: air puff, light

brush, cotton swab stroke, PinPrick probes (MRC systems) with weights: 8mN, 64mN and 512mN. Each stimulus was presented several times. These stimuli are routinely used for qualitative sensoric testing (QST), a technique used to determine sensitivity to touch and pain (Rolke et al., 2006).

To assess stump muscle activity, we used surface electromyography (EMG). We targeted the biceps and triceps of the residual arm, known to show muscle activity during phantom hand movements in amputees (Raffin, Giraux, et al., 2012; Raffin, Mattout, et al., 2012).

All three amputees were able to detect each of the stimuli when presented on their intact arm. Only one of the three tested amputees who reported to suffer from brachial plexus avulsion injury was unable to detect any of the stimuli on the residual arm. This participant also did not reveal a change in the EMG channels induced by cued phantom hand movements. This amputee therefore met our requirement for abolishment of afferent inputs and efferent outputs and was included in the standard field (3T) study.

2.2.4 MRI tasks

Digit representation was probed using a visually cued active (motor) task. In an intact sensorimotor system, movement recruits a combination of peripheral receptors encoding a range of somatosensory modalities (e.g. surface and deeper mechanoreceptors; proprioceptors), as well as efference information from the motor system. Using an active task, we have previously shown high consistency of S1 digit topography across multiple scanning sessions (Kolasinski et al., 2016).

The present study involved functional MRI (fMRI) paradigms designed to identify the two principles of topographic mapping of the hand, as previously shown using neuroimaging (Graziano & Aflalo, 2007): digit selectivity (Kolasinski et al., 2016) and inter-digit overlap (Ejaz et al., 2015). 1) To identify voxels showing digit preference (digit maps) a travelling wave approach was employed (also known as phase-encoding fMRI; Wandell, Dumoulin, & Brewer, 2007). This approach has previously been well-validated for sensory body mapping (Kolasinski et al., 2016; Mancini, Haggard, Iannetti, Longo, & Sereno, 2012; Orlov, Makin, & Zohary, 2010; Sanchez-Panchuelo, Francis, Bowtell, & Schluppeck, 2010; Sereno & Huang, 2006; Zeharia, Hertz, Flash, & Amedi, 2015). Whereas the travelling wave approach provides detailed information regarding digit preference, the winner-takes-all analysis (see below) makes this approach insensitive to overlapping cortical digit representations. Moreover, as the paradigm involves continuous cycles of digit movements without interruption of baseline periods, regions activated by multiple digits will be difficult to identify using a standard general linear model (GLM; Besle, Sánchez-Panchuelo, Bowtell, Francis, & Schluppeck, 2013). 2) To identify the extent of overlap between representations of individual digits (inter-digit representational similarity) a block design was therefore also employed. Below we describe the experimental design and analysis in further detail.

Participants were presented with five white circles, corresponding to the five digits, shown on a visual display projected into the scanner bore. To cue the participant which digit should be moved, the circle corresponding to this digit changed (i.e. in colour or by flashing). Participants were instructed to perform individual digit

movements using either their intact or phantom hand. Volitional (and not necessarily painful) movement of a phantom hand elicits both central (Makin, Cramer, et al., 2013; Makin, Scholz, et al., 2013; Raffin, Mattout, et al., 2012; Reilly & Sirigu, 2008b; see also Chapter 3) and peripheral motor signals (Raffin, Giraux, et al., 2012; Raffin, Mattout, et al., 2012; Reilly et al., 2006; Reilly & Sirigu, 2008b) that are different from those found during imagined movements. It was clearly stated to the amputees that they were required to perform actual movements with their phantom digits (i.e. try and move the digits of the missing hand), rather than motor imagery. To ensure good understanding of these instructions, the amputees were asked to demonstrate to the experimenter outside the scanner the extent of volitional movement carried out in each of their phantom digits, by mirroring each movement onto their intact hand. For the below elbow amputee, stump muscles were palpated by the experimenter outside the scanner to verify that actual movements were executed during movement of the phantom digits.

To compare between the amputees and controls, the phantom (left) hand was matched to the non-dominant (left) hand of control participants, and the intact (right) hand was matched to the (right) dominant hand of controls. Below we describe the parameters used for the main (ultra-high field) study. Adjusted parameters used for the standard field control experiment are mentioned when relevant.

Missing hand unimanual map

The traveling wave paradigm involved unimanual digit movements in a set sequence. The task consisted of blocks of 9s in which participants were instructed to move one digit. Each digit block was followed by a subsequent block of a neighbouring digit,

and repeated as follows: The forward sequence cycled through the movement blocks for digits: D1-D2-D3-D4-D5. The backward sequence cycled through the movement blocks in a reverse of the forward sequence (D5-D4-D3-D2-D1, Figure 2.1A). A sequence was repeated 8 times per run, with a duration of 6min and 25s. A forward and backward sequence was employed in separate runs. Each of the forward and backward runs was repeated twice, with a total duration of 25min and 40s.

When one of the white circles on the screen turned red, participants performed self-paced flexion and extension phantom (or left hand) digit movements with the digit corresponding to that circle, for the duration of the block (indicated by the presence of the red circle). The leftmost circle corresponded to D5 and the rightmost circle corresponded to D1 of the phantom (or left) hand. Amputees were instructed to move their phantom digits at a comfortable pace. Controls were instructed to perform slow movements, roughly corresponding to the pace and range of movement reported by the amputees (3-4s per flexion and extension movement). Participants practiced the movements extensively with an experimenter outside the scanner prior to the scan.

Missing hand inter-digit overlap

To assess inter-digit representational similarity of the missing hand, a block design was also employed. This task involved individual digit movement blocks for each of the five digits, as well as a no movement (rest) condition. Each of these 6 conditions was repeated 7 times in a counterbalanced order and each block lasted 12s, with a total duration of 8min and 24s. Participants were instructed to perform self-paced individual digit movements when the circle corresponding to this digit changed in

colour, as described above. All five circles remaining white, and a brief flash of the word ‘Rest’ indicated the rest condition.

Bimanual digit map

To replicate the missing hand maps using a separate dataset and additionally test whether topographic representation of the missing hand in amputees was independent of the intact hand, we asked our participants to perform a bimanual travelling wave task. Participants were provided with the visual display of five white circles (as described above) and were instructed to engage both hands in paired simultaneous digit movements when the relevant circle turned red, resulting in reversed digit movement cycles between the two hands. The leftmost circle corresponded to D5 of the left hand and D1 of the right hand; the second left circle corresponded to D4 of the left hand and D2 of the right hand; etc. (see Figure 2.3A). A forward and backward sequence was used in separate runs. Each of the forward and backward runs was repeated twice, for a total duration of 25min and 40s.

2.2.5 MRI acquisition

Ultra-high field

Ultra-high field fMRI data was acquired using a Siemens 7 tesla (7T) Magnetom system with a 32-channel head coil. Task fMRI data was acquired using a limited field of view (FOV), with 19-22 true axial slices centred on the anatomical location of the hand knob (Yousry et al., 1997) in the central sulcus bilaterally. The following acquisition parameters were used: sequence: multislice gradient echo EPI, TR:

1500ms, TE: 25ms, flip angle: 90°, GRAPPA factor: 2. The spatial resolution was 1.2mm isotropic.

To improve image registration, a whole brain and a partial field of view single volume high-saturation EPI image were acquired with the same slice positioning as the task fMRI. Anatomical T1-weighed scans, used for surface projection, were acquired using a 3 tesla (3T) system when available. For control participants 1, 5, 6, and 11 a 7T whole-brain T1-weighted image was acquired.

Standard field

Standard field MRI images were acquired using a 3T Verio MRI scanner (Siemens, Erlangen, Germany) with a 32-channel head coil. A multiband T2*-weighted pulse sequence with an acceleration factor of 6 was used (Moeller et al., 2010; Ugurbil et al., 2013). This provided the opportunity to acquire data with increased spatial (2mm isotropic) and temporal (TR: 1300ms) resolution than available with standard EPI sequences. The following acquisition parameters were used: TE: 40ms; flip angle: 66°, 72 transversal slices. A high-saturation first volume of each acquired multiband run was collected for registration purposes. Field maps were acquired for field unwarping.

2.2.6 MRI analysis

MRI analysis was implemented using tools from FSL and Connectome Workbench software (http://fsl.fmrib.ox.ac.uk/fsl; http://www.humanconnectome.org; Jenkinson, Beckmann, Behrens, Woolrich, & Smith, 2012; Smith et al., 2004; Woolrich et al., 2009) in combination with in house scripts developed using Matlab (version 8.4,

R2014b). Cortical surface reconstructions, used for visualisation of the fMRI results, were produced using FreeSurfer (http://freesurfer.net; Dale, Fischl, & Sereno, 1999; Fischl, Liu, & Dale, 2001).

MRI preprocessing

Common pre-processing steps for fMRI data were applied to each individual run in native (three dimensional, 3D) space, using FSL's Expert Analysis Tool FEAT (v6.00; fsl.fmrib.ox.ac.uk/fsl/fslwiki). The following steps were included: Motion correction using MCFLIRT (Jenkinson, Bannister, Brady, & Smith, 2002), brain extraction using automated brain extraction tool BET (Smith, 2002), spatial smoothing using a 1.5mm FWHM (full width at half maximum) Gaussian kernel for the ultra-high field scans and 2mm FWHM for the standard field scans, and high pass temporal filtering with a cut-off of 100s. All BOLD EPI data were assessed for excessive motion using motion estimate outputs from MCFLIRT: ultra-high field functional data from one participant exhibited greater than 1.2mm (functional voxel size) of absolute mean displacement and was excluded from all further analysis.

Image registration

Ultra-high field

Image registration was accomplished using FLIRT (FMRIB's linear image registration tool; Jenkinson et al., 2002; Jenkinson & Smith, 2001). To ensure good registration of the partial-FOV functional data to the anatomical image, image registration was carried out in individual, visually inspected, steps.

First, the task fMRI data from each run was registered to a partial-FOV single volume high-saturation EPI image, acquired at the first session. This partial-FOV image was registered to a whole brain FOV single volume high-saturation EPI image. The whole brain image was then registered to the T1-weighted image; initially using the mutual information cost function (6 degrees of freedom), and then optimised using boundary-based-registration (Greve & Fischl, 2009) (6 degrees of freedom, FMRIB's Automated Segmentation Tool (FAST) for white matter segmentation, no search). For two participants (C4 and C11), manual alignment was used to register the single volume partial-FOV high-saturation EPI image to the structural MEMPRAGE white matter and pial surfaces using blink comparison as implemented in Freeview.

Standard field

Functional and anatomical images were aligned using a similar pipeline as described above. Each individual run was first co-registered to the high-saturation first volume of the acquired multiband run, and then to the T1-weighted image. In addition, field map based unwarping was included to reduce spatial distortions and additionally improve co-registration.

Travelling wave analysis

The travelling wave runs were analysed for each individual participant in native (3D) space, using a cross-correlation approach previously applied in retinotopy (Engel, Glover, & Wandell, 1997). The approach is based on continuous presentation of stimuli in a set cycle that are expected to result in neighbouring cortical representations (e.g. rotating wedge in the visual field; sequential digit stimulation in a set cycle). It is designed to capture voxels showing increased response to one

condition, above and beyond all other conditions (in our case, preference for a specific digit). Beyond preference, this technique also provides a powerful tool for capturing the smooth progression of adjacent representations that are typical for topographic maps. It is therefore considered a preferable technique for capturing topographic representations (Wandell et al., 2007). With respect to somatotopy, the travelling wave approach (or the homologous phase-encoding approach) has previously been validated against blocked and event-related fMRI paradigms (Besle et al., 2013; Kolasinski et al., 2016; Orlov et al., 2010; Sanchez-Panchuelo et al., 2010).

We have recently utilized the traveling wave approach, in combination with ultra-high field fMRI to demonstrate highly reproducible maps of individual digits in S1 (Kolasinski et al., 2016). In the current study, we closely followed these previously validated experimental procedures, as described in Figure 2.1. Participants moved individual digits in a set cycle (see the fMRI tasks section above). A reference model was generated using a gamma-HRF convolved boxcar function, while taking into account the hemodynamic delay. The model was constructed using a 9s 'on' (the duration of a single digit movement) and 36s 'off' (the period of movement of all other digits), accounting for a single 45s cycle (Figure 2.1B). This cycle was repeated 8 times to reflect the full run duration. The reference model was systematically shifted in time to model activity throughout the full movement cycle. Because the runs were acquired using a TR of 1.5s, the model was shifted 30 times by 1 lag to account for the full 45s cycle of movement.

For each individual voxel, each of the 30 reference models was correlated with the preprocessed BOLD signal time course to estimate cross-correlation values. The resulting r-values were standardised using the Fisher's r-to-z transformation. By plotting these standardised r-values as a function of the lag, tuning curves can be created, and the optimal fit for each voxel can be inferred (Figure 2.1C).

The travelling wave approach uses a set cycle, and as such could be susceptible to order-related biases resulting from the sluggish hemodynamic response. For this reason, the order of the cycle was varied between forward (D1-D2-D3-D4-D5) and backward (D5-D4-D3-D2-D1) in different runs (Figure 2.1A). To average across the four runs, lags were initially assigned to each of the five digits (six lags per digit). Within each voxel, the r-values corresponding to each digit were averaged, resulting in five r-values, corresponding to each of the digits for a given run. The digit-specific r-values were then averaged across the forward and backward runs on a voxel-by-voxel basis. A winner-take-all approach was applied to produce maps in which each voxel was assigned exclusively to one individual digit, providing us with digit specificity.

To visualise the gradient of progression across digits, lag-specific maps were also produced. For each backward run, the resulting r-values from the cross-correlation analysis were standardised and time-reversed. Forward and backward runs were averaged, on a lag-by-lag basis. To construct a gradient map, a winner-take-all approach was used across all 30 lags, in which each voxel was assigned exclusively to one individual lag.

Cortical surface projections were constructed from T1-weighted images. The digit and gradient maps were registered to structural space and projected to two-dimensional surface space using a cortical ribbon mapping method. To account for multiple comparisons, thresholding was implemented on the surface using the false discovery rate (FDR) (Benjamini & Hochberg, 1995), calculated for each digit individually. This approach doesn't take into consideration the neighbourhood relationships of the voxels, and therefore doesn't force cluster patterns. The thresholded maps were set at a false detection criterion of $q < 0.05$ based on the native (3D) values. The FDR thresholded digit-specific clusters were overlaid into a single hand map. Within the resulting five-digit map, we used a 30-lag colour code to visualise the gradient of progression across digits (Figure 2.1D).

For the standard field digit maps, the same procedures were used, with the following exceptions. Due to the difference in temporal resolution (TR = 1.3s), each digit block lasted 9.1s, resulting in slightly longer movement cycles (45.5s). 35 HRF reference models were constructed (compatible with 35 lags), and a more conservative FDR criterion ($q < 0.01$) was selected, due to a reduced signal-to-noise ratio.

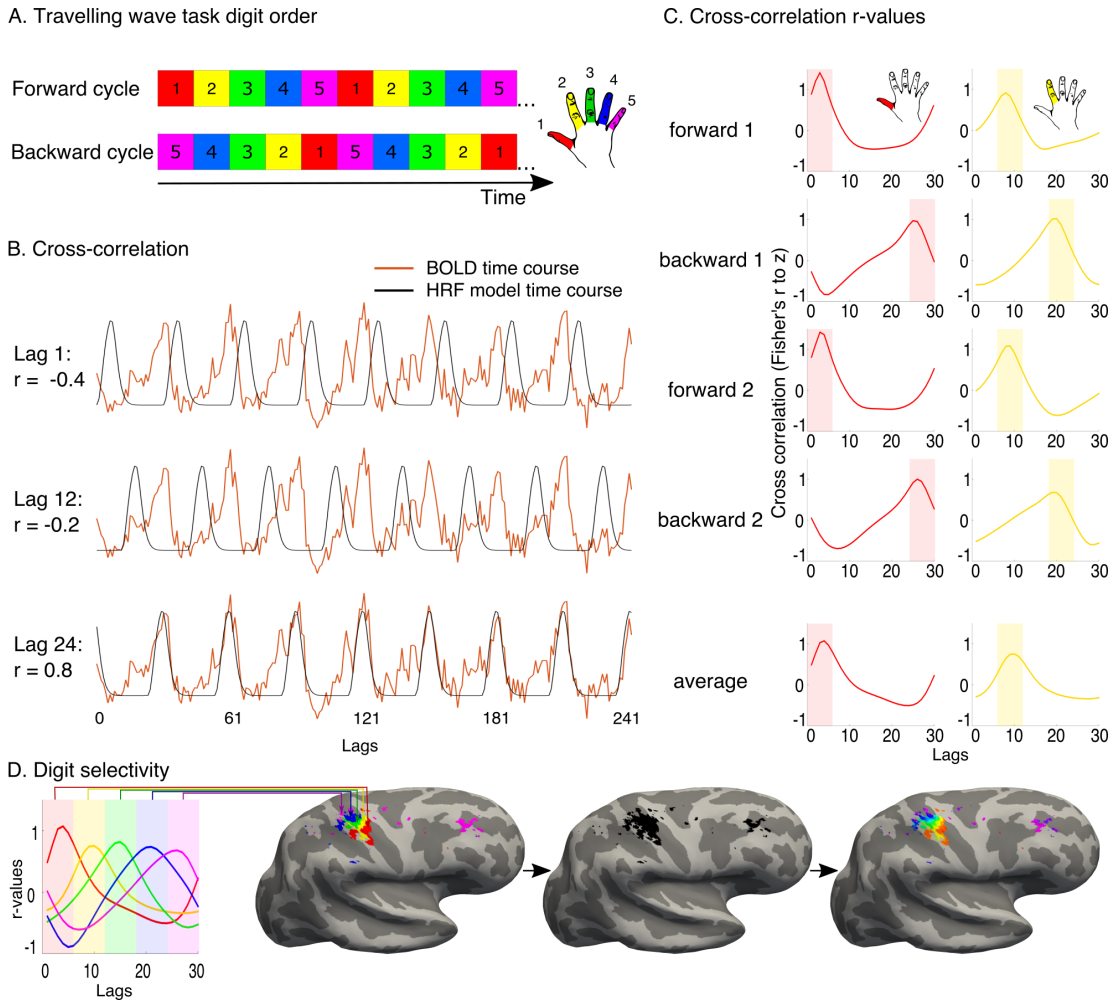


Figure 2.1: Travelling wave task and analysis. A travelling wave paradigm, involving digit movements in a set sequence, was used to capture digit preference and the smooth progression of adjacent digit representations in primary somatosensory cortex. (A) The travelling wave task involved 8 repeated cycles of continuous individual digit movements. Each 45s cycle consisted of five 9s blocks dedicated to each digit (as exemplified by the coloured squares), with each run cycling through either D1-D2-D3-D4-D5 (forward, top) or D5-D4-D3-D2-D1 (backward, bottom). Each of the forward and backward runs was repeated twice. The numbers 1-5 and colours correspond to the five digits, as visualised in the right side of the panel. (B) The preprocessed BOLD time courses from individual voxels (example time course of one voxel is shown in red) were cross-correlated against a reference model. The model corresponded to a single-digit movement (9s 'on', 36s 'off'- the period of movement of all other digits), and was systematically shifted in time to model activity throughout a full cycle (30 shifts, corresponding to the 30 lags of the 45s cycle). The figure shows three different model lags (1, 12 and 24), resulting in varying cross-correlation outcomes. Lag 24 was the optimal model lag for this preprocessed BOLD time course. (C) The standardised r-

values (Fisher's r-to-z, y-axis) resulting from the cross-correlation were plotted as a function of lag (x-axis) for each individual voxel in each run. In the left panel, cross-correlation values from the example voxel shown in B are plotted for each of the four runs. The optimal fit for the voxel is demonstrated by the peak cross-correlation (digit 1, in the left panel; digit 2 in the right panel, taken from a separate voxel). Lags associated with the same digits were averaged, first within and then across runs. A winner-take-all approach was used to determine digit preference, based on the highest averaged r-value, resulting in five separate digit maps. False discovery rate (FDR) was applied for each of these single digit maps to adjust the threshold based on the criterion q (FDR) < 0.05. (D) Each of the five digits was assigned a colour code, as demonstrated on the left. The five digit maps were projected to the cortical surface, to display digit preference maps. Note that no masking was applied when presenting the resulting maps. Within the resulting five-digit map a gradient of progression across digits was visualised, based on the voxel-wise r-values for each of the 30 lags. The resulting map was located in the central sulcus and postcentral gyrus, corresponding to the primary somatosensory cortex, around the anatomical hand knob.

Split-half consistency

To quantify consistency in digit preference, as identified using the travelling wave task, we split the data used to construct the digit preference maps, and compared the spatial correspondence between digit selective clusters. Split-half consistency of the digit-specific clusters was calculated using the Dice coefficient (Dice, 1945; Kolasinski et al., 2016). The Dice coefficient varies from 0 (no spatial correspondence between digit representations) to 1 (perfect spatial correspondence between digit representations). Where A and B are the areas of two digit representations, the Dice Coefficient is expressed as:

$$\frac{2 \times |A \cap B|}{|A| + |B|}$$

Each digit's winner-take-all map was minimally thresholded on the cortical surface ($Z > 2$). Spatial correspondence was calculated in S1 (as defined by FreeSurfer) between

each possible digit pair across the split-halves of the unimanual digit maps. The first forward and backward runs were combined to provide the first digit-specific clusters, and the second forward and backward runs were combined to form the second digit-specific clusters. By doing so, we established a split-half consistency measure for the travelling wave maps of the phantom (or left) hand and intact (or right) hand separately. One control participant was discarded from the subsequent analysis, as his mean spatial correspondence values (across all possible digit combinations) fell outside two standard deviations from the control group mean.

A benchmark for digit selectivity is greater split-half spatial correspondence across "same" versus "different" digits. Mean "same"-digit values (across all five "same"-digit pairs) were greater than mean "different"-digit values (across all twenty "different"-digit pairs) in each of the participants. The "same"-digit spatial correspondence values in the two amputees (0.30 for the above and below elbow amputees, average across all "same"-digit pairings) were smaller on average than those observed in the control participants (0.57 on average across all control participants; Figure 2.2D), suggesting lower consistency of digit selectivity in amputees. To further assess digit selectivity in the amputees, the "different"-digit distribution of Dice spatial correspondence values was estimated using a bootstrapping procedure (5,000 iterations) for each individual participant. "Same"-digit values were averaged for each participant, and compared against the 95% confidence interval (CI) on a subject-by-subject basis. For all participants (amputees and controls), the "same"-digit value fell well outside the range of spatial correspondence seen between "different" digits. This indicates that the consistency shown for digit-selective clusters was greater than expected by chance in all

participants. Next, the mean "same"-digit values in the two amputees were compared to the "different"-digit spatial correspondence distribution of each of the controls. "Same"-digit spatial correspondence values in both amputees fell outside the "different"-digit spatial correspondence distribution of each of the controls (CI: 0.03-0.08 on average). This was also confirmed by comparing the mean spatial correspondence between "same"-digit values for each of the amputees and "different"-digit values of the controls (two-tailed Crawford and Howell t-test (Corballis, 2009); $t(9) = 14.24$, $p < 0.001$ and $t(9) = 14.31$, $p < 0.001$ for above and below elbow amputees respectively). This indicated that although reduced, the digit maps of the amputees were consistent, even relative to controls.

In addition, we aimed to compare between the unimanual and bimanual digit maps within the missing hand hemisphere, providing us with an estimate of consistency when accounting for potential contributions of the intact hand. The "different"-digit distribution of Dice spatial correspondence values between the unimanual and bimanual maps was estimated using a bootstrapping procedure (5,000 iterations) for each individual participant. "Same"-digit spatial correspondence values (mean across all "same" digits) in both amputees (0.49 and 0.40 for above and below elbow amputees respectively) fell outside the "different"-digit spatial correspondence distribution. This was observed both compared to their own "different"-digit distribution (CI: 0.03-10 for both above and below elbow amputees) and each of the controls' "different"-digit distributions (CI: 0.03-0.13 on average). This was also confirmed by comparing the mean spatial correspondence between "same"-digit values for each of the amputees and "different"-digit values of the controls (two-tailed

Crawford and Howell t-test (Corballis, 2009); $t(3) = 29.14$, $p < 0.001$ and $t(3) = 22.57$, $p < 0.001$ for above and below elbow amputees respectively).

Inter-digit representational similarity analysis

We used an fMRI pattern component approach to identify the extent to which representations of the different digits overlapped with each other, while considering multivoxel patterns underlying the S1 digit maps. Voxels underlying the digit preference map surrounding the anatomical hand knob were combined to form a region of interest (ROI) in native space. The multivoxel pattern-component model is described in detail in (Diedrichsen, Ridgway, Friston, & Wiestler, 2011) and implemented in http://www.icn.ucl.ac.uk/ motorcontrol/imaging/multivariate_analysis.html. This method allows deriving unbiased estimates of the true correlations between the underlying activation patterns for each condition.

In brief, a generative model is created that assumes the observed patterns are associated with a set of underlying pattern components that relate to the different experimental conditions or noise. Activity patterns are decomposed within the ROI into a common (noise) component that is shared between all trials and one specific component for each of the five digits. By estimating the variability (or strength) of the similarity between the latter components, the inter-digit representational overlap in the ROI is revealed. Figure 2.4 and Appendices: Supplementary Materials Chapter 2 – Figure A.2.4 (Figure 2.5D for standard field) show the resulting matrices, demonstrating the level of representational similarity (or overlap) between each digit pair. The topographic inter-digit pattern is characterised by increased overlap between

neighbouring digits. Furthermore, digits showing increased synergies in daily life (e.g. digits 3 and 4) tend to show greater representational overlap than digits that are more independent during hand function (e.g. digits 1 and 2; Ejaz et al., 2015). The resulting inter-digit representational overlap pattern therefore provides a detailed "fingerprint" of hand representation.

We initially assessed overall (mean) overlap within the matrix of each participant, by averaging all unique inter-digit similarity r-values (across the 10 cells of the matrix, while excluding the diagonal). On average, the amputees showed higher inter-digit overlap (0.55 and 0.54 for above and below elbow amputees, respectively) compared to the control group (CI: 0.24-0.41). To investigate whether the missing hand inter-digit overlap pattern was comparable to normal hand representation, as found in controls, we generated the distribution (and 95% confidence intervals) of correlation across the control population. For this purpose, inter-digit overlap patterns (i.e. the cells in the similarity matrices) were correlated across pairs of controls, using a bootstrapping approach (10,000 iterations) and a Spearman test. One control participant was discarded from the subsequent analysis, as his mean Spearman correlation value (with all other controls) fell outside two standard deviations from the control group mean. (Note that the exclusion of the outlier participant did not affect the outcome of this analysis.) Next, the same procedure was carried out between each amputee and each of the controls' inter-digit overlap patterns. By plotting the average amputee-control Spearman rho values and confidence intervals against the confidence interval of the controls-to-controls correlation distribution, we were able to show that the amputees' inter-digit representational overlap pattern fell within the normal range of the controls. There was no significant difference between

the amputees-to-controls average Spearman correlation and the control-to-control correlations also when using more conventional statistics (two-tailed Crawford and Howell t-test (Corballis, 2009); $t(9) = -1.10$, $p = 0.30$ and $t(9) = 0.31$, $p = 0.76$ for above and below elbow amputees respectively).

Because the pattern component approach implemented here is minimally affected by differences in noise amplitude resulting from different scanners and acquisition parameters (Diedrichsen et al., 2011), we repeated the same analysis, using the brachial plexus amputees' data and the control participants' data (ultra-high field MRI). The average correlation of this amputee's inter-digit overlap pattern with each of the controls' inter-digit overlap patterns (0.76), fell within the controls-to-controls correlation range. There was no significant difference between the amputee-to-controls average Spearman correlation and the control-to-control correlations (two-tailed Crawford and Howell t-test (Corballis, 2009); $t(9) = 0.14$, $p = 0.89$)

2.3 Results

To study phantom digit topography, we used ultra-high field 7 tesla neuroimaging in two individuals who lost their left hand several decades ago (25 and 31 years post amputation) and eleven right-handed controls. Both amputees reported exceptionally vivid kinaesthetic phantom sensations during individual digit movements (see Table 2.1 and Table 2.2 for clinical and demographic details). Amputees and controls were visually cued to execute individual phantom digit movements (left hand digits in controls). Importantly, phantom movements are distinguishable from imagined movements. This is supported by empirical evidence demonstrating that phantom limb movements elicit both central and peripheral motor signals, that are different

from those found during imagined movements (Makin, Scholz, et al., 2013; Raffin, Mattout, et al., 2012; Reilly et al., 2006). To ensure adequate task performance, amputees were asked to demonstrate to the experimenter outside the scanner the extent of volitional movement carried out in each of their phantom digits during the task, by mirroring the phantom movements with their intact hand.

2.3.1 Travelling wave

To capture the first principle of topography, we employed a technique designed to identify digit preference in S1 (travelling wave design, see Figure 2.1 for design details; see Appendices: Supplementary Materials Chapter 2 – Figure A.2.1 for other brain areas activated by phantom hand movements). The resulting gradients of digit preference (hereafter digit maps) are presented in Figure 2.2. As indicated by the black arrows in the example control participants (Figure 2.2A), a characteristic digit map shows a gradient of digit preference, progressing from thumb (red, medially) to little finger (pink, laterally). Similarly, both amputees showed a clear gradient of digit preference in the central sulcus and postcentral gyrus (Figure 2.2B; see Appendices: Supplementary Materials Chapter 2 – Figure A.2.2 for intact hand maps). Qualitatively, the position, digit order, and extent of the missing hand maps were similar to those observed in controls. Analysis of spatial correspondence of "same" versus "different" digit clusters between two halves of the dataset further confirmed that while reduced (compared to controls), digit selectivity in amputees was consistent (Figure 2.2D; see materials and methods for further details).

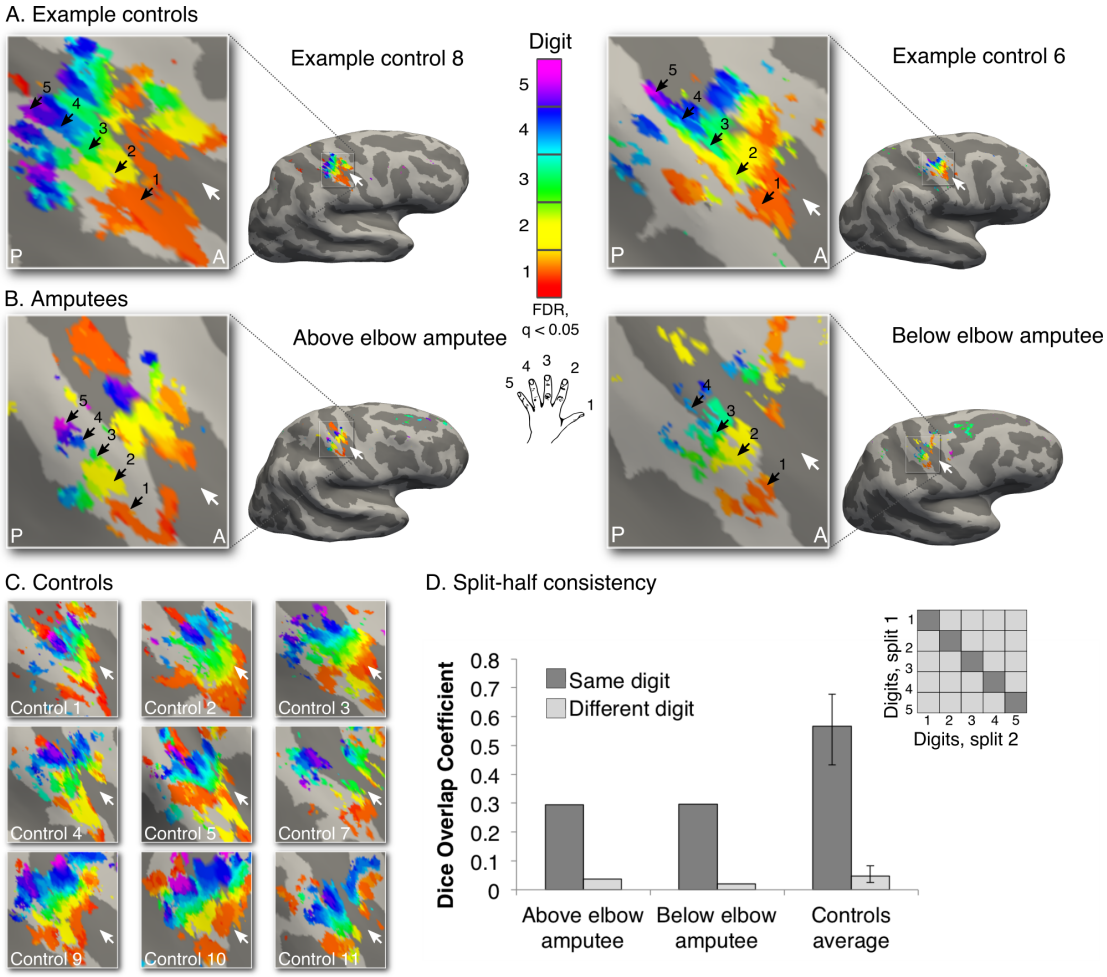


Figure 2.2: Missing hand maps revealed in amputees during phantom digits movement. Black arrow indicate preference for digits 1-5: thumb (red); index (yellow); middle (green); ring (blue) and little finger (purple) in two-handed controls (A, C) and amputees (B). Participants performed single digit flexion and extension movements with their non-dominant (controls) or phantom hand (amputees) in a travelling wave paradigm. Qualitatively similar digit topographies were found in each amputee and the controls. White arrows indicate the central sulcus. A = anterior; P = posterior. Multiple comparisons were adjusted using false discovery rate (FDR). (D) Maps' intra-individual split-half consistency, assessed using the Dice overlap coefficient. On average, "same"-digit selective clusters (dark bars) showed greater consistency than "different"-digit clusters (light bars) in amputees and controls. Amputees showed lower split-half consistency for "same"-digit clusters (averaged across digits) compared to controls (95% confidence intervals (CI) = 0.43-0.68, as assessed using a bootstrap approach). However, amputees' "same"-digit clusters were more consistent than "different"-digit clusters in controls (i.e. fell outside the CI of "different"-digit clusters split-half consistency in controls), indicating that although reduced, the digit maps of the amputees were consistent.

2.3.2 Preserved digit maps are independent of intact hand contributions

A hallmark of a functional sensorimotor system is the distinct representation of the two hands. To further confirm the existence of the missing hand map independently of intact hand contributions (Makin, Cramer, et al., 2013), we designed an opposing bimanual travelling wave task. Participants performed paired movements with digits of the phantom and intact hands in reverse sequences (i.e. one hand moved D1 to D5, while the other simultaneously moved D5 to D1; Figure 2.3A). Both amputees showed maps in the hemisphere contralateral to the intact hand, dissociated from a second map in the missing hand hemisphere (Figure 2.3B, C). The latter map corresponded to the original (unimanual movements) missing hand map (Figure 2.3B), as confirmed by higher spatial correspondence for "same" (0.49, 0.40 for above and below elbow amputees) versus "different" (0.06, 0.04) digit clusters across the two (unimanual and bimanual) missing hand datasets (Figure 2.3E). This provides a replication for the preserved missing hand maps. This result also demonstrates the independence of the missing hand topography from the representation of the intact hand. Our group and others previously showed that following unilateral arm amputation, the intact hand becomes over-represented in the missing hand territory (Makin, Cramer, et al., 2013; Philip & Frey, 2014; Raffin et al., 2016). Our results therefore confirm that the digit map in the missing hand territory is not driven by an emerging representation of the intact hand. Note, however, that our results do not exclude the possibility for reorganisation in the missing hand territory. As demonstrated in Appendices: Supplementary Materials Chapter 2 – Figure A.2.3, this study's participants showed over-representation of their intact hand in the missing

hand territory, indicating that the preserved missing hand topography can co-occur with remapping of body parts.

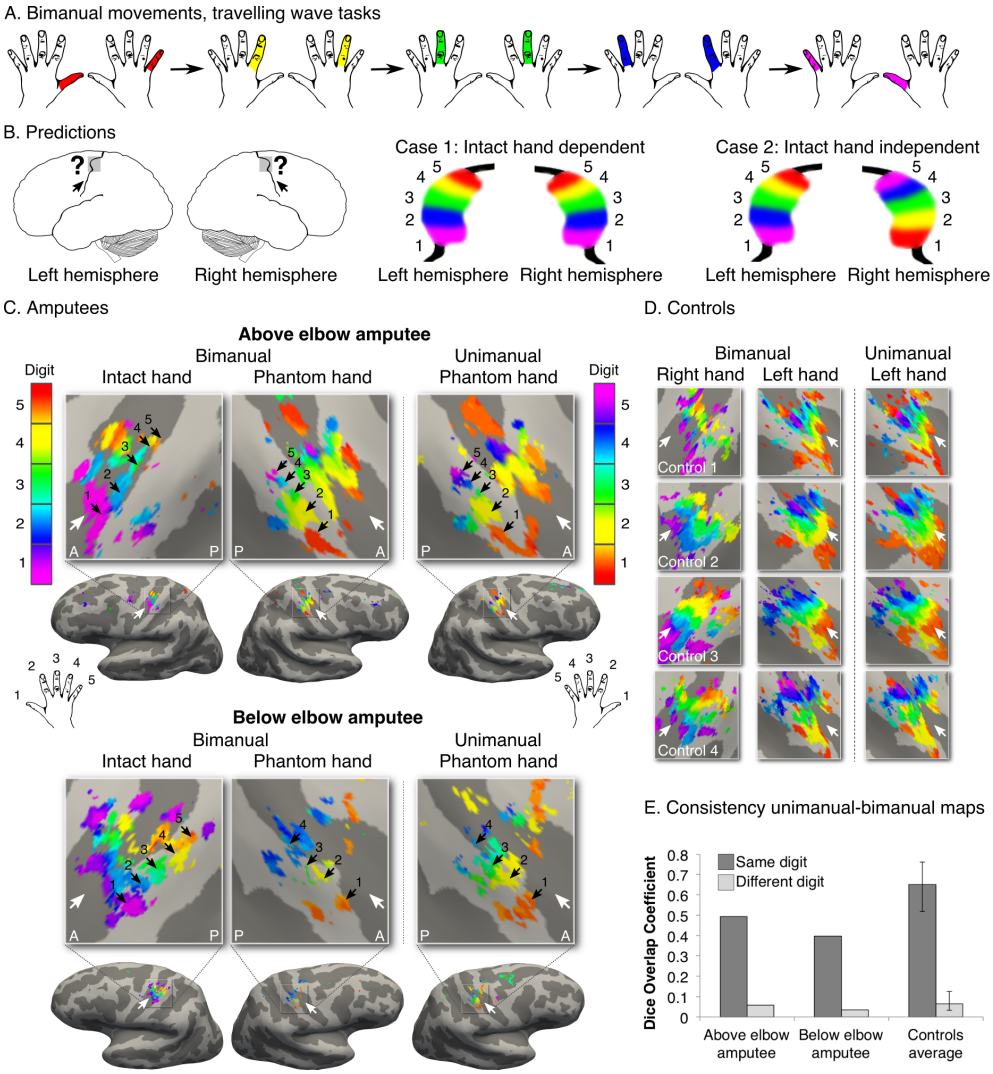


Figure 2.3: Missing hand maps are replicated during dissociated bimanual hand movements. (A) In the bimanual task, individuals performed paired digit movements with both hands, resulting in reversed digit cycles between the hands. The colour code in this figure indicates the cycle lag as shown in (A). Symmetrical colour gradients across the two hemispheres would reveal the missing hand map as dependent on intact hand movements (B: case 1). Colour gradient reversal across hemispheres indicates dissociated hand representations (B: case 2), as was seen in both amputees and controls (C, D respectively, left two panels). Maps contralateral to the missing hand (left hand in controls) resembled the unimanual tasks' maps (Figure 2.2), both qualitatively (C, D, right panel) and quantitatively, using the Dice overlap coefficient (E). The digit maps

were adjusted for multiple comparisons using false discovery rate (FDR). Other annotations are as in Figure 2.2.

2.3.3 Inter-digit overlap patterns in amputees are similar to controls

While the travelling wave maps demonstrate digit preference, they provide little information about the second principle of digit topography: inter-digit overlap. To study inter-digit overlap, we used pairwise digit representational similarity of multivoxel patterns (Diedrichsen et al., 2011). This approach fully reveals the intricate overlap pattern across all digits (Ejaz et al., 2015), as shown for controls in Figure 2.4B, D. In general, both amputees showed greater average overlap across digits (0.55 and 0.54 for above and below elbow amputees respectively), compared to controls (95% confidence intervals (CI) = 0.24-0.41). However, when examining the inter-digit overlap pattern in the missing hand map, both amputees demonstrated typical patterns (Figure 2.4A, C; see Appendices: Supplementary Materials Chapter 2 – Figure A.2.4 for intact hand). This was reflected in high correlation between each amputee's inter-digit overlap pattern and the controls, as assessed using a bootstrapping approach (average $r_s = 0.61$ and $r_s = 0.78$, 95% CI = 0.25-0.89 and 95% CI = 0.62-0.90 for above and below elbow amputees respectively). These average amputee-to-controls Spearman correlation values fell well within the controls-to-controls Spearman correlation range (95% CI = 0.35-0.95; Figure 2.4C), providing further evidence for characteristic missing hand representation decades after amputation.

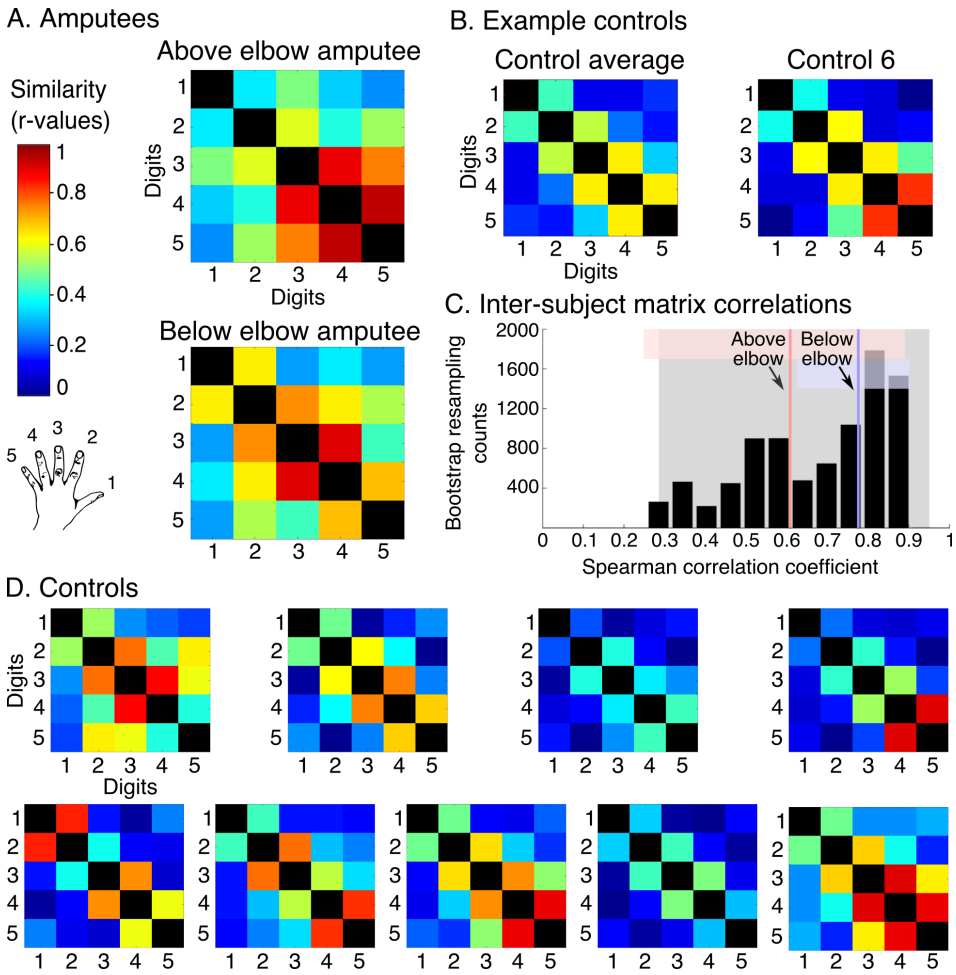


Figure 2.4: Amputees show characteristic inter-digit overlap patterns during phantom digit movements. Inter-digit representational similarity of multivoxel patterns underlying the maps shown in Figure 2.2, derived from a block-design paradigm in amputees (A) and controls (B, D). Similarity (or overlap) is decreased between non-neighbouring digits and tends to increase between digits 3-5, as shown in the controls' averaged matrix. (C) Positive distribution of inter-subject correlations, between controls' inter-digit overlap patterns. The grey area indicates the 95% confidence interval (CI) for controls. Pink and blue lines indicate average amputee-to-controls correlations for above and below elbow amputees respectively. Pink and blue shaded areas correspond to the 95% CIs. Both amputee-to-controls correlation averages values fell within the normal controls-to-controls correlation range, suggesting that the amputees exhibited a characteristic pattern of inter-digit overlap.

2.3.3 Preserved digit topography is not dependent on peripheral inputs

Finally, we also studied missing hand representation in a third amputee (31 years since amputation) whose cause of amputation involved a brachial plexus avulsion, abolishing communication between the residual arm and the central nervous system. Due to MRI safety limitations, 3 tesla neuroimaging was used (see Figure 2.5B for quality comparisons to ultra-high field digit maps). Using the bimanual task (specified above and in Figure 2.5A) we identified digit preference for the missing hand in the postcentral gyrus (Figure 2.5C). We also identified a typical inter-digit overlap pattern (Figure 2.5D), as confirmed in comparison with the control population described in Figure 2.4 (average Spearman correlation with controls = 0.76 with 95% CI = 0.30-0.92). This result provides further evidence for the existence of preserved digit topography in the absence of peripheral input.

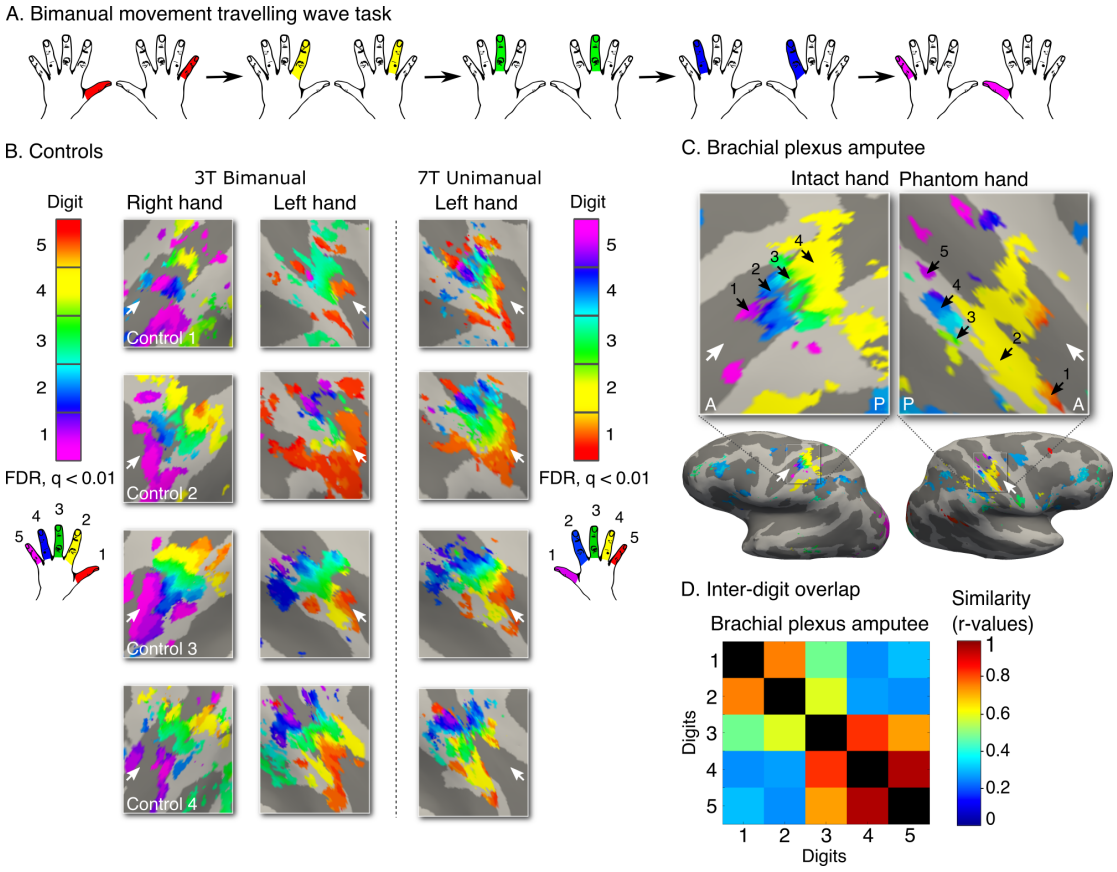


Figure 2.5: Topography is preserved despite the absence of peripheral input. To rule out the potential contribution of peripheral inputs from the injured nerve to preservation of the phantom hand map, we tested an upper-limb amputee suffering from brachial plexus avulsion injury with vivid kinaesthetic phantom digit sensations. This injury involves the tearing of the nerve from its attachment at the spinal cord, abolishing afferent inputs and efferent outputs to the residual limb. 3 tesla MRI was used here due to safety restrictions, meaning that standard field digit preference maps were acquired. The bimanual travelling wave task (A, Figure 2.3) elicited maps in the controls with reversed colour gradients (B - left 2 panels). In comparison to the ultra-high field left hand maps (right panel), the standard field left hand maps were cruder (e.g. less digit specificity, B - middle panel). (C) The brachial plexus amputee showed two maps with reversed colour gradients, comparable to those found in controls. The map in the missing hand hemisphere showed preference for digits in primary somatosensory cortex. (D) Inter-digit representational similarity was assessed for multivoxel patterns underlying the missing hand map. The correlation value of the brachial plexus amputee's inter-digit overlap pattern with the controls exemplified in Figure 2.4 fell within the normal controls-to-controls correlation range. Together, these results suggest that preserved representation of the missing hand existed independently of peripheral inputs. Annotations are as in Figure 2.2.

2.4 Discussion

Together we show that, although the missing hand maps were weaker and noisier than the maps found in controls, the functional digit layout of S1 prevails following arm amputation. Digit topography, previously thought to depend on experience (Ejaz et al., 2015; Merzenich et al., 1984), was detectable despite decades without organised peripheral inputs associated with normal hand function. Our findings call for a reassessment of the role of sensory input in regulating brain organisation and plasticity. By demonstrating characteristic topography of the missing hand decades after arm amputation, our findings reopen the question of what happens to a cortical territory once its main inputs are removed.

Textbooks teach us that the cortical territory previously assigned to processing the now lost input is invaded by new representations. For example, following arm amputation, the missing hand territory in S1 is taken over by representations of other body parts (e.g. the neighbouring representation of the face in monkeys (Pons et al., 1991), or the intact hand in humans (Makin, Cramer, et al., 2013)). Conversely, recent research in the visual cortex suggests that reorganisation in the adult brain may be restricted. For example following macular degeneration, the functional representation of the intact visual field was unchanged (Baseler et al., 2011; see Smirnakis et al. (2005) for similar results in non-human primates). Common to all these previous studies aiming to characterise reorganisation or the lack thereof, is that the authors probed the cortical neighbours of the area previously responsible for processing the lost input. While this approach is suitable for documenting shifted representation of the cortical neighbours, it leaves unexplored the possibility that the original function of the region deprived of sensory input may be preserved, though latent. Amputees

experiencing phantom sensations provide a unique model to study what happens to the deprived cortical territory itself during sensory input loss. Here we show that reorganisation in the missing hand territory following input loss does not abolish the original functional layout in sensory cortex.

How can our finding of preserved S1 topography of a missing hand be allied with the wealth of evidence showing cortical reorganisation in S1 following sensory input loss? (e.g. amputation and spinal cord injury (Jain, Qi, Collins, & Kaas, 2008; Merzenich et al., 1984; Pons et al., 1991); see Appendices: Supplementary Materials Chapter 2 – Figure A.2.3 for reorganisation in the current study's volunteer cohort). Already in their seminal work Merzenich et al. (1984) suggested that reorganisation following sensory input loss does not exclude the possibility for simultaneous preservation of the original function of that region. Accordingly, recent structural and functional evidence shows that the capacity for S1 reorganisation is more limited than initially thought, and that instead the functional changes previously observed in S1 following input loss could be attributed to reorganisation in sub-cortical areas in the afferent pathway, principally the brainstem (Chand & Jain, 2015; Jain, Catania, & Kaas, 1998; Kambi et al., 2014). In other words, previous findings of massive cortical reorganisation in S1 reflect reorganisation of inputs, rather than reorganisation within S1 itself. This recent evident nicely complements our own finding of S1 reorganisation, overlaid on preserved structure and function.

Which inputs could contribute to the maintenance of the missing hand topography? The variability in the level and nature of amputations in this study's cohort allows us to consider the potential contribution of the peripheral nervous system in the

preservation of missing hand topography. In the below elbow amputee, some forearm muscles normally controlling hand movements are spared and therefore proprioceptive inputs relating to phantom hand movements likely persist (Nystrom & Hagbarth, 1981). In the above elbow amputee, these inputs would be absent, though ectopic firing from the injured nerve (Nystrom & Hagbarth, 1981) or intact dorsal root ganglia could preserve some afferent inputs (as previously shown following peripheral nerve injury (Nordin, Nystrom, Wallin, & Hagbarth, 1984), see also Vaso et al. (2014) for related findings). However, in the amputee suffering from brachial plexus avulsion injury, the dorsal root ganglia are damaged, meaning that no such peripheral input should be available. Given the observation of preserved topography in all three cases, it is highly probable that the preserved missing hand maps are not maintained by peripheral input, but rather are driven by processing in the central nervous system itself.

What neural signals may be triggering the brain activations sub-serving the missing hand maps? Given the relatively unimpaired motor system in amputees, it is possible that these representations are driven by motor (efferent) information. The motor system is thought to provide information about its descending commands to the sensory system, by means of efference copy. When efference signals reach the sensory areas, they evoke activity in those areas. The pattern of this corollary discharge could resemble that of the sensory feedback to be expected from the movement (London & Miller, 2013). While predictive signals are fundamental components for current theories of motor control (Franklin & Wolpert, 2011), surprisingly little empirical evidence exists to demonstrate efferent signals in the primates' S1 hand representation independently of afferent processing (London &

Miller, 2013). Our evidence for digit topography in S1 despite the physical absence of a hand suggests the involvement of non-afferent processing in S1. The persistence of efference signals from the motor system could contribute to the maintenance of preserved structure and function in SI despite afferent input loss.

Our findings are based on the unique phenomenology of phantom sensations, and as such all tested amputees reported experiencing exceptionally vivid phantom sensations, allowing them to voluntarily move each of their phantom fingers. An open question remains whether a relationship exists between the experience of phantom sensations and preserved missing hand topography. Our previous findings, showing that phantom hand movements activate the missing hand territory in individuals experiencing varying levels of phantom sensation vividness (Makin, Scholz, et al., 2013, 2015) might indicate that this is a general phenomenon. However, we note that these previous studies do not provide information on whether the topographic features underlying the phantom-evoked activity were preserved. Further research is needed to determine whether the preservation of missing hand topography depends on (or gives rise to) the experience of phantom sensations, or whether our finding reflects a fundamental organising principle of the brain that is independent of experience.

The notion of brain reorganisation has posed an unexpected obstacle to recent technological developments of human-technology fusion, i.e. neuroprosthetics. Neuroprosthetics allow patients with sensorimotor impairments (e.g. amputation, paralysis) to directly interface with a robotic limb using cortical signals of the hand. However, the relevant information necessary for intuitive neuroprosthesis control may not be attainable once input is lost and functional reorganisation occurs. By

demonstrating persistence of topography despite input loss, our finding could be exploited to develop intuitive fine-grained control of neuroprosthetics (Bensmaia & Miller, 2014) (e.g. requiring representation of individual digits) in disabled populations.

3 | Reaffirming the link between chronic phantom limb pain and maintained missing hand representation

Adapted from

Kikkert, S., Johansen-Berg, H., Tracey, I., Makin, T. R. Reaffirming the link between chronic phantom limb pain and maintained missing hand representation. (Under revisions).

Chapter abstract:

Phantom limb pain (PLP) is commonly considered to be a result of maladaptive brain plasticity. The highly influential maladaptive plasticity model proposes that PLP is caused by reorganisation in primary somatosensory cortex, characterised by functional degradation of the missing hand representation and remapping of other body part representations. In the current chapter, I replicated the previous results by Makin et al. (2013), showing that PLP is associated with maintained representation of the missing hand during phantom hand movements. I asked sixteen unilateral upper-limb amputees to move their phantom hand, lips or other body parts and measured the associated neural activity using functional magnetic resonance imaging (fMRI). I confirm that amputees suffering from worse chronic PLP have stronger activity in the primary sensorimotor missing hand area during phantom hand movements. I find no evidence of lip representation remapping into the missing hand territory, as assessed using lip movements. I further show that the correlation between chronic PLP and

maintained representation of the missing hand cannot be explained by the experience of chronic non-painful phantom sensations or compensatory usage of the residual arm or an artificial arm (prosthesis). These results reaffirm a likely relationship between persistent peripheral inputs pertaining to the missing hand representation and chronic PLP, and emphasise a need to further study the role of peripheral inputs from the residual nerves to better understand the mechanisms underlying chronic PLP.

3.1 Introduction

Following amputation, individuals often perceive painful sensations coming from their missing limb (Weeks et al., 2010). Phantom limb pain (PLP) is typically unresponsive to conventional analgesic therapies and poses a significant medical problem (Knotkova et al., 2012). The underlying cause of PLP remains poorly understood and extensively debated (Boström, de Lussanet, Weiss, Puta, & Wagner, 2014; Devor, Vaso, Adahan, & Vyshka, 2014; Flor, 2002; Flor, Diers, & Andoh, 2013; Flor et al., 2006; Foell, Andoh, et al., 2014; Jutzeler, Curt, et al., 2015; Raffin et al., 2016).

Although previous and recent work highlighted peripheral PLP contributors (Borghi et al., 2010; Vaso et al., 2014), an influential model attributes this neuropathic pain syndrome to ‘maladaptive plasticity’, characterised by reorganisation in primary sensorimotor cortex (Flor et al., 1995, 2006; Lotze et al., 2001). While the maladaptive plasticity model suggests that PLP associates with degradation of missing hand representation and reorganisation, we recently reported that amputees with worse chronic PLP showed stronger maintained phantom hand representation during phantom hand movements (Makin, Scholz, et al., 2013). Our approach was

based on empirical evidence demonstrating that phantom hand movements elicit central and peripheral motor signals different from those found during movement imagery (Raffin, Mattout, et al., 2012; Reilly et al., 2006). By asking amputees to perform phantom hand movements, we directly targeted otherwise latent phantom hand representation in the primary sensorimotor missing hand area (see Chapter 2). This is unlike previous studies using sensory lip stimulation, lip movements or imaginary phantom hand movements to determine reorganisation in the missing hand cortex (Flor et al., 1995; Foell, Bekrater-Bodmann, et al., 2014; Lotze et al., 2001; MacIver, Lloyd, Kelly, Roberts, & Nurmikko, 2008).

Here we used the same approach (Makin, Scholz, et al., 2013), involving phantom hand movements, to replicate and extend our earlier findings by addressing some previously raised criticisms (Flor et al., 2013).

3.2 Materials and methods

3.2.1 Participants

Sixteen unilateral upper-limb amputees (mean age±s.e.m.=44±3, four right-arm amputees, see Table 3.1 for details) and twenty-two two-handed age-matched controls (age=40±3, 7 left-hand dominant) were recruited through Opcare. Ten amputees participating in the current study also participated in our original study (Makin, Scholz, et al., 2013). Note, however, that novel data was acquired for all participants and that a 3-year gap existed between the testing for the previous and the current study. Ethical approval was granted by Oxford University's Medical Sciences committee (Ref: MSD-IDREC-C2-2014-003). Written informed consent was obtained from all participants prior to the study. To compare between groups, amputees'

phantom/intact hand was matched to controls' non-dominant/dominant hand, respectively (the proportion of right-arm amputees and left-handed controls was similar: 25% and 32% respectively; $X^2_{(1)}=0.21$, p=0.65).

	Age	Age at amp.	Amp. level	Side/ dominant	Chronic PLS	Chronic PLP	Chronic residual arm (stump) pain	Cause of amp.	Pros. usage
A1	32	31	2	L/R	100	50	0	Trauma	2
A2	45	20	4	R/L	50	10	40	Trauma	2
A3	25	18	5	L/R	100	30	18	Trauma	2
A4	29	24	1	L/R	40	18	0	Trauma	2
A5	64	33	4	R/R	75	0	0	Trauma	5
A6	49	37	2	L/R	20	27	0	Trauma	1
A7	50	45	2	L/L	90	70	17	Tumour	2
A8	24	18	4	R/L	100	45	35	Trauma	0
A9	58	27	2	L/R	35	45	15	Nerve inf.	5
A10	46	38	4	L/R	90	94	20	Trauma	0
A11	53	28	4	L/R	10	20	15	Trauma	5
A12	41	27	2	R/L	100	80	100	Trauma	2
A13	48	17	2	L/R	100	25	10	Trauma	2
A14	37	27	2	L/R	90	13	17	Trauma	2
A15	59	40	2	L/L	48	23	48	Trauma	0
A16	57	20	4	L/L	23	60	0	Trauma	5

Table 3.1: Amputee demographic and clinical details (Chapter 3). Amp. = amputation; Amp. levels: 1 = through shoulder, 2 = above elbow, 3 = through elbow, 4 = below elbow, 5 = wrist and below; Side = side of amputation; dominant = hand dominance prior to amputation (based on self-report); L = left; R = right; PLS = phantom limb sensation; PLP = phantom limb pain; inf. = infection; Pros. usage = prosthetics usage: 0 = never, 1 = rarely, 2 = occasionally, 3 = daily (less than 4 hours), 4 = daily (more than 4 hours), 5 = daily (over 8 hours).

3.2.2 Pain ratings

At the start of the first testing session, amputees rated the frequency of PLP, as experienced within the last year, as well as the intensity of worst PLP experienced during the last week (or in a typical week involving PLP). Chronic PLP was

calculated by dividing worst PLP intensity (scale 0 - 100: ranging from no pain to worst pain imaginable) by PLP frequency (1 - all the time, 2 - daily, 3 - weekly, 4 - several times per month, and 5 - once or less per month). This approach reflects the chronic aspect of the PLP as it combines both frequency and intensity (Makin, Scholz, et al., 2013, 2015). Similar measures were obtained for non-painful phantom sensation vividness and stump pain. A rating of transient PLP intensity (scale 0 – 100, as above) was obtained prior to the MRI scanning.

3.2.3 Scanning procedures

Participants were visually instructed to make intact hand (all fingers flexion and extension), phantom hand (as for the intact hand), residual arm (elbow movements), lips, feet (bilateral toes), and intact arm (as for the residual arm) movements in a block-design fashion. Each movement condition was repeated four times in a semi-counterbalanced protocol, alternating 12s of movement with 12s of rest. Movement pace was instructed at 0.5Hz. Participants were instructed to make actual rather than imagined phantom hand movements (Raffin, Mattout, et al., 2012; Reilly et al., 2006) and were trained on the required movements before the scan.

3.2.4 MRI data acquisition

Similar scanning parameters and analysis procedures were used as in Makin, Scholz, et al. (2013). MRI images were collected using a 3 tesla Siemens Verio MRI scanner, with a 32-channel head coil. A high-resolution T1-weighted sequence was used to acquire a structural image (TR: 2040ms, TE: 4.7ms, flip angle 8°, voxel size: 1mm isotropic resolution). Functional images based on the blood oxygenation level-dependent (BOLD) signal were obtained using a multiple gradient echo-planar T2*-

weighted pulse sequence. The following acquisition parameters were used: TR: 2000ms, TE: 30ms, flip angle: 90°, voxel size: 3mm isotropic, FOV = 192mm axial slices, volumes: 300. Forty-six slices were acquired in the oblique axial plane, covering the whole cortex, with partial coverage of the cerebellum. Additional dummy volumes were acquired before the start of the scan. Field maps were acquired for field unwarping.

3.2.5 MRI data preprocessing and analysis

All imaging data were processed using FSL version 5.0 (https://fsl.fmrib.ox.ac.uk/fsl/fslwiki; Jenkinson et al., 2012; Smith et al., 2004; Woolrich et al., 2009). Cortical surface reconstructions, used for visualisation of the fMRI results, were produced using Workbench (http://www.humanconnectome.org). To align the missing/non-dominant hand hemisphere, data of individuals with a missing/non-dominant right hand was flipped on the mid-sagittal plane prior to all analysis. This flipping procedure is commonly applied in neuroimaging analysis of populations with lateralised injuries (Bogdanov, Smith, & Frey, 2012; Diers, Christmann, Koeppe, Ruf, & Flor, 2010; Foell, Bekrater-Bodmann, et al., 2014; Lotze et al., 2001; MacIver et al., 2008; Raffin, Mattout, et al., 2012).

Common pre-processing steps for fMRI data were applied to each individual run, using FSL's Expert Analysis Tool FEAT (version 6.00): motion correction using FMRIB's Linear Image Registration Tool (MCFLIRT; Jenkinson et al., 2002), brain extraction using automated brain extraction tool BET (Smith, 2002), spatial smoothing using a 5mm FWHM (full width at half maximum) Gaussian kernel, and high pass temporal filtering with a cut-off of 150s.

Functional data were aligned to structural images initially using linear registration (FMRIB's Linear Image Registration Tool, FLIRT; Jenkinson et al., 2002; Jenkinson & Smith, 2001) and optimised using boundary based registration (Greve & Fischl, 2009). Structural images were transformed to MNI standard space using nonlinear registration tool FNIRT, and the resulting warp fields were applied to the functional statistical images.

First-level parameter estimates were computed using a voxel-based general linear model (GLM) based on the double-gamma HRF function and its temporal derivatives. Time series statistical analysis was carried out using FILM (FMRIB's Improved Linear Model) with local autocorrelation correction. Contrasts were defined for phantom/non-dominant hand movements versus rest, residual arm movements versus rest, and lips movements versus rest. To construct the regions of interest (ROIs) a further contrast was defined between phantom/non-dominant hand and feet movements. Estimated head motion parameters (as estimated by MCFLIRT) were added to the model to remove residual motion effects.

Group-level analysis was performed using FMRIB's Local Analysis of Mixed Effects (Woolrich, Behrens, Beckmann, Jenkinson, & Smith, 2004). Whole-brain group differences were tested for phantom/non-dominant hand movements versus rest. Z-statistic images were thresholded using clusters determined by $Z > 3.1$ and $p < 0.05$ family-wise-error-corrected cluster significance thresholding was applied.

Hand ROIs were created based on the non-thresholded top 400 voxels activated during phantom/non-dominant hand versus feet movements in group-level analyses, surrounding the contralateral hand knob. Two ROIs were constructed and explored: ROI_1: based on averaged phantom/non-dominant hand movements across the amputee and control groups (as the original study (Makin, Scholz, et al., 2013), and ROI_2: based on amputees' phantom hand movements. Averaged percent signal change was extracted from each participant's first-level analyses for the phantom/non-dominant hand movements versus rest contrast in each hand ROI. Note that similar results were observed when using a phantom/non-dominant versus feet movements contrast (as used in our original study; Makin, Scholz, et al., 2013). Group differences were calculated using ROI_1 and correlations were investigated using both ROIs.

3.2.6 Statistical analysis

Statistical analysis was performed using SPSS (version 21) and Matlab (version 9.1). Data were inspected for normality violations using the Shapiro-Wilk test, and non-parametric tests were utilised when needed. Standard approaches were used for statistical analysis, as mentioned in the results.

3.3 Results

3.3.1 Phantom hand movements activity in amputees compared to controls

We first examined which areas amputees recruited during phantom hand movement, compared to controls. Amputees showed increased recruitment of bilateral insula (see Figure 3.1 and Table 3.2), but not of primary sensorimotor cortex. This observation

was confirmed using ROI analysis, showing no significant group differences in primary sensorimotor missing hand cortex activity during phantom/non-dominant hand movements (Figure 3.2A&B; ROI_1: $t_{(36)}$=-0.20, p=0.84). Similar hyperactivity during phantom hand movements were found using data obtained from a different subset of amputees (i.e. for Chapters 4 and 5; see Appendices: Supplementary Materials Chapter 4 – Figure A.4.4 for similar results in this different subset of amputees).

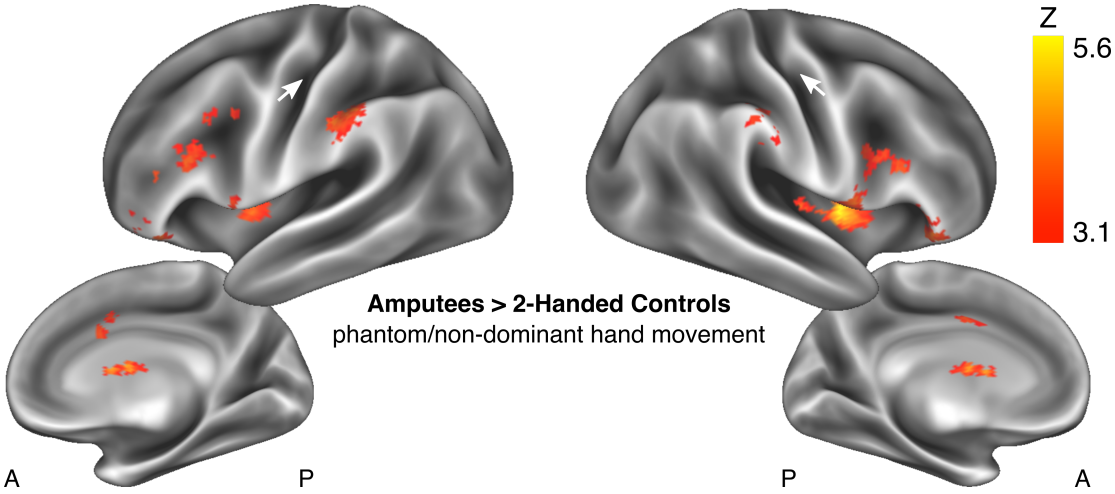


Figure 3.1: Hyperactivity during phantom hand movement in amputees. Amputees show increased excitability in bilateral insula, thalamus, middle frontal gyrus, anterior supramarginal gyrus, caudate, and anterior cingulate cortex during phantom hand movements, compared to two-handed controls (see Table 3.2 for a detailed overview of peak activations). A = anterior; P = posterior. White arrows indicate the central sulcus.

	Hemisphere	Z-value	x	y	z
Insular cortex	Phantom	5.6	23	65	35
	Intact	4.4	65	64	40
Thalamus	Phantom	4.9	41	63	39
	Intact	4.0	49	62	40
Caudate	Phantom	4.9	41	63	39
	Intact	4.0	49	62	40
Anterior cingulate cortex	Phantom	3.9	44	72	52
	Intact	3.7	46	62	56
Middle frontal gyrus	Phantom	4.2	28	83	40
	Intact	4.3	64	80	42
Supramarginal gyrus (anterior)	Phantom	5.3	15	47	56
	Intact	4.6	73	45	57

Table 3.2: Functional location peak activations parameters for whole brain contrasts between amputees and controls. Phantom hemisphere refers to the hemisphere contralateral to the phantom/non-dominant hand. Intact hemisphere refers to the hemisphere contralateral to the intact/dominant hand.

3.3.2 Maintained activity in S1's missing hand area associates with chronic phantom limb pain

Next we repeated our previous study's main analysis (Makin, Scholz, et al., 2013), demonstrating a positive association between chronic PLP and maintained phantom hand movement activity in the primary sensorimotor missing hand cortex. The missing hand cortex ROI was based on conjunct phantom/non-dominant hand activity in amputees and controls (ROI_1). As before, amputees with worse chronic PLP showed greater activity during phantom hand movements (ROI_1: $r=0.71$, $p=0.002$; Figure 3.2B). This relationship was not driven by experience of non-painful phantom sensations, as shown using a partial correlation including non-painful chronic phantom sensations as a nuisance regressor (ROI_1: $r_s=0.66$, $p=0.008$).

It has been suggested that our original analysis mis-estimated the "true" phantom hand area, as our ROI was based on conjunct phantom/non-dominant hand movement activity in amputees and controls (Flor et al., 2013). We therefore constructed an

additional ROI based on phantom hand movement in the amputee group only (ROI_2). Using this ROI, we again found a correlation between chronic PLP and phantom hand activity in the missing hand area (ROI_2: r=0.71, p=0.002), regardless of non-painful phantom sensations (ROI_2: r_s=0.59, p=0.02). These results demonstrate the robustness of our findings.

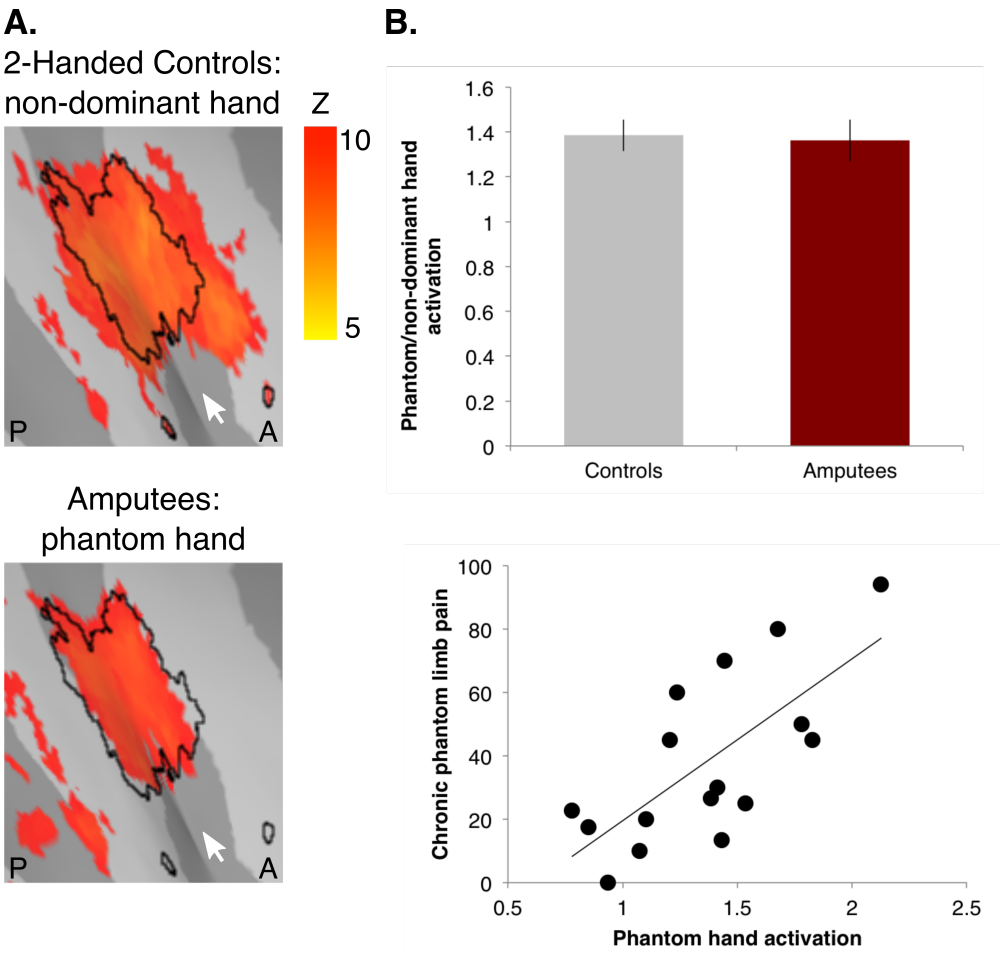


Figure 3.2: Chronic phantom limb pain relates to maintained cortical phantom hand representation. (A) Activity for controls (top) and amputees (bottom) in the primary sensorimotor hand cortex during non-dominant/phantom hand movements. Black outlines define the boundaries of the 'missing hand ROI_1'. (B). Activity in the primary sensorimotor missing hand cortex during phantom hand movements did not differ from activity during non-dominant hand movements of two-handed controls (top; ROI_1: t(36) = -0.20, p = 0.84). Amputees suffering worse chronic phantom limb pain activated the primary sensorimotor missing hand cortex more strongly during phantom hand movement (bottom; ROI_1: r = 0.71, p = 0.002).

3.3.3 Chronic PLP did not associate with lip or residual arm movement activity

It was also suggested that activity in the primary sensorimotor missing hand cortex could be facilitated by residual arm representation (Flor et al., 2013), which was recently associated with PLP (Raffin et al., 2016). However, amputees did not show more activity in the primary sensorimotor missing hand cortex during residual arm movements compared to controls (ROI_1: $t_{(36)}$=0.73, p=0.47; U=64, p=0.51 when only including below elbow amputees; see also (Makin, Cramer, et al., 2013)). No relationship existed between chronic PLP and residual arm activity (ROI_1: r=0.17, p=0.535, ROI_2: r=0.21, p=0.43). Furthermore, the observed correlation between chronic PLP and strength of phantom hand representation was independent of residual arm/prosthesis usage (partial correlation, regressing out residual arm/prosthesis usage; ROI_1: r=0.72, p=0.003, ROI_2: r=0.72, p=0.003; as measured using questionnaires described and validated in Hahamy et al., 2017; Makin, Cramer, et al., 2013; van den Heiligenberg, Yeung, Brugger, Culham, & Makin, 2017). Together, these results show that the relationship between chronic PLP and phantom hand activity is not related to the residual arm representation.

Finally, we revisited the potential relationship between chronic PLP and lip representation remapping into the primary sensorimotor missing hand cortex, as such remapping has been considered an indicator of maladaptive plasticity (Flor et al., 1995). As reported previously (Makin, Scholz, et al., 2013, 2015), we could not find significant group activity differences in the missing hand cortex ROI during lip movements (ROI_1: U=160, p=0.65). Furthermore, no significant correlation was found between chronic PLP and missing hand cortex activity during lip movements

(ROI_1: r=-0.004, p=0.987, ROI_2: r=-0.03, p=0.925). We found a significant difference between phantom hand and lip activity correlations with chronic PLP (ROI_1: Z=2.27, p=0.023, ROI_2: Z=2.34, p=0.019), demonstrating that in the current dataset, the persistent representation model was statistically better supported than the maladaptive plasticity model.

3.4 Discussion

Here we report again that chronic PLP associates with stronger maintained activity in the primary sensorimotor missing hand cortex during phantom hand movements. This was observed regardless of ROI selection, and was not confounded by the experience of chronic non-painful phantom sensations or residual arm representation.

Maladaptive reorganisation is still widely assumed to play a key role in PLP, as well as a range of other chronic pain conditions, with important implications for designing clinical treatments. While some treatments based on the maladaptive plasticity model have shown effective in relieving PLP (Chan et al., 2007; Ortiz-Catalan et al., 2016), placebo controls are often missing and the underlying mechanisms for such PLP relief are actively discussed (Jutzeler, Curt, et al., 2015; Mezue & Makin, 2016; Thieme et al., 2016). A key assumption of the maladaptive plasticity model is that cortical reorganisation is triggered by input loss (e.g. through arm amputation), thereby promoting remapping of adjacent representations (e.g. lips) into the deprived cortex, leading to a mismatch of body-part inputs. However, despite arm amputation, detailed preserved missing hand representation can be observed in primary sensorimotor cortex when amputees make phantom hand movements (see Chapter 2; Makin, Scholz, et al., 2013; Makin & Bensmaia, 2017; Mercier, Reilly, Vargas, Aballea, &

Sirigu, 2006; Raffin, Mattout, et al., 2012). Furthermore, displaced signals in primary somatosensory cortex (e.g. evoked by brain stimulation) do not trigger pain sensations (Flesher et al., 2016; Mazzola, Isnard, Peyron, & Mauguire, 2012). Lastly, while local lip representation shifts occur following arm amputation, these do not invade the primary sensorimotor missing hand area (Makin, Scholz, et al., 2015; Raffin et al., 2016).

It is important to note that in both our original and this replication study we used an active motor task to probe missing hand representation, whereas previous studies used an indirect and passive tactile face stimulation to demonstrate maladaptive reorganisation. It is conceptually possible that persistent representation will spatially coincide with reorganisation (see Chapter 2). However, in previous studies using active lip movements (Makin, Scholz, et al., 2013, 2015), and also here, we could not identify lip overrepresentation in the missing hand territory nor a relationship between displaced body-parts representation and chronic PLP. Furthermore, when comparing the correlation coefficients of chronic PLP with hand and lip movement activity in the missing hand area, we observed that phantom hand activity was a better predictor of chronic PLP variability in the current dataset. This suggests that persistent missing hand representation is a more appropriate neural correlate of chronic PLP. Indeed, evidence is growing to support a persistent representation model of chronic PLP (Blume et al., 2014; Borghi et al., 2010; Vaso et al., 2014; Yanagisawa et al., 2016), emphasising a need to investigate the role of maintained inputs (and/or organisation).

As proposed in early theories (Nystrom & Hagbarth, 1981) and emphasized again recently (Vaso et al., 2014), spontaneous activity from residual damaged nerves can

prevail after amputation and, as such, carry information relating to the missing hand into the brain. This likely input seems to powerfully contribute to maintained representation, that becomes unmasked during phantom hand movement. If this is correct, then amputees with worse chronic PLP (more residual peripheral inputs) will tend to show stronger activity in the primary sensorimotor missing hand cortex during phantom hand movements, as observed in the previous (Makin, Scholz, et al., 2013) and current studies. We tentatively suggest that sensorimotor cortex activity may not causally drive PLP, but instead could be a secondary consequence of peripheral disturbances. Further work is needed to better dissect the contributory factors.

4 | Non-invasive brain stimulation reduces phantom limb pain: an fMRI study

Adapted from

Kikkert, S., Mezue, M. O'Shea, J., Henderson-Slater, D., Beckmann, C. F., Johansen-Berg, H., Tracey, I., Makin, T. R. (In preparation). Non-invasive brain stimulation reduces phantom limb pain in amputees: an fMRI study.

Chapter abstract:

Chronic neuropathic pain is a common consequence of nerve injury. Phantom limb pain (PLP) following amputation is difficult to treat, in part due to a poor understanding of pain related disease mechanisms. Here, we used task-concurrent non-invasive brain stimulation, via anodal transcranial direct current stimulation over the primary sensorimotor missing hand cortex, as a means to alleviate PLP. Using a double-blind sham-controlled design, we show that a single intervention session caused significant PLP relief, with effects lasting up to 1 week. Neuroimaging showed that PLP relief was associated with a reduction of activity in the primary sensorimotor missing hand cortex after stimulation. This is consistent with previous evidence linking PLP with hyperactivity in that region. Critically, brain activity during stimulation in S2 and the mid- and posterior insula predicted both this subsequent reduction in primary sensorimotor missing hand cortex activity and PLP relief. These findings describe a novel intervention for PLP using non-invasive brain stimulation.

4.1 Introduction

Following peripheral nerve injury, neuropathic pain commonly arises. This highly debilitating condition is typically unresponsive to conventional analgesic treatments and, as such, poses a significant medical problem (Finnerup, Sindrup, & Jensen, 2010). Recent and past studies confirm that an improved understanding of the neural circuits underlying neuropathic pain can facilitate targeted, and therefore more effective, treatments for this condition (Colloca et al., 2017; von Hehn, Baron, & Woolf, 2012). Phantom limb pain (PLP) following amputation is an archetypal example of an intractable neuropathic pain syndrome. In recent years, several innovative PLP treatments have been designed based on putative PLP disease mechanisms. These treatments have provided an example for the development of non-conventional therapies against other neuropathic pain conditions (e.g. through the use of invasive brain stimulation, mirror therapy, virtual reality, graded motor imagery, real-time feedback etc.; Beaumont, Mercier, Michon, Malouin, & Jackson, 2011; Lefaucheur et al., 2017; Moseley, 2006)). Despite this effort into advancing novel therapies and some limited evidence of efficacy, there remains no consensus on the management of PLP. Furthermore, both the methodological quality and strength of previous evidence is highly variable, with several studies omitting the use of blinding, control of the placebo effect, and validation against control interventions. A major challenge in developing targeted treatments for PLP stems from an incomplete understanding of its neural basis.

Decades of research has identified neural networks believed to mediate chronic and neuropathic pain, incorporating the role of both subcortical and cortical structures (Apkarian, Bushnell, & P, 2013; Baron, 2006; Woolf, 2011). The mechanisms of PLP

have traditionally been thought to be distinct from other neuropathic conditions. However, while the missing limb most probably adds a unique nuance to PLP, there are likely overlapping sets of generating, exacerbating and maintaining mechanisms between PLP and other chronic pain conditions. Still, for the past decades there has been an exclusive focus on PLP being consequential to cortical plasticity in primary somatosensory cortex (Flor et al., 1995; Flor, Nikolajsen, & Staehelin Jensen, 2006). In particular, PLP has frequently been linked with cortical maladaptive reorganisation, stating that following arm amputation the "freed-up" missing hand representation becomes degraded and is invaded by the neighbouring facial representation. However, recent evidence of increased phantom hand movement activity in the primary sensorimotor missing hand cortex in amputees with worse chronic PLP (Makin, Scholz, et al., 2013; see also Chapter 3), has led us to propose an additional mechanism involved in PLP – notably that of 'maintained phantom hand representation'. This asserts that maintained phantom hand movement activity in the primary sensorimotor missing hand cortex may be aberrant, and links PLP to broad scale functional reorganisation at a network level. This newly identified mechanism offers a new potential target for PLP treatment as it may be possible to target persistent activity and modulate PLP by altering cortical plasticity.

Non-invasive brain stimulation has been used to modulate plasticity in a range of neuropathological diseases including chronic intractable pain (Lefaucheur et al., 2017). While brain stimulation has been previously applied to alleviate neuropathic pain (including PLP; Ahmed, Mohamed, & Sayed, 2011; Bolognini et al., 2015; Bolognini, Olgiati, Maravita, Ferraro, & Fregni, 2013; Lefaucheur et al., 2008), it remains unclear how brain stimulation contributes to pain relief. In particular,

transcranial direct current stimulation (tDCS) is known to cause widespread cortical and subcortical effects, which go well beyond the target stimulation area (Parazzini, Fiocchi, Rossi, Paglialonga, & Ravazzani, 2011; Stagg et al., 2013). While this spatial profile of current distribution opens up multiple potential pathways to impact aberrant neural circuits, it also presents a challenge for targeted treatment. It is well recognised that the effects of non-invasive brain stimulation are cognitive state dependent: for example, combining stimulation with a meaningful task can enhance or prolong the effects of tDCS (Brasil-Neto, 2012; Cohen Kadosh, Soskic, Iuculano, Kanai, & Walsh, 2010; Reis et al., 2009; Silvanto, Muggleton, & Walsh, 2008). This likely reflects spatial variations in the functional networks that are active during stimulation, offering a potential avenue for targeting stimulation to a specific network.

In the present study we assessed the efficacy of a single session of task-concurrent tDCS in alleviating PLP in a within subjects, double-blind, and sham-controlled design. As we aimed to influence the information processing of the peripheral missing hand signals that have previously been associated with PLP (Makin, Scholz, et al., 2013; see also Chapter 3), we instructed arm amputees to make phantom hand movements while undergoing tDCS. Our intervention stimulation consisted of applying excitatory tDCS over the primary sensorimotor missing hand cortex, as previously implemented for related neuropathic conditions (Bolognini et al., 2015; Lefaucheur, 2016). Neuroimaging was used during and after tDCS to evaluate the neural mechanisms underpinning PLP relief.

4.2 Materials and methods

4.2.1 Participants

Seventeen unilateral upper-limb amputees who experienced PLP episodes more than once a week in the month preceding recruitment (mean age ± s.e.m. = 47 ± 3, 6 right-arm amputees, 4 females; see Table 4.1 for demographic and clinical details) and fifteen age-matched controls (two-handers, age = 46 ± 3, 7 with a dominant left hand, 4 females) were recruited through the Oxford Centre for Enablement and Opcare. Exclusion criteria were: 1) contraindications for MRI and tDCS (Rossi et al., 2009); 2) the usage of drugs that affect the concentrations of the inhibitory neurotransmitter gamma-Aminobutyric acid (GABA; e.g. pregabalin); 3) active enrolment in other brain stimulation experiments. Ethical approval was granted by the NHS National Research Ethics service (Ref: 10/H0707/29) and written informed consent was obtained from all participants prior to the study. One amputee was excluded from the study due to safety considerations. A second amputee was excluded from the study due to an inability to perform the movement task in the MRI scanner.

	Age	Age at amp.	Amp. Level	Side/ dominant	Chronic PLS	Chronic PLP	Chronic residual arm pain	Cause of Amp.	Pros. Usage
A01	43	26	2	R/R	90	70	0	Trauma	5
A02	68	53	2	R/R	25	42.5	0	Trauma	5
A03	36	31	2	R/L	20	40	80	Trauma	0
A04	54	54	2	L/R	90	10	20	Vascular D	3
A05	28	24	1	L/R	15	26.7	5	Trauma	3
A06	52	28	4	L/R	80	35	10	Trauma	5
A07	49	45	2	L/L	80	70	10	Tumour	3
A08	47	17	2	L/R	100	15	3.3	Trauma	2
A09	48	27	2	R/R	100	45	0	Trauma	0
A10	23	18	4	R/R	90	25	0	Trauma	0
A11	49	19	2	L/R	70	50	0	Trauma	5
A12	60	31	2	L/R	70	12.5	0	Trauma	0
A13	56	20	5	L/L	70	70	0	Trauma	5
A14	40	27	2	R/L	100	80	26.7	Trauma	2
A15	45	38	4	L/R	89	92	17.5	Trauma	2

Table 4.1: Amputee demographic and clinical details (Chapters 4 and 5). Amp. = amputation; Amp. levels: 1 = shoulder, 2 = above elbow, 3 = through elbow, 4 = below elbow, 5 = wrist and below; Side = side of amputation; dominant = hand dominance prior to amputation (based on self-report); L = left; R = right; PLS = phantom limb sensation; PLP = phantom limb pain; Vascular D = Vascular disease; Pros. Usage = prosthetics usage: 0 = never, 1 = rarely, 2 = occasionally, 3 = daily (less than 4 hours), 4 = daily (more than 4 hours), 5 = daily (over 8 hours).

4.2.2 Experimental design

Testing was done as part of a larger study (please refer to https://osf.io/4a5zg/ for full methods). Amputees participated in four consecutive experimental sessions that were at least one week apart, to minimise carry-over effects. In these experimental sessions, we examined the effects of non-invasive brain stimulation on PLP (see Figure 4.1A for a timeline of the behavioural assessments). Besides the main intervention and sham conditions, two further active stimulation conditions were included in the current study as active controls.

One amputee completed only three testing sessions (i.e. data for this participant is missing for the control site stimulation condition). Control participants visited the lab once to enable baseline comparisons with the amputees (i.e. controls did not undergo any tDCS). To compare between the amputees and controls, the phantom hand was matched to the non-dominant hand of controls, and the intact hand was matched to the dominant hand of controls.

4.2.3 Transcranial direct current stimulation

We tested the effect of anodal tDCS to the primary sensorimotor missing hand cortex (hereafter intervention condition) in a double-blind, within subjects, counterbalanced, and sham controlled design.

A DC-Stimulator (Magstim) was used to deliver electric current to the brain via two 5x7cm electrodes (Easycap), fitted with 5kΩ resistors for safe use in the MRI environment. High-chloride electrolyte EEG gel was used as a conducting medium between the scalp and electrodes. Electrode position was determined according to the EEG 10-20 system. For anodal stimulation centred over primary sensorimotor missing hand cortex, the anodal electrode was positioned 5cm lateral to Cz (corresponding to C3/C4), with the cathode electrode placed over the contralateral supraorbital area. This is the standard set up for tDCS over primary sensorimotor cortex (Nitsche & Paulus, 2000). tDCS stimulation lasted 20min (fade-in/fade-out phases = 10s), with an intensity of 1mA. Similar electrode arrangement and stimulation parameters were used for sham tDCS. In the sham condition, the electrodes were positioned over the primary sensorimotor intact hand area and the contralateral supraorbital area, but the

stimulator was turned off after the impedance was stabilised (after approximately 30s).

Besides the main intervention and sham conditions, we included two further active tDCS control conditions in this study. The first condition was designed to control for stimulation site (hereafter control site condition) and the second condition was included to assess the effect of cathodal tDCS over the primary sensorimotor missing hand cortex (hereafter cathodal condition). In the control site condition, anodal tDCS was applied over the primary sensorimotor intact hand cortex. The anodal electrode was positioned 5cm lateral to Cz (corresponding to C3/C4), with the cathode electrode placed over the contralateral supraorbital area. To examine the effect of cathodal tDCS over the primary sensorimotor missing hand cortex, the cathodal electrode was positioned 5cm lateral to Cz (corresponding to C3/C4), with the anode placed over the contralateral supraorbital area.

4.2.4 Pain ratings

At the start of the first experimental session, amputees rated the frequencies of PLP as experienced within the last year, as well as the intensity of worst PLP experienced during the last week (or in a typical week involving PLP). Chronic PLP was calculated by dividing worst PLP intensity (scale 0-100: ranging from no pain to worst pain imaginable) by PLP frequency (1 - all the time, 2 - daily, 3 - weekly, 4 - several times per month, and 5 - once or less per month). This approach reflects the chronic aspect of the PLP as it combines both frequency and intensity (Makin, Filippini, et al., 2015; Makin, Scholz, et al., 2013, 2015). Similar measures were obtained for residual limb (stump) pain and non-painful phantom sensation vividness.

Ratings of transient PLP intensity (scale 0-100, as above) were obtained using short pain questionnaires (SPQs), administered at four time points in each experimental session to investigate stimulation effects (see Figure 4.1A). To assess PLP at the start and end of an experimental session, i.e. outside the MRI scanner ('offline'), participants completed the SPQ in writing. Inside the scanner ('online'), a blinded experimenter verbally asked the participant the SPQ questions.

To assess potential lasting tDCS effects, participants were further sent automated text messages asking for an average PLP intensity rating. These texts were sent daily, starting 1 week before the first experimental session, and ending 1 week after the last experimental session. Participants were instructed to respond to these text messages as soon as possible. If a participant did not respond for more than 3 days in the week after an experimental session, this participant's daily pain ratings data for that condition was discarded. PLP ratings in the week before the start of the relevant experimental session were used as a baseline for the construction of the timeline in Figure 4.1C.

In the current study, we aimed to examine stimulation induced changes in PLP at different time points. Baseline PLP ratings were subtracted from post stimulation PLP ratings. No differences were found in baseline PLP levels across stimulation conditions (online: $\chi^2(3) = 5.81, p = 0.12$, offline: $\chi^2(3) = 3.13, p = 0.37$). We contrasted the online PLP measures to assess stimulation effects immediately after stimulation offset (i.e. PLP ~0min post stimulation offset *minus* PLP ~20min prior to stimulation onset). Similarly, the offline pre- and post- stimulation PLP levels were

contrasted to obtain a measure of stimulation effects at end of the experimental session (i.e. PLP ~90min post stimulation offset *minus* PLP ~90min prior to stimulation onset). Lastly, to examine any stimulation induced PLP effects lasting one week post stimulation, two separate approaches were taken. Firstly, we contrasted PLP measured a week post stimulation (the first baseline PLP rating obtained in the next experimental session) with the offline pre-stimulation PLP rating (i.e. PLP > 6 days post stimulation offset *minus* PLP ~90min prior to stimulation onset). Secondly, we used the obtained daily text messages data as a measure of PLP effects lasting one week post stimulation. This daily pain ratings data was treated as an absolute measure and no difference scores were created for this data.

A linear regression analysis was conducted on the resulting scores to remove the influence of chronic PLP from the PLP ratings. This ensured that the intervention effects were not masked by the high variability in chronic PLP between participants and better characterised fluctuations in PLP. We conducted all statistical analysis (both stimulation induced effects on PLP and correlations with MRI measures) using the residuals of the regression analysis, i.e. after the influence of chronic PLP was removed from the PLP ratings.

Effect sizes were calculated for the intervention and the main control, i.e. sham, conditions only, using the raw PLP ratings (i.e. before regressing out chronic PLP). A percentage change was calculated between the average baseline score and the average post-stimulation score as follows:

*(post stimulation PLP - pre stimulation PLP) / pre stimulation PLP * 100*

The resulting effect sizes are reported in Table 4.2. This table presents the PLP effects sizes in percentages for the sham and intervention conditions separately, as well as a further estimated PLP relief effect size for the intervention condition considering the PLP effect in the sham condition. Indeed, the intervention condition could both relieve PLP (with regards to baseline) and prevent the PLP effect in the sham condition. As such, we created a measured that took into consideration both of these effects, by adding the effect size of the sham condition to the effect size of the intervention condition.

4.2.5 Scanning procedures

Prior to each experimental scanning session, we informed participants regarding the general procedure of the study. The experimenter explained the tasks to be performed inside the scanner and patients were given extensive training on the expected movements. Participants were clearly instructed to make actual instead of imagined phantom movements and received sufficient time to practice the movements outside the scanner. Importantly, phantom hand movements are distinguishable from imagined movements, as is supported by empirical evidence demonstrating that phantom limb movements elicit both central and peripheral motor signals, that are different from those found during movement imagery (Makin et al., 2013; Raffin, Mattout, Reilly, & Giraux, 2012; Reilly, Mercier, Schieber, & Sirigu, 2006; see also Chapter 5). If it was impossible to perform full movements with the phantom hand, we asked the amputees to attempt to perform the movements as instructed. Amputees were encouraged to move at a comfortable pace. To confirm that appropriate movements were made at the instructed times, we monitored task performance

visually both on- and offline using video recordings. Instructions were delivered visually using Presentation software (version 16.4), via a mirror mounted on the head coil. Head motion was minimized using padded cushions.

Body localiser

A body localiser scan was obtained post stimulation in each experimental session and at baseline in the first experimental session. Participants were visually instructed to make simple movements with their intact hand (all fingers flexion/extension), phantom hand (as the intact hand), feet (bilateral toes), and lips in a block-design fashion. Each movement condition was repeated four times in a counterbalanced protocol, alternating 12s of movement with 12s of rest. The movement pace was instructed at 0.5Hz.

Stimulation scan

During stimulation participants were visually instructed to perform phantom wrist flexing, all phantom fingers flexion/extension, phantom index finger flexing/extension, phantom ring finger flexing/extension, and phantom fingers adduction movements in a block design fashion. Each 45s movement condition was alternated with 15s of rest and each movement condition was presented once in a run. The first and third runs involved phantom hand movements only. In the second and fourth runs participants used their intact hand to mirror the precise degree and speed of movement of the phantom hand. Participants were instructed to make as many movements as possible in each 45s block, at a comfortable pace, whilst taking little breaks when needed. Movements made during stimulation were recorded on video

and inspected offline by a blinded experimenter for a subset of 11 amputees. Importantly, the movements made during stimulation were not different between the stimulation conditions (see the Appendices: Supplementary Materials Chapter 4 for details). This suggests that any differences observed between conditions (both in PLP ratings and neural activity) were not due to a difference in task performance.

4.2.6 MRI data acquisition

MRI images were collected by means of a 3 tesla Verio MRI scanner (Siemens, Erlangen, Germany), using a 32-channel head coil. A high-resolution T1-weighted sequence was used to acquire structural images (TR: 2040ms, TE: 4.7ms, flip angle 8°, voxel size: 1mm isotropic resolution). Functional images were acquired based on the Blood Oxygenation Level Dependent (BOLD) signal.

Body localiser scan

Functional images for the body localiser scans were obtained using a multiband T2*-weighted pulse sequence with an acceleration factor of 6 (Moeller et al., 2010; Xu et al., 2013). The following acquisition parameters were used: TR: 1300ms, TE: 40ms, spatial resolution: 2mm isotropic, flip angle: 66°, 72 transversal slices, 314 acquired volumes. A high-saturation first volume of each acquired multiband run was collected for registration purposes. Fieldmaps were acquired for field unwarping.

Stimulation scan

During stimulation, an echo-planar T2*-weighted pulse sequence was used to record images with 3mm isotropic resolution. The following acquisition parameters were

used: TR: 2000ms; TE: 30ms; flip angle: 90°; 192 transversal slices, 608 acquired volumes. Fieldmaps were acquired for field unwarping.

4.2.7 MRI preprocessing and image registration

All imaging data were processed using FSL version 5.0 (https://fsl.fmrib.ox.ac.uk/fsl/fslwiki; Jenkinson, Beckmann, Behrens, Woolrich, & Smith, 2012; Smith et al., 2004; Woolrich et al., 2009). Data collected for individuals with an amputated (or non-dominant for controls) right hand was flipped on the mid-sagittal plane before all analyses, such that the hemisphere corresponding to the phantom hand was consistently aligned (Bogdanov et al., 2012; Diers et al., 2010; Foell, Bekrater-Bodmann, et al., 2014; Lotze et al., 2001; MacIver et al., 2008; Raffin, Mattout, et al., 2012). This procedure is regularly exercised in functional connectivity studies involving lateralised populations (Douaud, Filippini, Knight, Talbot, & Turner, 2011; Park et al., 2011). To further investigate neural activity in brain regions that do not have strong lateralisation, the non-flipped data was also analysed.

Body localiser scan

Common pre-processing steps were applied to each individual scan, using FSL's Expert Analysis Tool FEAT (version 6.00): motion correction using FMRIB's Linear Image Registration Tool (MCFLIRT; Jenkinson et al., 2002), brain extraction using automated brain extraction tool BET (Smith, 2002), spatial smoothing using a 3mm FWHM (full width at half maximum) Gaussian kernel, and high pass temporal filtering with a cut-off of 100s.

A high saturation first volume of each acquired multiband scan was used as an alternative reference image to enhance registration. Functional images were first registered to the example functional image acquired in the first imaging session (7 degrees of freedom). This example functional image was then aligned to the structural image acquired in the first imaging session, initially using linear registration (FMRIB's Linear Image Registration Tool, FLIRT; Jenkinson et al., 2002; Jenkinson & Smith, 2001) and optimised using boundary based registration (Greve & Fischl, 2009). Structural images were transformed to MNI standard space using nonlinear registration tool FNIRT, and the resulting warp fields were applied to the functional statistical images.

Stimulation scan

Similar pre-processing as above was applied for the functional scans obtained during stimulation, with the following exceptions: spatial smoothing using a 5mm FWHM Gaussian kernel, and high pass temporal filtering with a cut-off of 150s.

Functional data were aligned to structural images initially using linear registration (FLIRT; Jenkinson et al., 2002; Jenkinson & Smith, 2001) and optimised using boundary based registration (Greve & Fischl, 2009). Structural images were transformed to MNI standard space using nonlinear registration tool FNIRT, and the resulting warp fields were applied to the functional statistical images.

4.2.8 MRI analysis

Time series statistical analysis was carried out using FILM (FMRIB's Improved Linear Model) with local autocorrelation correction. First-level (time-series)

parameter estimates were computed using a voxel-based general linear model (GLM) based on the double-gamma HRF function and its temporal derivatives, as implemented in FEAT. All fMRI data was assessed for excessive motion using motion estimate outputs from MCFLIRT: volumes with estimated absolute mean displacement greater than half of the functional voxel size were scrubbed (body localizer scans: scrubbing applied in 40% of scans, maximum percentage of volumes scrubbed in a given session: 2%; stimulation scans: scrubbing applied in 33% of scans, maximum percentage of volumes scrubbed in a given session: 2%).

Group-level analysis was performed using FMRIB's Local Analysis of Mixed Effects (FLAME; Woolrich, Behrens, Beckmann, Jenkinson, & Smith, 2004). Z-statistic images were thresholded using clusters determined by $Z > 2.3$ and a family-wise-error-corrected cluster significance thresholding of $P < 0.05$ was applied to the suprathreshold clusters.

For presentation purposes, statistical parametric activity maps were projected on the inflated surface using Connectome Workbench (http://www.humanconnectome.org).

Body localiser

The main contrast for the body localiser scans was defined as phantom (or non-dominant) hand versus feet movements. Whole brain baseline differences between the amputee and control groups were assessed using amputees' first acquired baseline body localiser scan (see the Appendices: Supplementary Materials Chapter 4 for details and Figure A.4.4 for results).

To assess the neural correlates of stimulation-induced PLP relief, we carried out a whole brain regression analysis for the intervention condition, using PLP relief observed at the end of the experimental session (i.e. ~90min post stimulation) as a regressor. To examine the primary sensorimotor missing hand cortex in further detail, we conducted a region of interest (ROI) analysis. The missing hand ROI was defined as follows: A mask was drawn around the anatomical hand knob, extending the pre- and postcentral gyrus and the central sulcus. Within this mask, the top 400 voxels of the controls' average spatial map for non-dominant hand versus feet movements were combined to form the missing hand ROI. Averaged percent signal change was extracted from all voxels underlying the missing hand ROI for each amputee's first-level phantom hand versus feet movement contrast in both the sham and intervention conditions.

Stimulation scan

Cerebral spinal fluid and white matter scan-wise time series were extracted and added to the model as nuisance regressors. The main contrast was defined as phantom hand (only) movements versus rest.

To link the PLP-related sensorimotor cortex activity post stimulation to neural processes occurring during stimulation, we extracted each participant's averaged activity level underneath the cluster depicted in Figure 4.2A and used this as a regressor in a whole brain regression analysis (see Figure 4.3A for a graphical illustration of this analysis). This analysis was carried out on the flipped brains to investigate brain regions with strong lateralisation (see Figure 4.3), as well as on the un-flipped brains to investigate activity in regions that do not adhere to strong

lateralisation principles (see Figure A.4.6). Note that this analysis could not be carried out for the sham condition, as no relationship was observed between PLP effects and activity levels in the primary sensorimotor missing hand cortex for this condition.

To assess the neural correlates of stimulation-induced PLP relief, a whole brain regresssion analysis was carried out for the intervention condition, using PLP relief observed at the end of the experimental session (i.e. 90min post stimulation) as a regressor.

4.2.9 Statistical analysis

Statistical analysis was carried out using SPSS (version 21) and Matlab (version 9.1). Cases greater than 3 standard deviations from the mean were considered outliers and replaced by within-participant means. Outliers in the PLP analysis were removed from all further analysis and treated as missing values as opposed to being replaced by within-participant means. PLP ratings were inspected for violations of normality using the Shapiro-Wilk test. One-samples two-tailed *t*-tests were used to investigate whether the mean difference in PLP within a stimulation condition was greater than 0. A repeated measures ANOVA was then used to assess whether there was a significant different in PLP ratings across conditions at a specific time point. Post-hoc within-groups comparisons were carried out using paired two-tailed student t-tests. Between groups comparisons were made using independent samples two-tailed student *t*-tests. When significant departure from normality was found (based on the Shapiro-Wilk test), nonparametric tests were- used (Friedman test, Man-Whitney U test or Wilcoxon signed rank test, as appropriate). Correlations were evaluated using two-

tailed Pearson's correlation coefficients, or a Spearman rank-order correlation coefficient if normality assumptions were violated.

To correct for multiple comparisons, we divided the α (normally set at 0.05) by the number of comparisons made. For the PLP ratings analysis one-samples t-tests (i.e. assessing whether the PLP change was greater than 0), the adjusted α was set at $\alpha = 0.0125$. For the post-hoc comparisons that were carried out to assess differences in PLP modulations between the intervention and the various control conditions, the adjusted α was set at $\alpha = 0.0167$.

4.3 Results

4.3.1 Non-invasive brain stimulation induces phantom limb pain relief

We first determined the efficacy of task-concurrent anodal (excitatory; Nitsche & Paulus, 2000) tDCS over the primary sensorimotor missing hand cortex (i.e. intervention stimulation), compared to sham tDCS, control site tDCS and cathodal tDCS, based on subjective PLP ratings. The results relating to the main intervention and the sham condition are presented visually in Figure 4.1. The results relating to the control site and cathodal conditions are presented visually in Figure A.4.1. The subjective ratings of transient PLP intensity (scale 0-100, ranging from no pain to worst pain imaginable) were obtained either verbally or in writing. tDCS effects on PLP ratings were calculated at several time points (i.e. immediately after stimulation offset, at the end of the experimental session and a week after stimulation; see Figure 4.1A), while accounting for inter-subject variability in baseline PLP. To ensure that

the stimulation effects were not masked by the high variability in chronic PLP between participants, linear regression analysis was conducted to remove the influence of chronic PLP from the transient PLP scores.

tDCS prevents movement-induced phantom limb pain increases

Immediately after stimulation offset, PLP was significantly increased in the sham condition ($t_{(13)} = 4.81$, $p < 0.001$). This is consistent with previous reports showing that phantom hand movements can increase PLP (see Chapter 5). As in the sham condition, PLP was significantly increased in the control site condition immediately after tDCS offset ($t_{(13)} = 3.60$, $p = 0.003$; Figure A.4.1A). No PLP change could be observed in the cathodal stimulation condition ($t_{(14)} = 060$, $p = 0.555$; Figure A.4.1A). Furthermore, no PLP increase was observed in the intervention condition ($Z = -1.73$, $p = 0.084$, note that with the adjusted α this p-value does not indicate a trend towards significance; Figure 4.1B).

A Friedman test showed that there was a significant difference between the 4 stimulation sessions in PLP modulation immediately after stimulation offset ($X_{(3)} = 15.65$, $p = 0.001$). Posthoc tests revealed a significantly different PLP effect in the intervention compared to the sham condition ($Z = -2.73$, $p = 0.006$; see Figure 4.1B) and between the intervention and the control site condition ($Z = -2.83$, $p = 0.005$; Figure A.4.1A). No difference was observed between the intervention and cathodal stimulation condition ($Z = -.85$, $p = 0.397$; Figure A.4.1A).

tDCS relieves phantom limb pain

At the end of the experimental session (~90min after stimulation offset; see Figure 4.1B) there was a trend towards a significant PLP increase in the sham condition ($t_{(13)}$ = 2.77, p = 0.016). We no longer observed a change in PLP for the control site (Z = -0.87, p = 0.382; Figure A.4.1A) or the cathodal stimulation conditions ($t_{(13)}$ = -0.30, p = 0.766; Figure A.4.1A). Contrarily, we observed significant PLP relief in the intervention condition ($t_{(14)}$ = -6.20, p < 0.001).

A Friedman test showed that there was a significant difference between the 4 stimulation sessions in PLP modulation at the end of the experimental session ($X_{(3)}$ = 16.2, p = 0.001). Post hoc testing revealed a significant difference in PLP ratings in the intervention condition compared to the sham ($t_{(13)}$ = 8.18, p < 0.001; see Figure 4.1B) and the cathodal stimulation condition ($t_{(13)}$ = -4.25, p = 0.001; Figure A.4.1A). There was no significant difference between the intervention and control site condition ($t_{(12)}$ = 2.06, p = 0.039; Figure A.4.1A).

tDCS-induced phantom limb pain relief lasts for at least one week

To assess longer-term effects of the intervention stimulation, two separate approaches were taken. Firstly, PLP ratings were assessed in the week after each stimulation condition with respect to baseline ratings (as above). No change in PLP was observed in the sham (Z = 0.00, p = 1.00; Figure 4.1B) or control site condition (Z = -1.42, p = 0.155; Figure A.4.1A). PLP was significantly increased in the cathodal stimulation condition (Z = -2.70, p = 0.007; Figure A.4.1A). Importantly, PLP remained significantly reduced in the intervention condition (Z = -2.80, p = 0.005; Figure 4.1B).

Because of the counterbalancing, no participant will have a difference score for each stimulation condition, making it impossible to carry out a repeated measures test across the four stimulation conditions. Therefore, only Wilcoxon signed rank tests between individual pairs can be used to analyse these PLP ratings. Statistical analysis found no significant difference between the intervention and any of the control conditions (sham: $Z = -1.36$, $p = 0.173$; control site: $Z = -1.51$, $p = 0.128$; cathodal: $Z = -2.20$, $p = 0.028$). This lack of significant differences may reflect the reduced number of participants that could be tested for these comparisons, due to the counterbalancing of sessions ($n = 6$-7).

We further assessed longer-term intervention effects using daily PLP ratings obtained in the week after each stimulation condition (Figure 4.1C&D). A repeated measures ANOVA showed that there was a significant difference across the stimulation sessions in average PLP in the week after stimulation ($F_{(3,30)} = 4.87$, $p = 0.007$). Post hoc tests demonstrated a strong trend towards lower average PLP for the intervention condition in the week after stimulation, compared to both the sham ($t_{(14)} = 2.65$, $p = 0.019$; Figure 4.1D) and cathodal stimulation conditions ($t_{(11)} = 2.68$, $p = 0.022$; see Figure A.4.1C). PLP was significantly lower in the week after intervention stimulation compared to the control site condition ($t_{(11)} = 3.77$, $p = 0.003$; see Figure A.4.1C).

Is the observed tDCS-induced phantom limb pain relief dependent on a carry-over effect?

As our results showed a lasting PLP effect of our condition, we aimed to make sure that the success of our intervention stimulation, as indicated by significant PLP relief

assessed at the end of the experimental session (~90min after stimulation offset), was not dependent on which condition preceded intervention stimulation (i.e. our results were not dependent on a potential carry-over effect). As such, we divided our sample in subgroups, depending on which condition preceded intervention stimulation. In subgroup 1 (n = 4) intervention stimulation was presented in the first experimental session (i.e. there was no preceding stimulation condition). In subgroup 2 (n = 2) sham stimulation preceded intervention stimulation. In subgroup 3 (n = 6) control site stimulation preceded intervention stimulation. And, lastly, in subgroup 3 (n = 3) cathodal stimulation preceded intervention stimulation.

We found, using a one-sample Wilcoxon signed rank test, that there was no significant change in PLP in any of the subgroups immediately after stimulation offset, consistent what was seen when sampling all subgroups together (subgroup 0: $Z = -1.83$, $p = 0.068$, subgroup 1: $Z = -1.34$, $p = 0.180$, subgroup 2: $Z = -0.67$, $p = 0.500$, subgroup 3: $Z = -0.00$, $p = 1.000$; the adjusted α was set at $\alpha = 0.0125$). There were not enough cases to run a Kruskal-Wallis H test to assess whether there were significant differences in PLP change across the four subgroups.

Different to what we found when sampling the four subgroups together, we found no significant PLP change in any of the subgroups at the end of the experimental session (one-sample Wilcoxon signed rank test; subgroup 0: $Z = -1.10$, $p = 0.273$, subgroup 1: $Z = -1.34$, $p = 0.180$, subgroup 2: $Z = -2.20$, $p = 0.028$, subgroup 3: $Z = -1.60$, $p = 0.109$; the adjusted α was set at $\alpha = 0.0125$). This lack of significance is most likely due to the highly reduced number of participants that could be tested for each subgroup. As before, there were not enough cases to run a Kruskal-Wallis H test to

assess whether there were differences in PLP change across the four subgroups. Due to the reduced number of samples we were unable to conduct any statistical tests for the ratings that assess PLP (changes) in the week after stimulation.

The tests carried out above may not be optimal to determine whether carry-over effects may have affected our results, as our study sample (n = 15) is arguably too small to be split into subgroups. The highly reduced number of participants that can be tested for each subgroup when making such a split drastically reduces the power to find any effect – potentially explaining why we unable to find significant PLP relief at the end of the experimental session the data in any of the subgroups.

Counterbalancing is a method to control for order effects in a repeated measures design. If counterbalancing is successfully achieved, then the chance that an order effect would influence study results is reduced. To ensure that counterbalancing was carried out correctly in our study, we used a chi-square test to confirm that each condition was preceded an equal number of times by the other conditions (intervention condition: $X^2_{(3)} = 2.33$, $p = 0.506$; sham condition: $X^2_{(3)} = 2.33$, $p = 0.506$; control site condition: $X^2_{(3)} = 8.57$, $p = 0.836$, cathodal condition: $X^2_{(3)} = 0.73$, $p = 0.865$). Note, however, that even optimal counterbalancing does not fully prevent the possibility that a carry-over effect influences one's study results. Indeed, it may be interesting to explore the potential confound of carry-over of our study set-up in more detail in future studies.

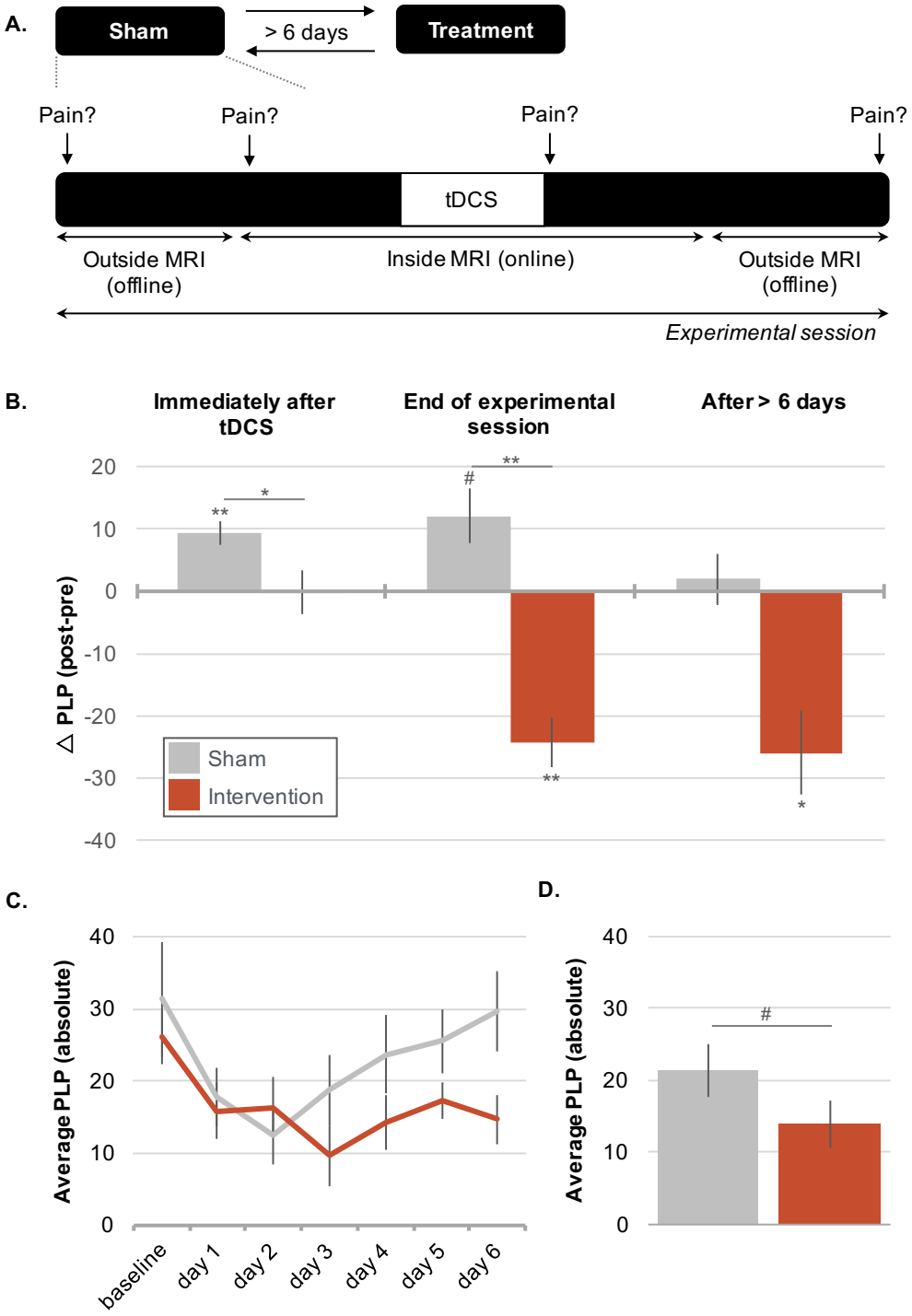


Figure 4.1: Non-invasive brain stimulation relieves phantom limb pain with effects lasting up to one week. (A) Experimental timeline. Transient phantom limb pain (PLP) ratings were obtained at four different time points within each experimental session. To account for inter-subject variability, post-stimulation online and offline PLP ratings were contrasted with their respective baselines in (B). To examine longer-term effects of stimulation, participants were asked to respond to daily text messages requesting PLP ratings for 6 days post stimulation. (B) Intervention stimulation effects on PLP, assessed in the experimental sessions. Positive values on the y-axis indicate PLP increases and negative

values indicate PLP relief. The sham condition is depicted in grey and the intervention condition in red. (B, left) While PLP was increased in the sham condition immediately after stimulation, no such PLP increase was observed in the intervention condition, leading to a significant difference between conditions. (B, middle) At the end of the experimental session, PLP remained increased in the sham condition, while significant PLP relief was observed after intervention stimulation. The PLP change was significantly different between the sham and intervention conditions. (B, right) At least one week after stimulation, there was no longer a change in PLP in the sham condition, but significant PLP relief was still observed for the intervention condition. (C&D) A second measure of week-long tDCS effects on PLP was obtained using text messages, asking amputees to rate their average PLP on a daily basis. Note that no difference scores were calculated for this measure and as such, the y-axis reflects absolute PLP ratings. (C) PLP ratings over the course of 6 days post stimulation. (D) The results in (C) tested as a main effect. In the week after stimulation, PLP was significantly lower in the intervention condition, compared to sham. Together, these results show that a single 20min application of task-concurrent intervention stimulation relieved PLP with effects lasting up to one week after stimulation. Asterisks indicate statistical significance as follows: # = corrected $p < 0.10$; * = corrected $p < 0.05$; ** = corrected $p < 0.01$. Correction for multiple comparisons is carried out as in the text, i.e. while also considering the tests that were carried out for the two active control conditions that are not illustrated in this figure (see Figure A.4.1 for an illustration of the results related to the two active tDCS control stimulation conditions). PLP = phantom limb pain.

	Immediately after tDCS	End of experimental session	After > 6 days
Sham	+42.9	+28.3	+1.2
Intervention	-6.1	-20.4	-29.5
PLP relief estimate (i.e. intervention, considering sham)	-49	-48.7	-30.7

Table 4.2: Non-invasive brain stimulation induced PLP relief in percentages (effect sizes). Effect sizes were calculated using the raw PLP ratings (i.e. before regressing out chronic PLP). A percentage change was calculated between the averaged pre- and post-stimulation scores as follows: *(post stimulation PLP - pre stimulation PLP) / pre stimulation PLP * 100.* Since PLP increased in the sham condition, it may be argued that the actual PLP effect in the intervention condition consisted of the combined intervention PLP effect *plus* the sham condition PLP effect. As such, we created a PLP relief estimate,

taking into account the effect size of the intervention condition, considering the effect observed in the sham condition.

4.3.2 Phantom movement activity relates to PLP relief

We first inspected phantom hand movement activity at the first baseline recording. As we have shown previously (Makin, Scholz, et al., 2013; see also Chapter 3 and 5) phantom hand movement evoked activity in the primary sensorimotor missing hand cortex (see Figure A.4.2). We further confirmed that this maintained phantom hand movement activity in the primary sensorimotor missing hand cortex positively associated with chronic PLP (see Figure A.4.3; Makin et al., 2013; see also Chapter 3).

Compared to two-handed controls, we found increased activity (hereafter hyper-activity) in the bilateral insula in amputees, and no activity differences in the primary sensorimotor missing hand cortex (as reported in Chapter 3 and Makin, Scholz, et al. (2013); see Figure A.4.4A). To determine whether this hyperactivity in the bilateral insula associated with the phantom hand representation, we ran a baseline resting state functional connectivity analysis. This analysis confirmed increased functional connectivity (hereafter hyper-connectivity) between the missing hand territory and bilateral insula in amputees compared to controls (see Figure A.4.4B).

We concentrated our examination of the neural correlates of PLP relief on the intervention condition, as this was the only stimulation condition that achieved significant PLP relief. We only conducted neural comparisons between the intervention and sham condition and disregarded the two further two control conditions, to prevent over-cluttering of the results section. To determine the neural

correlates of PLP relief we focused our analysis on neural activity elicited by phantom hand movements performed during and after stimulation in the intervention condition. Based on the PLP ratings presented above, the earliest time-point at which PLP relief was significant was at the end of the experimental session. As such, all neuroimaging analysis, aimed at identifying the neural correlates of PLP relief, was focused on PLP measures obtained at the end of the experimental session (~90min after stimulation offset; see Figure 4.1A for the experimental timeline). Note that for this analysis we used the same PLP ratings as described above (i.e. after regressing chronic PLP).

Linking PLP relief with maintained phantom hand representation

To test the neural correlates of PLP relief, we conducted a whole-brain group regression analysis of phantom hand movement activity levels after stimulation in the intervention condition, with individual amputees' PLP relief scores as a regressor. We found that after stimulation in the intervention condition, amputees who experienced greater PLP relief showed less activity (hereafter also termed 'downregulation') in the primary sensorimotor cortex (located to anatomical 'hand knob') contralateral to the missing hand (Figure 4.2A).

This was further confirmed using an independently specified region of interest (ROI) of the primary sensorimotor missing hand cortex. Amputees who experienced greater PLP relief after stimulation in the intervention condition showed less activity in the missing hand cortex after stimulation ($r = 0.54$, $p = 0.036$; Figure 4.2B). This is consistent with our previous studies showing that amputees who have stronger maintained activity in this region during phantom hand movements have worse chronic PLP (Makin et al., 2013; see also Chapter 3). No such relationship was

observed in the sham condition (r = -0.18, p = 0.542), resulting in a significant difference in correlations between phantom hand activity and PLP scores between the intervention and sham conditions (Z = 1.98, p = 0.047).

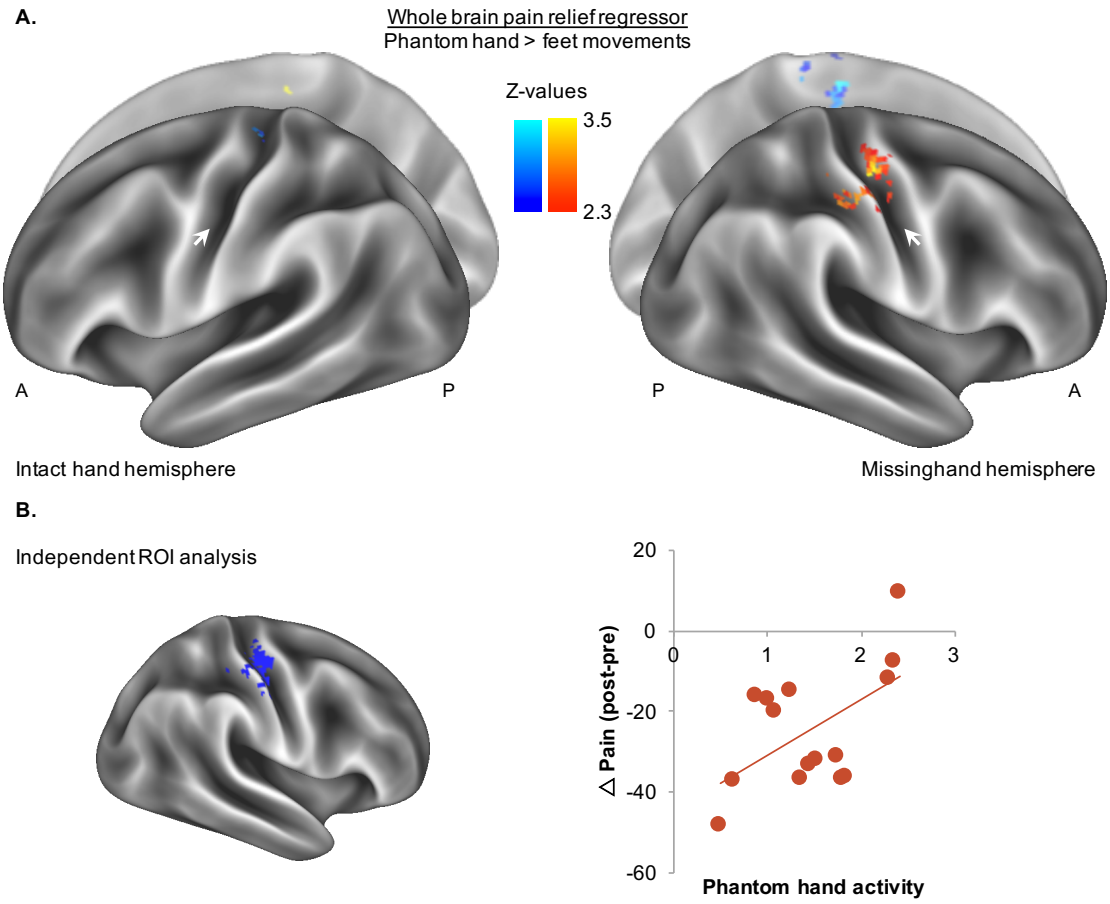


Figure 4.2: Downregulation of phantom hand representation activity reflects phantom limb pain relief. (A) We aimed to assess how the neural readout of phantom hand movements after intervention stimulation reflected PLP relief. To do so, we conducted a whole brain regression analysis for phantom hand movement activity levels after intervention stimulation with PLP relief scores taken at the end of the experimental session as a regressor. Voxels showing a positive relationship with PLP relief scores are indicated in red and voxels exhibiting a negative correlation are in blue. Lower activity levels around the primary sensorimotor missing hand cortex correlated with greater PLP relief. White arrows indicate the central sulcus. P = posterior; A = anterior; Intact hand hemisphere = hemisphere contralateral to the intact hand; Phantom hand hemisphere = hemisphere contralateral to the missing hand. (B) An independent region of interest (ROI) analysis of the primary sensorimotor missing hand

cortex confirmed that amputees with greater PLP relief (negative values on x-axis) showed less phantom hand movement activity in the missing hand cortex after intervention stimulation (y-axis).

Linking sensorimotor downregulation with activity in nociceptive pain-related areas during stimulation

Next, we explored which brain activity changes *during* stimulation predict the reduction in primary sensorimotor missing hand cortex activity that occurred *after* stimulation. For this purpose, we extracted the brain activity levels from the primary sensorimotor missing hand cortex after the intervention stimulation for each individual (i.e. under the cluster shown in Figure 4.2A; quantifying the degree of reduction in sensorimotor BOLD response) and used this as a regressor in a whole brain group regression analysis of phantom hand activity levels during intervention stimulation (see Figure 4.3A).

The resulting correlation map shows peaks in the insula (mid-, rostro-dorsal posterior and posterior ipsilateral to the missing hand), as well as the primary and secondary somatosensory cortex, posterior cingulate gyrus and globus pallidus (Figure 4.3B). This result demonstrates that across individuals, the magnitude of activity increase during stimulation, in all of these regions, predicted the magnitude of activity decrease in the phantom hand area after intervention stimulation.

Follow-up analysis showed that PLP relief was predicted by increased activity in the ipsilateral insula during stimulation in the intervention condition (Figure A.4.5). We further test for laterality of the results presented in Figure 4.3B by repeating analysis without aligning individuals' brains based on the missing hand laterality. This showed

that the correlation between higher insula activity during intervention and low phantom hand area activity after intervention stimulation was confined to the right hemisphere (see Figure A.4.6). Together, our results indicate a role for pain-related brain areas in reducing maintained activity in the primary sensorimotor missing hand cortex, as well as relieving PLP.

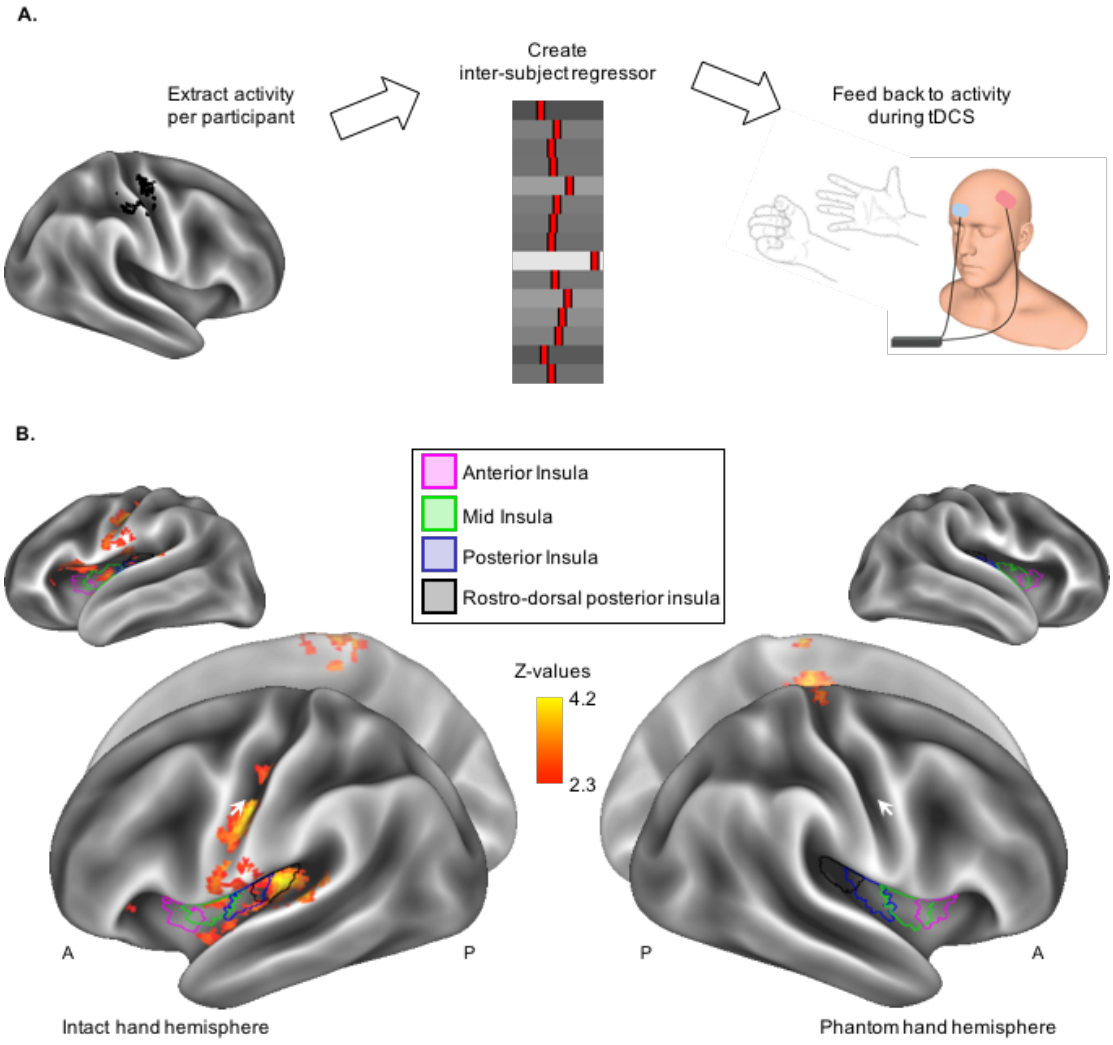


Figure 4.3: Increased insular activity during stimulation associated with downregulation of activity in the primary sensorimotor missing hand cortex after stimulation. (A) We aimed to assess what neural processes during intervention predicted the subsequent downregulation of sensorimotor cortex activity. To do so, we first extracted the phantom hand movement activity levels post-stimulation within the cluster shown in Figure 4.2A, and created an inter-subject regressor. This was then used as a whole brain regressor of phantom hand movement activity during intervention. (B) Increased ipsilateral insular recruitment during task-concurrent intervention stimulation

was predictive of a subsequent downregulation of activity in the primary sensorimotor missing hand cortex (see Figures A.4.5 and A.4.6 for related results). Annotations are as in Figure 4.2. No phantom hand movement activity was significantly positively correlated with sensorimotor cortex downregulation.

4.4 Discussion

In this study, we report that a single session of 20 minutes of non-invasive brain stimulation (anodal tDCS) over the primary sensorimotor missing hand cortex caused both short and longer term PLP relief. The intervention stimulation was effective in preventing movement-induced PLP immediately after stimulation and resulted in significant PLP relief, which lasted for at least one week after intervention. The analgesia effect sizes we report are in the range of 30-50% - which is suggested to be a clinically relevant effect (Farrar, Young, LaMoreaux, Werth, & Poole, 2001). Our findings provide a potential platform for further development of mechanism based targeted brain stimulation therapies for chronic pain. In addition, we partially reveal the neural correlates of stimulation-induced PLP relief. Stimulation, together with the related task, increased activity in nociceptive brain areas during intervention stimulation, and this was significantly related to the reduction of activity in primary sensorimotor missing hand cortex after intervention and PLP relief.

PLP relief significantly correlated with reduced activity in the primary sensorimotor missing hand cortex after intervention stimulation. This reduction in sensorimotor activity is highly compatible with our previous findings that linked higher levels of phantom hand movement activity in this area with greater PLP (Makin et al., 2013; see also Chapter 3). As reduced activity was only observed after stimulation, we note

that this may be a correlate of PLP relief rather than its driver. We therefore explored which brain regions during stimulation predicted this neural correlate of PLP relief.

Activity changes during intervention stimulation in several pain-related regions, including the insula, predicted post-intervention reduction of activity in the primary sensorimotor missing hand cortex. Amputees who recruited the insula more during intervention stimulation showed both a greater reduction in primary sensorimotor missing hand cortex activity after intervention and greater PLP relief. A wealth of past and recent convergent evidence indicates a key role for the insula (particularly the rostro-dorsal posterior aspect) in encoding the sensory aspects of pain perception and its modulation (Craig, 2014; Duff et al., 2015; Garcia-Larrea, 2012; Lin et al., 2017; Segerdahl, Mezue, Okell, Farrar, & Tracey, 2015; Wager et al., 2013). Yet, the role of the insula in PLP has remained largely unexplored.

The current Chapter and the work presented in Chapter 3 demonstrate that amputees have increased activity in bilateral insula when moving their phantom hand, compared to controls performing a similar non-dominant hand movement. Here, we also observed increased baseline resting state functional connectivity between the primary sensorimotor missing hand cortex and the insula (bilateral mid/posterior) in amputees compared to controls. This suggests that aberrant peripheral phantom hand inputs influence both the primary sensorimotor and insular cortices. As the insula is a core region encoding the perception of pain, the increased insular-sensorimotor cortex functional coupling found here is intriguing and potentially a key segue to the regulation of PLP through primary sensorimotor cortex stimulation.

In line with previous studies demonstrating the analgesic effect of tDCS in other chronic pain conditions, we positioned the excitatory electrode over the primary sensorimotor missing hand cortex. Interestingly, cathodal stimulation over the primary sensorimotor missing hand cortex, which has been suggested to result in reduced excitability (Nitsche & Paulus, 2000), and anodal stimulation applied to the primary sensorimotor intact hand cortex were ineffective in reducing PLP (see Figure A.4.1). This suggests that the beneficial effects of stimulation on PLP are specific to anodal (excitatory) stimulation of the primary sensorimotor missing hand cortex. This may seem to conflict with our prior findings showing that increased activity in the primary sensorimotor missing hand cortex relates to chronic PLP, which we proposed to be consequential to persistent peripheral inputs (Makin et al., 2013; Vaso et al., 2014; see also Chapter 3). However, the mechanisms underlying tDCS efficacy remain unknown and likely involve modulation of multiple brain networks (Lin et al., 2017; Stagg et al., 2013). Beyond a direct excitatory effect on the underlying cortex, stimulation may lead to the restoration of intracortical inhibitory processes (Antal, Terney, Kühnl, & Paulus, 2010; Lefaucheur, Drouot, Ménard-Lefaucheur, Keravel, & Nguyen, 2006) or indirect effects on other pain modulating structures such as the thalamus (Lang et al., 2005; Lin et al., 2017; Polanía, Paulus, & Nitsche, 2012). Accordingly, we found that intervention stimulation resulted in modulations both within and beyond the stimulation site. While it is possible that the hyperconnectivity we observed between the primary sensorimotor missing hand cortex and bilateral insula could have played a role in the success of the anodal stimulation, more research is required in order to understand how the intervention montage benefits PLP.

While single tDCS sessions have previously shown short-term alleviation of neuropathic pain (Antal et al., 2010; Bolognini et al., 2013), lasting benefits (e.g. over the course of a week) have commonly only been achieved after multiple sessions over consecutive days (Bolognini et al., 2015; Lefaucheur et al., 2017). Our results demonstrate that single-session intervention, coupled with phantom hand movements, induced PLP relief with effects lasting up to the one week. While not explicitly tested, our longer-term intervention efficacy might reflect the use of a task-concurrent stimulation protocol, which was designed to activate pathways associated with the read-out of aberrant peripheral inputs. This approach may have helped to better target our stimulation to brain regions maintaining PLP and thus attained longer lasting PLP relief (see Chapter 6: Discussion for further information).

In conclusion, we demonstrate the efficacy of stimulation over the primary sensorimotor missing hand cortex in relieving PLP. We further identify neural correlates of PLP relief, identifying potential novel targets for guiding future therapies. Our findings suggest that tDCS is a promising tool for targeting the mechanisms and symptoms of PLP. Furthermore, the ease of applying tDCS, the relatively low cost of the method, the portability of the device, its tolerability and its safety profile make the technique potentially very suitable for clinical treatment of PLP.

5 | Motor correlates of chronic phantom limb pain

Adapted from

Kikkert, S., Mezue, M., Henderson-Slater, D., Johansen-Berg, H., Tracey, I., & Makin, T. R. (2017). Motor correlates of phantom limb pain. *Cortex*.

Chapter abstract:

Following amputation, individuals ubiquitously report lingering sensations of their missing limb. While phantom sensations can be innocuous, they are often manifested as painful. Phantom limb pain (PLP) is notorious for being difficult to monitor and treat. A major challenge in PLP management is the difficulty in assessing PLP symptoms, given the physical absence of the affected body part. Here, we offer a means of quantifying chronic PLP by harnessing the known ability of amputees to voluntarily move their phantom limbs. Upper-limb amputees suffering from chronic PLP performed a simple finger-tapping task with their phantom hand. We confirm that amputees suffering from worse chronic PLP had worse motor control over their phantom hand. We further demonstrate that task performance was consistent over weeks and did not relate to transient PLP or non-painful phantom sensations. Finally, we explore the neural basis of these behavioural correlates of PLP. Using neuroimaging, we reveal that slower phantom hand movements were coupled with stronger activity in the cortical sensorimotor phantom hand territory, previously shown to associate with chronic PLP. By demonstrating a specific link between motor control and PLP, our findings open up new avenues for PLP management and improvement of existing PLP treatments.

5.1 Introduction

Following arm amputation individuals generally perceive vivid sensations of the amputated limb as if it is still present, with varying ability to voluntarily move this phantom hand. In up to 80% of arm amputees these phantom sensations are experienced as painful and can manifest as an intractable chronic neuropathic pain syndrome (Weeks et al., 2010). Phantom limb pain (PLP) often does not respond to conventional analgesic therapies and poses a significant medical problem (Knotkova et al., 2012).

A large number of studies have associated PLP with plastic changes in the sensorimotor nervous system (Flor et al., 1995; Makin, Scholz, et al., 2013; Mercier & Leonard, 2011; Raffin et al., 2016; Reilly & Sirigu, 2008a). Following this, a surge of behavioural therapies that aim to normalise the representation of the phantom hand have been developed in recent years (MacLachlan, McDonald, & Waloch, 2004; Moseley, 2006; Moseley & Flor, 2012; Ramachandran & Rogers-Ramachandran, 1996). The overarching objective of these behavioural therapies is to relieve PLP by improving the ability to move the phantom limb (e.g. mirror therapy (Chan et al., 2007; Rothgangel et al., 2011), graded motor imagery (Moseley, 2006; Thieme et al., 2016)). The assumption behind these therapies is that increased motor control (or motor imagery) over the phantom hand can cause PLP relief. Despite the large number of PLP therapies relying on this notion, the link between PLP and phantom hand motor control is only recently starting to be uncovered behaviourally (Gagné, Reilly, Hétu, & Mercier, 2009; Raffin, Giraux, et al., 2012), or using neuroimaging (Makin, Scholz, et al., 2013; Yanagisawa et al., 2016). Systematic evidence for the

role of phantom hand motor control in predicting (let alone modulating) PLP is lacking.

The current study aimed at characterising the assumed link between PLP and phantom hand motor control in fourteen upper limb amputees suffering from chronic PLP. Functional magnetic resonance imaging (fMRI) was used to further examine the neural correlates of deteriorated phantom hand motor control. Specifically, we investigated the relationship between deteriorated motor control and the cortical representation of the phantom hand.

5.2 Materials and methods

5.2.1 Participants

Fifteen unilateral upper-limb amputees who experienced PLP episodes more than once a week in the month preceding recruitment (mean age ± s.e.m. = 47 ± 3, mean years since amputation ± s.e.m. = 16 ± 3, 6 right-arm amputees, 4 females; the same sample as tested for Chapter 4 - see Table 4.1 for demographic and clinical details) and fifteen age- and sex-matched controls (2-handers, age = 46 ± 3, 7 with a dominant left hand, 4 females; the same sample as in Chapter 4) were recruited through the Oxford Centre for Enablement and Opcare. In this study, we specifically targeted amputees suffering from relatively high chronic PLP. As such, the variance and range of chronic PLP sampled was reduced in the current study (variance: 670, range: 82) compared to our previous study (Chapter 3) that demonstrated a relationship between chronic PLP and primary sensorimotor missing hand representation (variance: 754, range: 94; see Chapter 3). However, we note that this difference in variance of chronic PLP was not significant, as assessed using Levene' test of homogeneity of

variances ($F_{(1,29)} = 0.03$, $p = 0.86$). Ethical approval was granted by the NHS National Research Ethics service (10/H0707/29) and written informed consent was obtained from all participants prior to the study. Data from one amputee was discarded due to an inability to perform the motor task with the phantom hand.

As described in Chapter 4, amputees participated in four consecutive testing sessions that were separated by at least one week, as part of a larger study (see https://osf.io/4a5zg/ for full protocol). Here, we focus on the baseline measurements of the dataset described in Chapter 4. Only methods related to results reported in the current Chapter are detailed. Two amputees completed only three testing sessions. Control participants took part in a single session. To compare between the amputees and controls, the phantom hand was matched to the non-dominant hand of controls, and the intact hand was matched to the dominant hand of controls.

5.2.2 Pain ratings

Pain ratings data was obtained as described in Chapter 4: At the start of the first testing session, amputees rated the frequency of PLP, as experienced within the last year, as well as the intensity of worst PLP experienced during the last week (or in a typical week involving PLP). Chronic PLP was calculated by dividing worst PLP intensity (scale 0 - 100: ranging from no pain to worst pain imaginable) by PLP frequency (1 - all the time, 2 - daily, 3 - weekly, 4 - several times per month, and 5 - once or less per month). This approach reflects the chronic aspect of the PLP as it combines both frequency and intensity (Makin et al., 2013; Makin, Filippini, et al., 2015; Makin, Scholz, Henderson Slater, Johansen-Berg, & Tracey, 2015). Similar measures were obtained for non-painful phantom sensation vividness and stump pain.

Ratings of transient PLP intensity (scale 0 – 100, as above) were obtained in each testing session prior to the finger-tapping test.

As we have now used this measure of chronic PLP in multiple studies (Makin, Scholz, et al., 2013; see also Chapter 3; a further dataset used for the following assessment is currently unpublished), we are able to assess consistency of this measure across studies (i.e. over years). When considering all amputees that participated in at least two of our three studies (n = 21), we found excellent inter-studies consistency for our measure of chronic PLP (ICC = 0.88, 95% CI = 0.72-0.95, $F_{(20,20)} = 15.42$, $p < 0.001$). We also found excellent inter-studies consistency when considering amputees that participated in at least three of our past studies (n = 9; ICC = 0.78, 95% CI = 0.48-0.94, $F_{(8,16)} = 11.67$, $p < 0.001$).

5.2.3 Finger-tapping test

Motor control was assessed using the 'finger-to-thumb opposition task' (hereafter finger-tapping task). In this task, participants sequentially opposed each of the four fingertips to the tip of their thumb, starting with the index finger. Participants were instructed to repeat this movement cycle five times, and verbally indicated the ending of each cycle. Participants first performed the finger-tapping task with their intact hand and then repeated the task using their phantom hand. Importantly, phantom hand movements are distinguishable from imagined movements, as is supported by empirical evidence demonstrating that phantom limb movements elicit both central and peripheral motor signals that are different from those found during movement imagery (Makin, Scholz, et al., 2013; Raffin, Mattout, et al., 2012; Reilly et al., 2006). As such, emphasis was given to making "actual" instead of imagined phantom hand

movements (Raffin, Giraux, et al., 2012; Raffin, Mattout, et al., 2012; Reilly et al., 2006). Participants were encouraged to perform the finger-tapping task as well as possible, given the volitional motor control over the fingers. If it was impossible to make the full finger-to-thumb movements with the phantom fingers, participants were asked to attempt to perform the instructed movement. During the task, participants were requested to keep their eyes closed, their intact hand relaxed in their lap and all other body parts still.

Participants were further asked to perform the finger-tapping task bimanually, where they used their intact hand to mirror the precise degree and speed of movement of the phantom hand (see Appendices: Supplementary Materials Chapter 5 for related results). Lastly, participants were asked to perform the finger-tapping task using imagined intact and phantom hands movements separately (see Appendices: Supplementary Materials Chapter 5 for related results).

Response timing for completing the five movement cycles was recorded in real time by an experimenter using a stopwatch, based on participants' verbal reports. To establish a normalised measure for phantom hand movement response time (hereafter phantom hand movement), accounting for inter-subject response variability, the intact hand movement response time was subtracted from the phantom hand movement response time.

Upon completion of each trial, participants were asked to rate the movement difficulty (scale 0-100: ranging from easy to most difficult; see Appendices: Supplementary Materials Chapter 5 for related results) as well as whether the movement induced

transient PLP (scale 0-100, as above). Performing the phantom hand movement task increased transient PLP in 38% of all trials, with an average PLP increase of 10 points. Intact hand movements never induced PLP. The bimanual movement task elicited PLP in 44% of all trials, with an average PLP increase of 10 points. The imagined phantom hand movement task increased transient PLP in 13% of all trials, with an average PLP increase of 2 points. Imagined intact hand movements induced PLP in 3% of all trials, with an average PLP increase of 1 point.

5.2.4 Functional MRI sensorimotor task

Participants were visually instructed to make simple feet (bilateral toes), lips, intact hand (all fingers flexion/extension), and phantom hand (as the intact hand) movements, in a block-design fashion. Each movement condition was repeated four times in a counterbalanced protocol, alternating 12s of movement with 12s of rest. The movement pace was instructed at 0.5Hz. Participants were clearly instructed to make actual rather than imagined phantom hand movements. If it was impossible to perform full phantom hand movements, participants were asked to attempt to perform the movements. We have previously shown that this task is successful in producing cortical sensorimotor activity across a heterogeneous group of upper limb amputees (i.e. in terms of PLP, phantom sensations, level of amputation, etc.; Makin et al., 2013; see also Chapters 2 and 3). Instructions were delivered visually using Presentation software (version 16.4). Head motion was minimized using padded cushions.

5.2.5 MRI data acquisition

MRI images were collected by means of a 3-Tesla Verio MRI scanner (Siemens, Erlangen, Germany), using a 32-channel head coil. A high-resolution T1-weighted sequence was used to acquire a structural image (TR: 2040ms, TE: 4.7ms, flip angle 8°, voxel size: 1mm isotropic resolution). Functional images based on the blood oxygenation level-dependent (BOLD) signal were obtained using a multiband T2*-weighted pulse sequence with an acceleration factor of 6 (Moeller et al., 2010; Xu et al., 2013). This provided the opportunity to acquire data with increased spatial ($2mm^3$) and temporal (TR: 1300ms) resolution. The following acquisition parameters were used: TE: 40ms, flip angle: 66°, 72 transversal slices, 314 acquired volumes. A high-saturation first volume of each acquired multiband run was collected for registration purposes. Field maps were acquired for field unwarping.

5.2.6 MRI preprocessing and analysis

Data collected for individuals with an amputated (or non-dominant for controls) right hand was flipped on the mid-sagittal plane before all analyses, such that the hemisphere corresponding to the phantom hand was consistently aligned (Bogdanov et al., 2012; Diers et al., 2010; Foell, Bekrater-Bodmann, et al., 2014; Lotze et al., 2001; MacIver et al., 2008; Raffin, Mattout, et al., 2012). This procedure is regularly exercised in functional connectivity studies involving lateralised populations (Douaud et al., 2011; Park et al., 2011). Common pre-processing steps for fMRI data were applied to each individual run, using FSL's Expert Analysis Tool FEAT (version 6.00; fsl.fmrib.ox.ac.uk/fsl/fslwiki; Jenkinson et al., 2012; Smith et al., 2004; Woolrich et al., 2009): motion correction using FMRIB's Linear Image Registration Tool (MCFLIRT; Jenkinson et al., 2002), brain extraction using automated brain

extraction tool BET (Smith, 2002), spatial smoothing using a 3mm FWHM (full width at half maximum) Gaussian kernel, and high pass temporal filtering with a cut-off of 100s.

The first volume of each acquired multiband scan was used as an alternative reference image to enhance registration purposes. Functional images were registered to the example functional image of the acquired run in the first imaging session for each participant (7 degrees of freedom). This example functional image was then aligned to the structural image acquired in the first imaging session for each participant, initially using linear registration (FMRIB's Linear Image Registration Tool, FLIRT; Jenkinson et al., 2002; Jenkinson & Smith, 2001) and optimised using boundary based registration (Greve & Fischl, 2009). Structural images were transformed to MNI standard space using nonlinear registration tool FNIRT, and the resulting warp fields were applied to the functional statistical images.

Time series statistical analysis was carried out using FILM (FMRIB's Improved Linear Model) with local autocorrelation correction. First-level (time-series) parameter estimates were computed using a voxel-based general linear model (GLM) based on the double-gamma HRF function and its temporal derivatives. Two main contrasts were specified between different task movement conditions: 1) intact (or dominant) hand versus feet, and 2) phantom (or non-dominant) hand versus feet. To investigate a potential relationship between chronic PLP and activity in the cortical phantom hand area phantom hand movements were also defined versus rest. Estimated head motion parameters (as estimated by MCFLIRT) were added to the model to remove residual motion effects. All fMRI data was further assessed for

excessive motion using motion estimate outputs from MCFLIRT: volumes with estimated absolute mean displacement greater than 1mm (half of the functional voxel size) were scrubbed (amputees: scrubbing applied in 26% of all scans, maximum percentage of volumes scrubbed in a given session: 1.6%; controls: scrubbing applied in 6.7% of all scans, maximum percentage of volumes scrubbed in a given session: 1%).

Correlational analysis was carried out using a region of interest (ROI) approach. To define the two primary sensorimotor cortex hand areas, an average spatial map for the control group was created using FMRIB's Local Analysis of Mixed Effects (FLAME). A mask was drawn around the anatomical hand knob, extending the pre- and postcentral gyrus and the central sulcus. Within this mask, the top 400 voxels of the controls' average spatial map for each of the two main contrasts (dominant hand versus feet movements; non-dominant hand versus feet movements) were combined to form the two hand ROIs. The percent signal change was extracted for all voxels underlying the hand ROIs and then averaged across scans for each amputee.

5.2.7 Statistical analysis

Statistical analysis was carried out using SPSS software (version 21) and Matlab (version 9.1). For each measure, cases more than 3 standard deviations from the mean were replaced with within-participant means. Two-tailed significance testing was applied unless stated otherwise and standard approaches were used for statistical analysis. Between groups comparisons were assessed using independent samples two-tailed student *t*-tests. If the homogeneity of variances assumption was violated, as indicated by Levene's test for equality of variances, the Welch-Satterthwaite method

was used to adjust the degrees of freedom. Within groups, means were statistically compared using paired two-tailed student *t*-tests. When significant departure from normality was found (based on the Shapiro-Wilk test), nonparametric tests were used (Man-Whitney U test or Wilcoxon signed rank test, as appropriate). Correlations were evaluated using Pearson's correlation coefficients, or a Spearman rank-order correlation coefficient if normality assumptions were violated. We further calculated two-way random single measures of intraclass correlations (ICCs) to assess consistency between sessions.

5.3 Results

Here we focus on the normalised measure for phantom hand movements, i.e. phantom minus intact hand response times. To confirm that the results were not driven by intact hand response times, results were also examined for phantom and intact hand response times separately. These results are summarised in Table A.5.1. All results reported below were similar to phantom hand response times only, unless stated otherwise. In the main results of this Chapter we only report results based on *a priori* hypotheses derived from previous research (Gagné et al., 2009; Makin, Scholz, et al., 2013; Raffin, Giraux, et al., 2012; see also Chapter 3), as described in the introduction. Specifically, we focus on correlations between chronic PLP, phantom hand movement response times and activity in the primary sensorimotor missing hand cortex. Secondary control analyses showing null results were not adjusted for multiple comparisons. More exploratory analyses (e.g. relating to difficulty of movements, motor imagery and bimanual movements) are reported in the Appendices: Supplementary Materials Chapter 5.

5.3.1 Inter-session consistency

No significant difference in phantom hand movement response times was found across the four sessions (repeated measures ANOVA; $F_{(3,33)} = 1.10$, $p = 0.36$). Phantom hand movement inter-session consistency was further confirmed using intraclass correlations (ICC). ICC values range from 0 to 1: ICC values < 0.4 are considered poor, 0.4 to 0.59 are fair, 0.6 to 0.74 are good, and > 0.75 suggest excellent inter-session consistency (Fleiss, Levin, & Cho Paik, 2003). For phantom hand movements, this measure indicated good inter-session consistency with an ICC value of 0.64 (two-way random-model, consistency type), with 95% confidence interval (CI) = 0.37-0.86 ($F_{(11,33)} = 8.05$, $p < 0.001$). Inter-session consistency was only fair for imagined phantom hand movements (see Appendices: Supplementary Materials Chapter 5 for full results). Average response times across sessions were used for further analysis. Good inter-session consistency was found for phantom hand activity in the primary sensorimotor missing hand cortex (contrast: phantom hand movements versus rest; ICC = 0.63, 95% CI = 0.37-0.85, $F_{(12,36)} = 7.80$, $p < 0.001$).

5.3.2 Intact versus phantom hand movements

We found that phantom hand movement response times were greater in the amputee group compared to the control group ($t_{(13.62)} = -6.99$, $p < 0.001$). When considering phantom hand and intact hand response times separately, control over the phantom hand was deteriorated, as demonstrated by increased phantom hand movement response times (Figure 5.1A, see Figure A.5.1A for similar results for difficulty ratings). Amputees' phantom hand response times were slower both compared to intact hand response times ($t_{(13)} = -7.01$, $p < 0.001$) and compared to controls non-

dominant hand response times (U = 6, p < 0.001). Intact hand response times were not significantly different between amputees and controls: $t_{(27)}$ = 0.70, p = 0.49), and no difference in response time was found between dominant and non-dominant hand movements in controls (Z = -0.71, p = 0.48). These results are consistent with previous reports (Raffin, Giraux, et al., 2012).

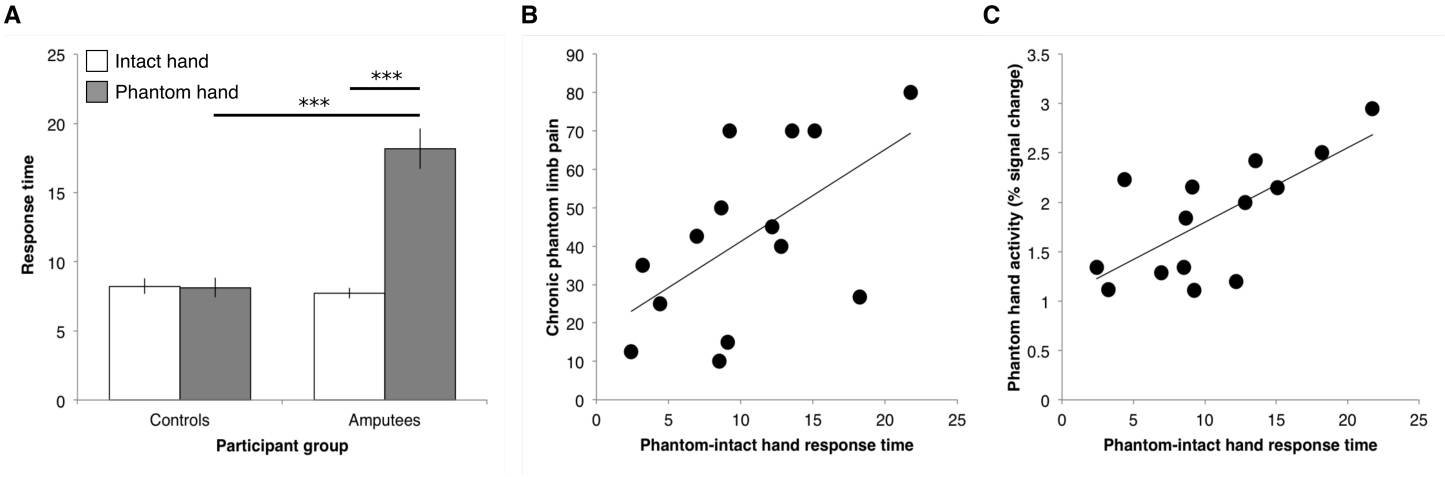


Figure 5.1: Phantom hand motor control is impaired and relates to chronic phantom limb pain and cortical sensorimotor phantom hand representation. (A) Amputees were slower in performing the motor execution task with their phantom hand, both compared to their intact hand and to the non-dominant hand of controls. (B) Amputees who experienced worse chronic PLP took longer to perform the finger-tapping task with their phantom hand (r = 0.57, p = 0.03). (C) Amputees who took longer to perform the finger-tapping task with their phantom hand showed stronger activity in the primary sensorimotor missing hand cortex when moving their phantom hand (r = 0.66, p = 0.01). Asterisks denote p < 0.001. Response time is shown in seconds. Error bars indicate the s.e.m.

5.3.3 Correlations with chronic phantom limb pain

Phantom hand movement response times associated with chronic PLP (Figure 5.1B, see Figure A.5.1B for similar results for difficulty ratings), consistent with previous studies (Gagné et al., 2009; Raffin, Giraux, et al., 2012). Amputees experiencing

worse chronic PLP were slower at performing phantom hand movements ($r = 0.57$, $p = 0.03$). As an exploratory test, we also examined the links between phantom hand movement response times and other measurements relating to chronic PLP, such as chronic non-painful phantom sensations and transient PLP. We observed that the relationship with phantom hand movement response times did not translate to chronic non-painful phantom sensations ($r_s = 0.08$, $p = 0.79$). Furthermore, no significant correlation was found between transient PLP and phantom hand movement response times in the individual sessions (average $r_s = 0.30$, $p = 0.30$). The observed correlation between chronic PLP and phantom hand movement response times was not driven by PLP evoked by the task, as shown using a partial correlation including task-evoked PLP as a nuisance regressor ($r_s = 0.54$, $p = 0.04$). A further exploratory analysis revealed that there was no significant correlation between imagined phantom hand movement response times and chronic PLP ($r = 0.22$, $p = 0.46$; see Appendix A: Supplementary materials for full results). These results extend previous findings (Gagné et al., 2009; Raffin, Giraux, et al., 2012), by showing that the link between phantom hand movements and chronic PLP is non-transmutable.

5.3.4 Phantom hand representation

Activity in the cortical sensorimotor phantom hand area was associated with phantom hand movement response times (Figure 5.1C). Amputees who were slower in performing the finger-tapping task with the phantom hand outside the scanner activated the primary sensorimotor missing hand cortex more during flexion and extension of all phantom fingers ($r = 0.70$, $p = 0.005$). When regressing out task-evoked PLP using a partial correlation, a strong trend towards a correlation between phantom hand activity in the primary sensorimotor missing hand cortex and phantom

movement response times was observed (r_s = 0.51, p = 0.06). Correlations between activity in the primary sensorimotor missing hand cortex and chronic PLP reached significance in the first and second scanning sessions (one-tailed r = 0.55, p = 0.02 and r = 0.48, p = 0.04 respectively), but not in subsequent scanning sessions (third scanning session: r = 0.18, p = 0.26, fourth scanning session: r = 0.20, p = 0.25; Figure A.5.3; see Appendices: Supplementary Materials Chapter 5 for further details).

Note that variations in cortical sensorimotor activity levels across participants did not result from differences in task difficulty: First, phantom movements used in the neuroimaging task were customised per participant such that they were comfortable to perform for all participants. Second, the correlation between phantom hand movements and primary sensorimotor missing hand cortex activity was independent of difficulty ratings in the finger-tapping task (partial correlation; r = 0.63, p = 0.03). This confirms that the observed increased activity in the phantom hand territory reflected movement representation, and not difficulty.

The correlation between response time and activity in the primary sensorimotor cortex was not significant for the intact hand or for controls (see Appendices: Supplementary Materials Chapter 5 for details). Although suggestive, the observed relationship with phantom hand movements might reflect abnormal movement representation, potentially pointing at aberrant processing.

5.4 Discussion

Previous studies reported that chronic PLP positively correlated with the duration of movement execution with the phantom hand (Gagné et al., 2009), as well as

difficulty. Furthermore, it was shown that this relationship with chronic PLP did not hold for imagined phantom movements (Raffin, Giraux, et al., 2012). In the current study, we confirm and extend these initial findings. First, we validate the reliability of phantom hand movement response times in the finger-tapping task by demonstrating good inter-session consistency. We therefore propose that this measure offers a means to quantify phantom hand motor control. Second, we show that deteriorated phantom hand motor control (i.e. slower response times) positively associated with the strength of primary sensorimotor missing hand representation, suggesting that deteriorated phantom hand motor control may be rooted in aberrant cortical representation. Third, we demonstrate that phantom hand movements are associated with chronic PLP, but not transient PLP or chronic non-painful chronic phantom sensations, thus consolidating the exclusive link between phantom hand motor control and chronic PLP.

Over the past decades, various theories have been proposed to explain the neural mechanisms underlying chronic PLP within the context of motor control and sensory inputs. For example, PLP has been suggested to be caused by a incongruency between motor and sensory signals (Harris, 1999; McCabe, Haigh, Halligan, & Blake, 2005), problems in the cortical body matrix representation (Moseley, Gallace, & Spence, 2012), a vicious cycle between pain and avoidance behaviour (in this case phantom hand movements; Vlaeyen & Linton, 2000) or prediction errors (Mohan & Vanneste, 2016). We wish to highlight the maintenance of nociceptive peripheral signals following amputation, previously shown to drive PLP (Vaso et al., 2014), as a potential source for the observed association between PLP and deteriorated motor control. It is possible that aberrant inputs from the residual nerves to the primary

sensorimotor missing hand cortex (e.g. through ectopic firing; Nystrom & Hagbarth, 1981) also disrupt the functioning of the sensorimotor system, leading to deteriorated phantom hand motor control. As such, the current results are in line with our previous neuroimaging findings that link chronic PLP with activity in the primary sensorimotor missing hand cortex during phantom hand movements (as originally shown in (Makin, Scholz, et al., 2013) and replicated in Chapter 3). Here we did not observe a consistent significant relationship between chronic PLP and activity in the primary sensorimotor missing hand cortex. This could potentially be explained by the restricted range of chronic PLP sampled in the current study, as we specifically targeted individuals with relatively high chronic PLP. When the variation in chronic PLP is reduced, this can explain less variation in brain activity, leading to a lower observed correlation coefficient. Indeed, lower variability is known to reduce the sensitivity of identifying correlations (Bland & Altman, 2011). As such, further research is needed to determine whether the observed relationship between deteriorated phantom hand motor control and chronic PLP is mediated by the cortical sensorimotor representation of the missing hand.

The accumulating evidence for a correlation between phantom hand movements and chronic PLP highlights the importance of studying phantom hand motor control as a key feature of chronic PLP, and provides opportunities for refining currently available clinical applications. Current behavioural therapies aiming to relieve PLP through phantom limb movement therapy (e.g. mirror therapy, graded motor imagery) have shown mixed effectiveness (Bowering et al., 2013; Ortiz-Catalan et al., 2016; Thieme et al., 2016). While these therapies are based on the assumption that increased motor control over the phantom hand can cause a change in PLP, many of these therapies

make use of motor imagery, rather than motor execution. Despite the mounting evidence linking phantom hand motor execution and PLP, the existence of a link between phantom hand motor imagery and chronic PLP remains tenuous, and our current findings highlight the diminished consistency of motor imagery performance (see the Appendices: Supplementary Materials Chapter 5 and Raffin, Giraux, et al., 2012). It is therefore possible that phantom limb movement therapy outcomes could be improved when using actual, instead of imagined, movements in rehabilitation approaches. An alternative explanation for the limited effectiveness of phantom limb movement therapies is that the observed link between phantom hand movements and chronic PLP may not be causal. Indeed, insufficient evidence currently exists to support the assumed causality of this link.

The motor test investigated in this study provides an option for implicit, and potentially more objective, measurement of chronic PLP. Since no implicit measure currently exist for assessing chronic PLP, clinicians rely solely on self-report for diagnostics and monitoring of treatment outcomes. Self-report is known to be sometimes unreliable, biased (Paulhus, Vazire, 2005) and influenced by mood states (Berna et al., 2010; Schweinhardt et al., 2008; Wiech & Tracey, 2009). In certain circumstances (e.g. when determining the impact of a novel treatment through longitudinal pain ratings) our motor task may provide an implicit proxy measure that is more resistant to the confounds sometimes inherent to self-report, as has been shown to be useful in several previous studies exploring analgesic efficacy (Iannetti et al., 2005; Tracey, 2013; Wanigasekera, Mezue, Andersson, Kong, & Tracey, 2016). A potential confound of our approach is that performing the phantom hand finger-tapping test increased transient PLP in a subset of the amputees, and one participant

was unable to perform the task. For amputees who are unable to move the phantom hand, performing the task using motor imagery could be an alternative (though sub-optimal) option, but more research is needed to validate this approach.

6 | Discussion

6.1 Thesis overview

This thesis comprises a set of experiments designed to investigate how the primary sensorimotor cortex, and in particular the missing hand cortex, changes following a major loss of sensory input, i.e. following upper-limb amputation. This thesis further aims to uncover the neural underpinnings of phantom limb pain (PLP). For this purpose, I employed a variety of MRI modalities, non-invasive brain stimulation (i.e. transcranial direct current stimulation, tDCS) and behavioural measures of phantom hand motor control.

I designed a series of experiments in my DPhil to answer three main (but partially overlapping) questions; (1) What happens to the neural fingerprint of a hand following its amputation (Chapter 2)? (2) What are the behavioural (Chapter 5) and neural underpinnings of PLP (Chapter 3)? (3) Can we identify novel targets for PLP treatment, by combining neuroimaging and non-invasive brain stimulation (Chapter 4)?

Together, my studies provide the first comprehensive overview of the neural correlates and mechanisms underlying missing hand sensations (i.e. phantom limb sensations and PLP), offering novel opportunities for PLP treatment.

6.2 Persistent representations of a missing hand

Retaining sensations of a missing hand following arm amputation is a mysterious, but frequently occurring, phenomenon. Surprisingly, the neural origins of such phantom limb sensations have not previously been related to a potential persistent representation of the missing hand in primary somatosensory cortex (S1). Instead, phantom limb sensations and PLP have mostly been considered to be caused by a degraded missing hand representation and S1 reorganisation. This thesis demonstrates, for the first time, that the neural fingerprint of a hand is not abolished following arm amputation.

Textbooks teach us that when the main input is removed from the sensory cortex, the "freed-up" brain territory is invaded by new representations. This brain reorganisation was famously exemplified in S1 (Merzenich et al., 1984; Pons et al., 1991) and was seminal not only as a striking example of the adult brain's capacity to reorganise, but also in guiding research and clinical treatment. Today, sensory input removal is a prominent model for studying brain reorganisation, both at the microscopic and macroscopic levels (Baseler et al., 2011; Feldman & Brecht, 2005; Kambi et al., 2014; Makin, Cramer, et al., 2013). A common feature across all studies is that scientists probe the invading representations to characterise the freed-up brain area, leaving unexplored whether the original function of this region may be preserved, though latent. Amputees experiencing vivid phantom sensations provide a unique model to study what happens to the deprived (i.e. missing hand) cortical territory itself during sensory input loss. In Chapter 2, we address this question by making use of ultra-high field 7 tesla (7T) neuroimaging and amputees' ability to move the individual digits of the phantom hand. We demonstrate that even decades after arm

amputation, the functional digit layout (i.e. digit topography) of the missing hand in S1 was preserved and similar to that of two-handed controls. As such, we unravel a fundamental brain principle that has not been considered before by showing that the organisation of sensory cortex is preserved despite several decades of sensory input loss.

The results presented in Chapter 2 are a categorical advance on results presented previously (Makin, Scholz, et al., 2013; Raffin, Mattout, et al., 2012) and in Chapters 3 and 4, as the latter were based on increased net and therefore nonspecific brain activity and have previously been attributed to abnormal processing (e.g. aberrant inputs, cortical disinhibition). In these Chapters we demonstrate activity in the primary sensorimotor missing cortex during whole phantom hand opening and closing movements in two different 3 tesla (3T) datasets for which 16 and 15 amputees (respectively) were tested. These phantom hand movement activity levels were similar to those found in two-handed controls during whole non-dominant hand opening and closing movements. The methodology used in Chapters 3 and 4 does not allow us to investigate the fine topographic representation of the missing hand and, as such, limits us in exploring whether these amputees' hand representation is normal (i.e. compared to two-handed controls). Nonetheless, these further results that were obtained in larger samples may suggest that the preserved missing hand representation observed in Chapter 2 is generalizable to a larger sample than the few participants we were able to test for this chapter (i.e. due to the safety restrictions of ultra-high field neuroimaging).

An open question remains: what neural signals are driving the maintenance of missing hand topography in S1? In Chapters 3 and 4 we demonstrate that chronic PLP positively scaled with brain activity levels in the primary sensorimotor missing hand cortex (see also Makin, Scholz, et al., 2013). Since PLP has been suggested to be driven by aberrant peripheral inputs from the residual arm (see section 6.3.2; Nystrom & Hagbarth, 1981; Vaso et al., 2014), it could be suggested that these peripheral inputs are also driving the maintenance of the missing hand representation in S1. In Chapter 2, we tested whether maintained peripheral inputs may be necessary for preserving missing hand representation by investigating missing hand topography in an amputee suffering from brachial plexus avulsion (BPA) injury. This injury involves the tearing of the nerves in the residual arm from their root in the spinal cord (see section 6.3.3 for further details). As such, the peripheral inputs from the amputees' residual arm were no longer feeding into his central nervous system – thus preventing sensory feedback from the arm to the brain. Still, we found preserved topographical representation of his missing hand that was similar to that found in two-handed controls. Thus, while peripheral inputs from the residual arm may alter excitability levels in the primary sensorimotor missing hand cortex (see Chapters 3 and 4), they are not necessary to maintain a topographical missing hand representation in S1.

What neural signals may be triggering the brain activations subserving the missing hand topographic maps? We suggest that missing hand topography may be driven by motor (efferent) information. Indeed, the motor system remains relatively intact in amputees despite a major loss of sensory inputs (Raffin, Mattout, et al., 2012). The motor system is thought to provide information about its descending commands to the

sensory system, by means of efference copies. When a motor command is sent out (e.g. in the form of a phantom hand movement), efference signals reach S1. This corollary discharge is suggested to resemble the sensory feedback activity that would be expected from the movement (London & Miller, 2013). The persistence of such efference signals could contribute to the maintenance of preserved information content in S1, despite afferent input loss.

6.3 The neural underpinnings of phantom limb pain

6.3.1 Challenging the maladaptive plasticity model

As introduced in Chapter 1 and discussed further in Chapter 3, the highly influential maladaptive plasticity model attributes PLP to a mismatch in sensory input signals that arise due to S1 reorganisation (Flor et al., 1995, 2006). The maladaptive plasticity model proposes that following arm amputation the missing hand representation deteriorates, causing cortical reorganisation in S1 where the neighbouring face representation invades the missing hand territory. This leads to a mismatch in input signals. Despite its common acceptance by both the scientific and clinical field, multiple study outcomes presented in the various chapters of this thesis argue against the maladaptive plasticity model. A comprehensive overview of these results is presented below.

The first assumption of the maladaptive plasticity model, proposing that the missing hand representation in S1 deteriorates following arm amputation, is strongly challenged by the results presented in Chapter 2. These results reveal that even 30+ years post arm amputation, the topographic layout of the missing hand's individual digits is preserved in S1. Moreover, missing hand topography in S1 is similar to that

found in two-handed controls. Maintained activity in the primary sensorimotor cortex during phantom hand movements is further demonstrated in two different datasets in Chapters 3 and 4. In Chapter 3, we replicate the results previously presented by Makin et al. (2013), showing that amputees' phantom hand movements activity in the primary sensorimotor missing hand cortex is not significantly different to that of two-handed controls during non-dominant hand movements. In Chapter 4, we further present a whole brain analysis contrasting phantom hand movements activity in amputees with non-dominant hand movements activity in two-handed controls. Again, no difference in activity was found in the primary sensorimotor cortex. Together, the data presented in these three chapters demonstrate that missing hand representation is not deteriorated following arm amputation, but rather is preserved as 'normal'.

The second assumption of the maladaptive plasticity model states that following arm amputation, reorganisation occurs whereby the lip representation invades the missing hand territory in S1. In Chapter 3, we tested this assumption directly by investigating levels of activity in the primary sensorimotor cortex missing hand territory during lip movements. Firstly, we did not find a significant difference in levels of lip movement activity in the primary sensorimotor missing hand cortex between amputees and two-handed controls, suggesting that no lip reorganisation had taken place in the amputees. Furthermore, we did not find a significant correlation between chronic PLP and lip movement activity levels in the primary sensorimotor missing hand cortex. Instead, we reaffirmed that chronic PLP correlates with levels of maintained phantom hand movement activity in the primary sensorimotor missing hand cortex. Further, the results presented in Chapter 3 show a significantly stronger correlation between

chronic PLP and phantom hand activity, compared to the correlation between chronic PLP and lip movement activity in the primary sensorimotor missing hand cortex. This suggests that the 'maintained representation model' was more accurate at predicting chronic PLP levels, compared to the lip reorganisation anticipated by the maladaptive plasticity model.

The maintained representation model was also in accordance with the results presented in Chapter 4. Here we demonstrated PLP relief following a single session of task-concurrent tDCS, and explored the neural correlates of this induced PLP relief. The maladaptive plasticity model would predict PLP relief to correlate with an increase in activity in the primary sensorimotor missing hand cortex, as the missing hand representation should get 'reinstated' to enable PLP relief. Instead, we demonstrated that reduced phantom hand movement activity levels in the primary sensorimotor missing hand cortex following tDCS correlated with PLP relief. Indeed, amputees with more PLP reduction had lower phantom hand movement activity levels in the primary sensorimotor missing hand cortex following tDCS. It is important to note that this alteration in activity only occurred following tDCS, suggesting it may be a consequence of PLP relief, rather than its driver. Indeed, tDCS-concurrent fMRI revealed that altered activity in nociceptive areas (i.e., the insula and secondary somatosensory cortex, S2) was predictive of both PLP relief and this subsequent downregulation of activity in the primary sensorimotor missing hand cortex.

As the influence of the maladaptive plasticity model has been vast since its introduction twenty-two years ago (Flor et al., 1995), numerous treatments have been developed that aim to reverse the brain changes that this theory predicts (MacLachlan,

McDonald, & Waloch, 2004; Moseley, 2006; Moseley & Flor, 2012; Ramachandran & Rogers-Ramachandran, 1996). Accordingly, the clinical efficacy of these therapies has been challenged (Bowering et al., 2013; Thieme et al., 2016)). These treatments aim to normalise the 'degraded' representation of the phantom hand by means of phantom limb movements or phantom limb imagery therapy (e.g. mirror therapy (Chan et al., 2007; Rothgangel et al., 2011) and graded motor imagery (Moseley, 2006; Thieme et al., 2016)). The assumption behind these treatments is that increased motor control over the phantom hand would cause PLP relief. Despite the large numbers of therapies banking on this notion, this link between motor control and PLP is only recently starting to be uncovered behaviourally (Gagné et al., 2009; Raffin, Giraux, et al., 2012) or using neuroimaging (Makin, Scholz, et al., 2013; Yanagisawa et al., 2016). In Chapter 5 we investigate the relationship between phantom hand motor control and PLP. We show that amputees with worse chronic PLP have worse motor control over their phantom hand. This behavioural correlate of chronic PLP could be interpreted as being in agreement with the maladaptive plasticity model, as degraded motor representation could imply worsened motor control. We, however, demonstrate that amputees with worse phantom hand motor control had higher phantom hand movement activity levels in the primary sensorimotor missing hand cortex. This last result, again, challenges the maladaptive plasticity model.

It remains unclear why previous studies have been able to find evidence in favour of the maladaptive plasticity model (Flor et al., 1995, 1998; Foell, Bekrater-Bodmann, et al., 2014; Grüsser et al., 2001; Karl, Birbaumer, Lutzenberger, Cohen, & Flor, 2001; Lotze et al., 2001; MacIver et al., 2008; Raffin et al., 2016), and we do not (see Chapter 3; Makin et al., 2013; Makin, Scholz, Henderson Slater, Johansen-Berg, &

Tracey, 2015). While some methodological concerns have previously been raised with regards to studies showing a relationship between PLP and reorganisation (Jutzeler, Curt, et al., 2015; Makin, Scholz, et al., 2015), I believe it is more interesting to explore potential conceptual reasons for a dissimilarity in results. A possible explanation for the difference in results is that, by asking amputees to perform phantom hand movements, we directly targeted otherwise latent motor pathways of the phantom hand (Chapter 2), potentially triggering efferent representation in the primary sensorimotor missing hand cortex. This is unlike previous studies using lip activity or imaginary phantom hand movements activity to investigate representations in the missing hand cortex (Flor et al., 1995; Foell, Bekrater-Bodmann, et al., 2014; Lotze et al., 2001; MacIver et al., 2008). Furthermore, previous studies showing a relationship between chronic PLP and reorganisation mainly used passive tactile lip stimulation to assess reorganisation (Flor et al., 1995, 1998; Grüsser et al., 2001; Karl et al., 2001), while we used active lip movements. Patterns of activity observed in S1 are different during active lip movement compared to those observed during passive lip stimulation, as the first elicits efference copies activity in S1 and the latter does not (see also section 6.2 for a discussion on efference copies; London & Miller, 2013). As such, the difference in lip reorganisation findings in the PLP literature has previously been attributed to dissimilarities in study protocols (active lip movements versus passive lip stimulation; Flor, Diers, & Andoh, 2013). However, a few previous studies have used active lip movements to demonstrate a relationship with PLP (Foell, Bekrater-Bodmann, et al., 2014; MacIver et al., 2008; Raffin et al., 2016) and, as such, this explanation may not hold. A direct comparisons of the contributions of afferent versus efferent plasticity is needed in the future.

6.3.2 Peripheral attributes of PLP

In opposition to what would be expected according to the highly influential maladaptive plasticity model, the research presented in this thesis demonstrates that both increased activity in the primary sensorimotor cortices (Chapters 3, 4 and 5) and altered activity in nociceptive brain areas, in particular the insula and S2 (Chapter 4), associates with PLP experience. Collectively, our findings are in accordance with theories that attribute PLP to nociceptive peripheral inputs that persist despite limb amputation.

As proposed in early theories (Nystrom & Hagbarth, 1981) and emphasized again in recent research (Vaso et al., 2014), spontaneous activity from the residual nerves prevails after amputation and carries information relating to the missing hand. Studies using peripheral microelectrode recording (i.e., microneurography) in upper-limb amputees revealed that tapping the neuroma at the end of the residual limb resulted in bursts of ectopia (i.e. disturbed activity in the residual nerves) and a corresponding burst of PLP (see Chapter 1: Introduction for further discussion). The long latency of these ectopic responses was interpreted as a conduction velocity corresponding to that of the slow (afferent nociceptive) C-fibres. Similarly, spontaneous ectopic discharge could also be observed and was suggested to explain spontaneous PLP episodes (Fried et al., 1991; Nystrom & Hagbarth, 1981). This residual peripheral input may contribute to the maintenance of the fibre pathway that feeds into the central nervous system (see below for a mechanistic description).

Based on the introduction of this peripheral theory of PLP, treatments were developed that attempted to block the nerves stemming from these neuroma formations that appeared to be responsible for this ectopic discharge. Unfortunately, local anaesthesia block does not eliminate PLP in all cases (Flor, 2002; Flor et al., 2006; Nystrom & Hagbarth, 1981). A potential reason for the poor clinical efficacy of peripheral nerve block in PLP treatment, is that a full peripheral block is difficult to achieve (Serra et al., 2015). A further explanation that has been proposed is that much of the spontaneous (background) ectopic discharge actually originates from the dorsal root ganglia. This would explain why a peripheral nerve block may not be effective, as this is not the only source of the ectopia. Indeed, dorsal root ganglia electrogenesis could account for the therapeutic failure of neuroma, nerve and plexus infiltration because these distal blocks do not affect the dorsal root ganglia. Vaso et al. (2014) demonstrated that locally anaesthetising the dorsal root ganglia, thereby preventing ectopic signals from the dorsal root ganglia to reach the central nervous system, consistently attenuated and often completely eliminated PLP as well as non-painful phantom limb sensations. The minimal duration of this effect was equal to the duration of the lidocaine block. Control (saline) injections in the dorsal root ganglia had no such effect.

How does this aberrant peripheral inputs explanation for PLP fit with the results presented in this thesis? In Chapter 2, we demonstrate that peripheral inputs are not necessary to preserve organisation in the primary somatosensory cortex. Indeed, we observed preserved topographic representation of the missing hand in a participant that suffered from brachial plexus avulsion, in whom all communication between the peripheral nerves of the residual arm and the central nervous system were lost. We

suggested that efference copies, reaching the primary somatosensory cortex via cortico-cortical connections (London & Miller, 2013), gave rise to these preserved topographic maps. In Chapters 3-5 we address the relationship between processing in the sensorimotor cortex and PLP, which is suggested to be caused by aberrant peripheral inputs. We show that amputees with worst PLP show stronger activity in the missing hand cortex during phantom hand movements (Chapters 3-4) and have worse motor control over the phantom hand (Chapter 5). Specifically, we suggest that aberrant input from the residual nerves may elicit PLP and proportionately scale brain excitability in areas normally receiving inputs from the missing hand (i.e. the primary sensorimotor missing hand cortex). These aberrant activity levels in the primary sensorimotor cortex may disrupt the functioning of the sensorimotor system and affect motor control over the phantom hand (Chapter 5).

So, what is the functional significance of peripheral inputs in driving PLP and cortical organisation? How can we integrate these, perhaps seemingly contradictory, findings? Firstly, it should be noted that efference copies and input from the residual afferent nerves may drive activity in the primary somatosensory/sensorimotor cortex in distinct ways. The primary somatosensory cortex (layer IV) receives afferent signals from the periphery via the thalamus, but also receives cortico-cortical inputs (layers I-III) (Kandel, Schwartz, & Jessell, 2000). Efference copies, through cortico-cortical signals, may elicit preserved topographic organisation in the primary somatosensory cortex (Chapter 2) while aberrant afferent inputs from the periphery, feeding aberrant information into the primary sensorimotor missing hand cortex, may simultaneously drive aberrant activity in this brain region (Chapter 3-5). Efference copies would not necessary relate to PLP, though this could not be tested in the current thesis due to the

low number of participants that could be tested in Chapter 2. Peripheral inputs, on the other hand, would not necessarily change organisation and may not consist of organised topographical signals, but will influence net activity levels in the primary sensorimotor missing hand cortex. Indeed, while both inputs may co-occur simultaneously, they arise from different sources and may have different functional relevance.

Indeed, while retained peripheral inputs are not necessary to maintain a missing hand representation in the primary sensorimotor cortex (see Chapter 2 and section 6.2 for further discussion), maintained peripheral inputs would influence the levels of activity observed in the primary sensorimotor cortex. This is in accordance with the results presented in Chapter 3, demonstrating that PLP proportionately scales brain excitability in areas normally receiving inputs from the missing hand (i.e., the primary sensorimotor missing hand cortex). Amputees with worst PLP (more residual input from the periphery) show stronger activity in the missing hand cortex during phantom hand movements, as observed previously (Makin, Scholz, et al., 2013) and reaffirmed in Chapter 3.

This nociceptive peripheral input to the primary sensorimotor missing hand cortex may lead to an abnormally excitable missing hand representation, which in turn may affect motor control over the phantom hand (e.g., by sending more aberrant input into the sensorimotor system). In accordance with this idea, we demonstrate in Chapter 5 that amputees with higher levels of phantom hand movement activity in the primary sensorimotor missing hand cortex and worse chronic PLP had worse motor control over their phantom hand.

This thesis further suggests that increased activity in sensorimotor cortex may not be causally driving PLP, but instead reflects an epiphenomenon of peripheral disturbances. The results presented in Chapter 4 support this suggestion of maintained activity in the primary sensorimotor missing hand cortex as a correlate rather than a driver of PLP. Indeed, reduced activity in the missing hand cortex *after* tDCS correlated with PLP relief. Interestingly, altered insular activity *during* tDCS was predictive of this subsequent sensorimotor downregulation and PLP relief. We propose that PLP does not originate from altered activity in the primary sensorimotor missing hand cortex. Instead, we suggest that nociceptive inputs from the residual nerves are the base of chronic PLP. The results presented in this thesis reaffirm the strong relationship between persistent inputs pertaining to the missing hand representation and chronic PLP. Collectively, our findings emphasize the need to study the role of persistent inputs to better understand the mechanisms underlying chronic PLP.

6.3.3 Phantom limb pain in the absence of peripheral inputs

A special case of PLP patients, are those suffering from brachial plexus injury. In particular, patients suffering from brachial plexus avulsion (BPA) injury frequently experience PLP (Ciaramitaro et al., 2010). As also described above and in Chapter 2, BPA injury is a pre-ganglionic lesion that involves a tearing of the arm nerves from their origin (i.e. the spinal cord; Teixeira et al., 2015). As such, communication between the nerves branching into the arm and the spinal cord is lost. Since both the sensory and motor nerves are disconnected from the spinal cord in BPA, symptoms of BPA include a loss of muscle control over the limb and a loss of sensation in the limb.

Patients with BPA often undergo arm amputation, either at the time of injury of as a consequence of BPA injury symptoms (e.g. loss of limb vitality). Unfortunately, a common consequence of BPA (either in combination with arm amputation or not) is the experience of PLP. This introduces a mystery: If PLP is caused by aberrant peripheral input stemming from the residual nerves and dorsal root ganglia, then how is it possible that amputees with BPA injury (in whom the central nervous system no longer receives input from the residual nerves and dorsal root ganglia) commonly experience PLP?

If PLP is caused by aberrant inputs from the residual nerves, then one could predict that when peripheral inputs stemming from the residual nerves and dorsal root ganglia are lost, PLP would be cured. Indeed, Vaso et al. (2014) showed that anaesthetisation of the dorsal root ganglia in lower-limb amputees attenuated PLP and the experience of phantom limb sensations drastically. How come a similar effect is not seen in brachial plexus avulsion injury? What could explain PLP in these special cases of amputees? Firstly, it is important to note that BPA, caused by an accident, often doesn't result in complete abolishment of peripheral input from the hand and arm (e.g. due to divergence over dermatomes). Second, even when considering complete BPA, this injury does not involve a clean cut of the brachial nerves from the spinal cord. Due to the abrupt disconnection of the nerve roots from the spinal cord, central lesions are induced. These lesions have been suggested to be involved in the generation of PLP in BPA patients (Teixeira et al., 2015). This lesioning is thought to lead to disinhibition and therefore hyperactivity in the posterior horn of the spinal cord, a first integration centre of the primary sensory afferents. Inducing further (controlled) lesions to such tracts through dorsal root entry zone procedures have been

shown to lead to significant pain relief in BPA (Chivukula et al., 2015; Prestor, 2001; Samii, Bear-Henney, Lüdemann, Tatagiba, & Blömer, 2001). Therefore, BPA involves highly difference tissue damage compared to 'regular' amputation and, as such, perhaps dissimilar neural mechanisms may underlie a similar sensory (PLP) experience.

Still, it remains unclear whether similar mechanisms may perhaps subserve the PLP symptoms that are observed following BPA and 'regular' amputation (i.e. without BPA). Direct comparisons of PLP mechanisms in BPA and 'regular' amputees are needed to determine whether we should consider PLP in BPA as a separate case of PLP or whether we should research and treat it similarly as 'regular' PLP. These questions need further consideration and may be important in the search for the origin of PLP.

6.4 Novel targets for phantom limb pain treatment

6.4.1 Potential mechanisms of tDCS induced PLP relief

In Chapter 4 we used anodal tDCS over the primary sensorimotor missing hand cortex, while amputees were performing a phantom hand movement task, to relieve PLP. We combined this task-concurrent non-invasive brain stimulation with fMRI to identifying novel targets for PLP treatment. We demonstrated that a single 20min session of our intervention stimulation was effective at relieving PLP with effects lasting at least one week after stimulation. We identified altered insular and S2 activity as potential drivers of the observed tDCS-induced PLP relief.

But how may our intervention stimulation condition have achieved this effect? How could tDCS over the primary sensorimotor missing hand cortex have altered activity in these nociceptive brain regions? Results presented in Chapters 3 and 4 demonstrate (in two separate datasets) that amputees had increased functional connectivity at rest between the primary sensorimotor missing hand cortex and bilateral insula compared to two-handed controls. Furthermore, when amputees move their phantom hand they showed increased activity in bilateral insula compared to two-handed controls. This insular hyperconnectivity and hyperactivity in amputees may have allowed the primary sensorimotor missing hand cortex stimulation, during the performance of a phantom hand movement task, to also alter activity in the insular cortex (see section 6.4.2 for further discussion concerning how the use of task-concurrent tDCS may have been key for the efficacy of our protocol). Indeed, as the insula is a core region in encoding the perception of pain (Duerden & Albanese, 2013; Mazzola, Isnard, & Mauguière, 2006; Mazzola, Isnard, Peyron, Guénot, & Mauguière, 2009; Segerdahl, Mezue, Okell, Farrar, & Tracey, 2015; Wager et al., 2013), the increased insula-sensorimotor cortex functional coupling found here is intriguing and potentially key to the regulation of PLP through primary sensorimotor cortical stimulation.

Was the PLP relief observed following intervention stimulation specific to the site of and the current flow during stimulation? In other words: could similar PLP relief be achieved by stimulating a different cortical area or by altering the current flow direction of the stimulation? To test whether the observed tDCS effects were specific to our intervention protocol (i.e., anodal tDCS to the primary sensorimotor missing hand cortex), two further active tDCS conditions were included in this study. The first active tDCS control condition was designed to control for stimulation site and

included the application of task-concurrent anodal tDCS over the primary sensorimotor *intact* hand cortex (hereafter control site stimulation condition). The second active tDCS control condition included the application of task-concurrent *cathodal* tDCS over the primary sensorimotor missing hand cortex. This cathodal condition, that consisted of applying tDCS over the same stimulation site as our intervention condition but with the current flowing in the opposite direction, allowed us to investigate whether our tDCS effects were specific to current flow direction. Importantly, both these alternate active tDCS condition conditions did not achieve PLP relief. Indeed, the only tDCS condition that induced PLP relief was the intervention condition. This specificity in effectiveness could potentially be attributed to the unique ability of our intervention protocol to target nociceptive brain regions as the insula and S2. As mentioned above, the increased functional coupling between the insula and primary sensorimotor missing hand cortex may have been key in altering insular activity during intervention stimulation. A potential reason for the lack of PLP relief following control site stimulation is that this condition may not have been able to effectively target the phantom hand movement activity network. Indeed, positioning the anodal electrode over the intact hand area may mean it was not positioned over a cortical area that was involved in this network and, as such, it would not alter activity in nociceptive brain regions or relieve PLP. Cathodal stimulation over the primary sensorimotor cortex, during the performance of phantom hand movements, may also not have effectively altered activity in the insular cortex and, as such, did not relieve PLP.

Does the observed PLP relief indicate that our intervention stimulation protocol was optimal? While the research presented in Chapter 4 proposes task-concurrent tDCS

over the primary sensorimotor missing hand cortex as a promising tool to manage PLP, better results may be achieved by stimulating a different brain area. Indeed, our results suggest the involvement of the insula in the observed PLP relief. Targeting the insula more directly may allow the more effective alteration of activity in this area (e.g. by placing the tDCS electrodes closer to this area or by means of neurofeedback) and, as such, may have superior beneficial effects on PLP. Furthermore, while the research presented in Chapter 4 suggests that tDCS may be a promising technique to manage PLP, tDCS may not be an ideal treatment to PLP. While our intervention stimulation was effective in relieving PLP, it did not fully abolish PLP. An ideal approach would consist of using a similar block as used by Vaso et al. (2014) on lower-limb amputees. However, doing such a dorsal root ganglia anesthetisation in upper-limb amputees would be much riskier due to the higher location of the arm's dorsal root ganglia.

6.4.2 Task-concurrent tDCS versus tDCS at rest

Bolognini, Olgiati, Maravita, Ferraro, & Fregni (2013) previously demonstrated immediate PLP relief after applying anodal tDCS to the primary sensorimotor missing hand cortex. These effects were abolished 90min after tDCS, while our intervention stimulation protocol relieved PLP with effects lasting at least one week post stimulation. It is interesting to note that the same tDCS parameters were used by Bolognini, Olgiati, Maravita, Ferraro, & Fregni (2013) and in the study presented in Chapter 4. However, a large difference between these two studies is that this previous research applied tDCS at rest while we combined our intervention stimulation with a task. Indeed, our usage of a phantom hand movement task-concurrent tDCS protocol

may be a potential explanation for the longer lasting effect of our intervention (as explained below).

tDCS is known to cause widespread cortical and subcortical effects that go well beyond the target stimulation area (Lin et al., 2017; Parazzini et al., 2011; Stagg et al., 2013). This spread of electrode current is thought to have different patterns of distribution and different behavioural consequences depending on whether a person is at rest or in a task state during tDCS (Andrews, Hoy, Enticott, Daskalakis, & Fitzgerald, 2011; Gill, Shah-Basak, & Hamilton, 2015; Hsu, Juan, & Tseng, 2016; Woods et al., 2016). Indeed, applying the same brain stimulation (i.e. in terms of current flow and stimulation site) could have a different spatial current distribution profile depending on which functional networks are active while it is being delivered. In Chapter 4, we aimed to target the functional network responsible for the processing of peripheral inputs that relate to the missing hand. The observed link between phantom hand motor control and PLP (Chapter 5) further suggested that we may be able to effectively target neural pathways associated with PLP by combining tDCS with a phantom hand movement task.

The results of the neuroimaging analysis carried out in Chapter 4 point at altered insular activity as a neural correlate for the observed tDCS-induced PLP relief. As stated above, it may be possible that the reason our stimulation protocol was able to successfully target this brain region, was the combination of tDCS with a phantom hand movements task. Supporting this, we found that amputees have increased functional connectivity between the primary sensorimotor missing hand cortex compared to two-handed controls (Chapter 4). Moreover, in the two different datasets

explored for Chapters 3 and 4, we found that amputees activate their bilateral insula more when making phantom hand movements, compared to two-handed controls. This hyperconnectivity and hyperactivity of the insular cortices in amputees may have allowed our stimulation protocol to target the insula. Applying current to the primary sensorimotor missing hand cortex during phantom hand movements may have affected the insula, a region that has previously been associated with pain perception (Duerden & Albanese, 2013; Mazzola et al., 2006, 2009; Segerdahl et al., 2015; Wager et al., 2013), due to the altered spatial current distribution profile induced by the task.

However, since we did not test the effectiveness of our intervention protocol at rest, it remains a speculation whether tDCS to primary sensorimotor missing hand cortex is more effective in relieving PLP when it is combined with a phantom hand movement task compared to when it is applied at rest.

6.5 Remaining questions and future directions

The results presented in Chapter 2 are highly promising for the development of more intuitive fine-grained control of neuroprosthetics, requiring neural signals of individual digits. However, an intriguing and important question remains to what degree such persistent representations exist following spinal cord injury (SCI; e.g. tetraplegia), where both the sensory and motor systems are affected. This question is critical as the current BMI development mainly focuses on SCI patients, whose injury is inherently different from amputees. While amputees suffer from sensory input loss, their motor output system remains relatively intact. In SCI, the injured fibres often encompass both sensory and motor spinal cord fibres. Furthermore, both the

ascending (sensory) and descending (motor) uninjured spinal cord fibres are affected by demyelination, causing further signal conduction failures (Raineteau & Schwab, 2001). It remains unclear to what extent a more impaired motor output system would affect preserved missing hand's digit topography. While a promising first study showed that it was possible to induce sensation of individual digits using intra-cortical stimulation in the S1 hand area of a tetraplegic patient (Flesher et al., 2016), preserved representation has yet to be shown in a larger (and preferable heterogeneous) group of SCI patients.

How we can relate our findings in Chapter 2 with the wealth of evidence showing reorganisation following sensory input loss? Most importantly, it remains unclear whether reorganisation following sensory input loss impacts the original functional representation of the deprived cortex (Jain et al., 2008; Merzenich et al., 1984; Pons et al., 1991). This is a particularly interesting question when considering evidence from other studies showing that the missing hand cortex in amputees is hyper-activated during intact hand movements (Makin, Cramer, et al., 2013; Philip & Frey, 2014). Does sensory input loss lead to a newly emerging (e.g. intact hand) functional representation while simultaneously maintaining the original functional representation? I.e., can persistent representation of a missing hand coincide with reorganisation? And if functional reorganisation and preservation of original function can co-occur, does this mean that they are subserved by separate neural mechanisms? These are important questions for future research.

The results presented in Chapter 2, showing preserved missing hand topography decades post arm amputation, were found using a protocol that depended on

amputees' exceptionally vivid phantom digit sensations, allowing them to voluntarily move each of the phantom digits. As such, it remains undetermined whether a relationship exists between the experience of phantom sensations and preserved missing hand topography. Our previous work (Makin, Scholz, et al., 2013) and the results presented in Chapters 3 and 4 show that phantom hand movements elicit activity in the primary sensorimotor missing hand territory in a heterogeneous group of amputees (in terms of phantom sensations). While this work may suggest that preserved missing hand representation is a general phenomenon, these studies focused on whole phantom hand movement net activity and, as such, do not provide information on the topographic features underlying the evoked phantom hand activity. It therefore remains to be investigated whether amputees experiencing less vivid phantom sensations also have preserved missing hand topography in S1. The protocol used in the current study was unable to answer this question, and further research is necessary to determine whether the preservation of missing hand topography depends on (or gives rise to) the experience of phantom sensations or whether it is a fundamental brain organising principle.

Can preserved organisation also be observed following other types of major sensory input loss, e.g. following loss of vision? A previous study by Baseler et al., (2011) demonstrated an absence of peripheral representation remapping in the occipital pole of human subjects who suffered foveal visual loss in adulthood. These results suggest that preserved organisation following major sensory input loss (as observed in Chapter 2) may be a fundamental brain principle. However, the authors were unable to target the representation of the foveal visual representation directly and are

therefore unable to make any claims whether the detailed retinotopic mapping of the deprived or freed-up cortex was preserved.

In the past decades, numerous treatments have been developed to reverse the cortical reorganisation changes that the maladaptive plasticity model suggests. However, our results (together with previous research and the clinical inefficacy of these treatments) suggest that the maladaptive theory is incorrect and instead emphasise the need to consider the peripheral attributes of PLP in future research. However, while our results suggest the involvement of peripheral mechanisms in PLP, conclusive causal evidence to link peripheral activity with persistent cortical representation is still lacking. Thus, there is a pressing need for an investigation combining fMRI, behavioural measures, and assessments of ectopic firing in the residual nerves and dorsal root ganglia.

While we have strong empirical reasons to speculate on the mechanism (as described above), it remains unresolved how the intervention tDCS protocol in Chapter 4 affected PLP. While our results demonstrate the involvement of the insula in PLP relief, we can only speculate how task-concurrent anodal tDCS over the primary sensorimotor missing hand cortex may have altered activity in this region. Furthermore, it would be interesting to investigate whether multiple consecutive sessions of our intervention stimulation would attain longer-lasting PLP relief. Lastly, it will be important to investigate whether more effective targeting of the insula in chronic PLP patients would achieve superior PLP relief.

While our research shows multiple correlations between clinical features and neural activity (i.e. PLP or PLP relief and neural activity, PLP and motor control, motor control and neural activity), we were unable to determine causation in these relationships. More research is needed to determine potential causation in these observed associations. Future developments in elucidating the causative mechanisms of PLP will aid the development of medically viable treatments that may help alleviate the suffering of PLP patients.

References

Ahmed, M. a, Mohamed, S. a, & Sayed, D. (2011). Long-term antalgic effects of repetitive transcranial magnetic stimulation of motor cortex and serum beta-endorphin in patients with phantom pain. *Neurological Research*, *33*(9), 953–958. https://doi.org/10.1179/1743132811Y.0000000045

Andrews, S. C., Hoy, K. E., Enticott, P. G., Daskalakis, Z. J., & Fitzgerald, P. B. (2011). Improving working memory: The effect of combining cognitive activity and anodal transcranial direct current stimulation to the left dorsolateral prefrontal cortex. *Brain Stimulation*, *4*(2), 84–89. https://doi.org/10.1016/j.brs.2010.06.004

Antal, A., Terney, D., Kühnl, S., & Paulus, W. (2010). Anodal Transcranial Direct Current Stimulation of the Motor Cortex Ameliorates Chronic Pain and Reduces Short Intracortical Inhibition. *Journal of Pain and Symptom Management*, *39*(5), 890–903. https://doi.org/10.1016/j.jpainsymman.2009.09.023

Apkarian, A., Bushnell, M., & P, S. (2013). Representation of Pain in the Brain. In *Textbook of Pain* (pp. 111–128). Elsevier Saunders.

Baron, R. (2006). Mechanisms of disease: neuropathic pain - a clinical perspective. *Nature Clinical Practice. Neurology*, *2*(2), 95–106. https://doi.org/10.1038/ncpneuro0113

Baseler, H. A., Gouws, A., Haak, K. V, Racey, C., Crossland, M. D., Tufail, A., … Morland, A. B. (2011). Large-scale remapping of visual cortex is absent in adult humans with macular degeneration. *Nature Neuroscience*, *14*(5), 649–655. https://doi.org/10.1038/nn.2793

Beaumont, G., Mercier, C., Michon, P. E., Malouin, F., & Jackson, P. L. (2011). Decreasing Phantom Limb Pain Through Observation of Action and Imagery: A Case Series. *Pain Medicine*, *12*(2), 289–299. https://doi.org/10.1111/j.1526-4637.2010.01048.x

Benjamini, Y., & Hochberg, Y. (1995). Controlling the false discovery rate : a practical and powerful approach to multiple testing. *Journal of the Royal Statistical Society. Series B (Methodological)*, *57*(1), 289–300.

Bensmaia, S. J., & Miller, L. E. (2014). Restoring sensorimotor function through intracortical interfaces: progress and looming challenges. *Nature Reviews Neuroscience*, *15*(5), 313–325. https://doi.org/10.1038/nrn3724

Berna, C., Leknes, S., Holmes, E. A., Edwards, R. R., Goodwin, G. M., & Tracey, I. (2010). Induction of Depressed Mood Disrupts Emotion Regulation Neurocircuitry and Enhances Pain Unpleasantness. *Biological Psychiatry*, *67*(11), 1083–1090. https://doi.org/10.1016/j.biopsych.2010.01.014

Besle, J., Sánchez-Panchuelo, R.-M., Bowtell, R., Francis, S., & Schluppeck, D. (2013). Single-subject fMRI mapping at 7 T of the representation of fingertips in S1: a comparison of event-related and phase-encoding designs. *Journal of Neurophysiology*, *109*(9), 2293–305. https://doi.org/10.1152/jn.00499.2012

Bland, J. M., & Altman, D. G. (2011). Correlation in restricted ranges of data. *BMJ (Clinical Research Ed.)*, *342*, d556. https://doi.org/10.1136/bmj.d556

Blume, K. R., Dietrich, C., Huonker, R., Götz, T., Sens, E., Friedel, R., … Weiss, T. (2014). Cortical reorganization after macroreplantation at the upper extremity: A magnetoencephalographic study. *Brain*, *137*(3), 757–769. https://doi.org/10.1093/brain/awt366

Bogdanov, S., Smith, J., & Frey, S. H. (2012). Former Hand Territory Activity

Increases After Amputation During Intact Hand Movements, but Is Unaffected by Illusory Visual Feedback. *Neurorehabilitation and Neural Repair*, *26*(6), 604–615. https://doi.org/10.1177/1545968311429687

Bolognini, N., Olgiati, E., Maravita, A., Ferraro, F., & Fregni, F. (2013). Motor and parietal cortex stimulation for phantom limb pain and sensations. *Pain*, *154*(8), 1274–1280. https://doi.org/10.1016/j.pain.2013.03.040

Bolognini, N., Spandri, V., Ferraro, F., Salmaggi, A., Molinari, A. C. L., Fregni, F., & Maravita, A. (2015). Immediate and sustained effects of 5-day transcranial direct current stimulation of the motor cortex in phantom limb pain. *The Journal of Pain*. https://doi.org/10.1016/j.jpain.2015.03.013

Borghi, B., D'Addabbo, M., White, P. F., Gallerani, P., Toccaceli, L., Raffaeli, W., … Mercuri, M. (2010). The use of prolonged peripheral neural blockade after lower extremity amputation: The effect on symptoms associated with phantom limb syndrome. *Anesthesia and Analgesia*, *111*(5), 1308–1315. https://doi.org/10.1213/ANE.0b013e3181f4e848

Boström, K. J., de Lussanet, M. H. E., Weiss, T., Puta, C., & Wagner, H. (2014). A computational model unifies apparently contradictory findings concerning phantom pain. *Scientific Reports*, *4*, 5298. https://doi.org/10.1038/srep05298

Bowering, K. J., O'Connell, N. E., Tabor, A., Catley, M. J., Leake, H. B., Moseley, G. L., & Stanton, T. R. (2013). The Effects of Graded Motor Imagery and Its Components on Chronic Pain: A Systematic Review and Meta-Analysis. *The Journal of Pain*, *14*(1), 3–13. https://doi.org/10.1016/j.jpain.2012.09.007

Brasil-Neto, J. P. (2012). Learning, memory, and transcranial direct current stimulation. *Frontiers in Psychiatry*, *3*(SEP). https://doi.org/10.3389/fpsyt.2012.00080

Brodmann, K. (1909). *Broadmann's Localisation in the Cerebral Cortex.* New York: Springer.

Chan, B. L., Witt, R., Charrow, A. P., Magee, A., Howard, R., Pasquina, P. F., … Tsao, J. W. (2007). Mirror therapy for phantom limb pain. *The New England Journal of Medicine*, *357*(21), 2206–7. https://doi.org/10.1056/NEJMc071927

Chand, P., & Jain, N. (2015). Intracortical and thalamocortical connections of the hand and face representations in somatosensory area 3b of macaque monkeys and effects of chronic spinal cord injuries. *Journal of Neuroscience*, *35*(39), 13475–13486. https://doi.org/10.1523/JNEUROSCI.2069-15.2015

Chivukula, S., Tempel, Z. J., Chen, C. J., Shin, S. S., Gande, A. V., & Moossy, J. J. (2015). Spinal and Nucleus Caudalis Dorsal Root Entry Zone Lesioning for Chronic Pain: Efficacy and Outcomes. *World Neurosurgery*, *84*(2), 494–504. https://doi.org/10.1016/j.wneu.2015.04.025

Ciaramitaro, P., Mondelli, M., Logullo, F., Grimaldi, S., Battiston, B., Sard, A., … Cocito, D. (2010). Traumatic peripheral nerve injuries: Epidemiological findings, neuropathic pain and quality of life in 158 patients. *Journal of the Peripheral Nervous System*, *15*(2), 120–127. https://doi.org/10.1111/j.1529-8027.2010.00260.x

Cohen Kadosh, R., Soskic, S., Iuculano, T., Kanai, R., & Walsh, V. (2010). Modulating neuronal activity produces specific and long-lasting changes in numerical competence. *Current Biology*, *20*(22), 2016–2020. https://doi.org/10.1016/j.cub.2010.10.007

Colloca, L., Ludman, T., Bouhassira, D., Baron, R., Dickenson, A. H., Yarnitsky, D., … Raja, S. N. (2017). Neuropathic pain. *Nature Reviews Disease Primers*, *3*, 17002. https://doi.org/10.1038/nrdp.2017.2

Corballis, M. C. (2009). Comparing a single case with a control sample: Refinements and extensions. *Neuropsychologia*. https://doi.org/10.1016/j.neuropsychologia.2009.04.007

Craig, A. D. (Bud). (2014). Topographically organized projection to posterior insular cortex from the posterior portion of the ventral medial nucleus in the long-tailed macaque monkey. *Journal of Comparative Neurology*, *522*(1), 36–63. https://doi.org/10.1002/cne.23425

Dale, A. M., Fischl, B., & Sereno, M. I. (1999). Cortical surface-based analysis. *NeuroImage*, *9*(2), 179–194. https://doi.org/10.1006/nimg.1998.0395

Devor, M., Vaso, A., Adahan, H. M., & Vyshka, G. (2014). PNS origin of phantom limb sensation and pain: Reply to Letter to the Editor regarding Foell et al., Peripheral origin of phantom limb pain: Is it all resolved? *Pain*, *155*(10), 2207–2208. https://doi.org/10.1016/j.pain.2014.08.018

Dice, L. R. (1945). Measures of the amount of ecologic association between species. *Ecology*, *26*(3), 297–302. https://doi.org/doi:10.2307/1932409

Diedrichsen, J., Ridgway, G. R., Friston, K. J., & Wiestler, T. (2011). Comparing the similarity and spatial structure of neural representations: A pattern-component model. *NeuroImage*, *55*(4), 1665–1678. https://doi.org/10.1016/j.neuroimage.2011.01.044

Diers, M., Christmann, C., Koeppe, C., Ruf, M., & Flor, H. (2010). Mirrored, imagined and executed movements differentially activate sensorimotor cortex in amputees with and without phantom limb pain. *Pain*, *149*(2), 296–304. https://doi.org/10.1016/j.pain.2010.02.020

Douaud, G., Filippini, N., Knight, S., Talbot, K., & Turner, M. R. (2011). Integration of structural and functional magnetic resonance imaging in amyotrophic lateral sclerosis. *Brain : A Journal of Neurology*, *134*(Pt 12), 3470–9. https://doi.org/10.1093/brain/awr279

Duerden, E. G., & Albanese, M. C. (2013). Localization of pain-related brain activation: A meta-analysis of neuroimaging data. *Human Brain Mapping*, *34*(1), 109–149. https://doi.org/10.1002/hbm.21416

Duff, E. P., Vennart, W., Wise, R. G., Howard, M. A., Harris, R. E., Lee, M., … Smith, S. M. (2015). Learning to identify CNS drug action and efficacy using multistudy fMRI data. *Science Translational Medicine*, *7*(274), 274ra16-274ra16. https://doi.org/10.1126/scitranslmed.3008438

Ejaz, N., Hamada, M., & Diedrichsen, J. (2015). Hand use predicts the structure of representations in sensorimotor cortex. *Nature Neuroscience*, *18*(7), 1034–1040.

Engel, S. A., Glover, G. G., & Wandell, B. A. (1997). Retintopic organization in human visual cortex and the spatial precision of functional MRI. *Cereb Cortex*, *7*(2), 181–192. https://doi.org/10.1093/cercor/7.2.181

Farrar, J. T., Young, J. P., LaMoreaux, L., Werth, J. L., & Poole, R. M. (2001). Clinical importance of changes in chronic pain intensity measured on an 11-point numerical pain rating scale. *Pain*, *94*(2), 149–158. https://doi.org/10.1016/S0304-3959(01)00349-9

Feldman, D. E., & Brecht, M. (2005). Map plasticity in somatosensory cortex. *Science*, *310*(November), 810–815. https://doi.org/10.1126/science.1115807

Finnerup, N. B., Sindrup, S. H., & Jensen, T. S. (2010). The evidence for pharmacological treatment of neuropathic pain. *Pain*, *150*(3), 573–581. https://doi.org/10.1016/j.pain.2010.06.019

Fischl, B., Liu, A., & Dale, A. M. (2001). Automated manifold surgery: Constructing geometrically accurate and topologically correct models of the human cerebral

cortex. *IEEE Transactions on Medical Imaging*, *20*(1), 70–80. https://doi.org/10.1109/42.906426

Fleiss, J., Levin, B., & Cho Paik, M. (2003). Statistical Methods for Rates and Proportions. *John Wiley & Sons*, 800. https://doi.org/10.1198/tech.2004.s812

Flesher, S. N., Collinger, J. L., Foldes, S. T., Weiss, J. M., Downey, J. E., Tyler-Kabara, E. C., … Gaunt, R. A. (2016). Intracortical microstimulation of human somatosensory cortex. *Science Translational Medicne*, 1–11. https://doi.org/10.1126/scitranslmed.aaf8083

Flor, H. (2002). Phantom-limb pain: Characteristics, causes, and treatment. *Lancet Neurology*. https://doi.org/10.1016/S1474-4422(02)00074-1

Flor, H., Diers, M., & Andoh, J. (2013). The neural basis of phantom limb pain. *Trends in Cognitive Sciences*. https://doi.org/10.1016/j.tics.2013.04.007

Flor, H., Elbert, T., Knecht, S., Wienbruch, C., Pantev, C., Birbaumer, N., … Taub, E. (1995). Phantom-limb pain as a perceptual correlate of cortical reorganization following arm amputation. *Nature*, *375*(6531), 482–484.

Flor, H., Elbert, T., Mühlnickel, W., Pantev, C., Wienbruch, C., & Taub, E. (1998). Cortical reorganization and phantom phenomena in congenital and traumatic upper-extremity amputees. *Experimental Brain Research*, *119*(2), 205–212. https://doi.org/10.1007/s002210050334

Flor, H., Nikolajsen, L., & Staehelin Jensen, T. (2006). Phantom limb pain: a case of maladaptive CNS plasticity? *Nature Reviews Neuroscience*, *7*(11), 873–881.

Florence, S. L. (1998). Large-Scale Sprouting of Cortical Connections After Peripheral Injury in Adult Macaque Monkeys. *Science*, *282*(5391), 1117–1121. https://doi.org/10.1126/science.282.5391.1117

Foell, J., Andoh, J., Bekrater-Bodmann, R., Diers, M., Fuchs, X., Colloca, L., & Flor, H. (2014). Peripheral origin of phantom limb pain: Is it all resolved? *Pain*, *155*(10), 2205–2206. https://doi.org/10.1016/j.pain.2014.08.028

Foell, J., Bekrater-Bodmann, R., Diers, M., & Flor, H. (2014). Mirror therapy for phantom limb pain: Brain changes and the role of body representation. *European Journal of Pain (United Kingdom)*, *18*(5), 729–739. https://doi.org/10.1002/j.1532-2149.2013.00433.x

Franklin, D. W., & Wolpert, D. M. (2011). Computational mechanisms of sensorimotor control. *Neuron*, *72*(3), 425–442. https://doi.org/10.1016/j.neuron.2011.10.006

Fried, K., Govrin-Lippmann, R., Rosenthal, F., Ellisman, M. H., & Devor, M. (1991). Ultrastructure of afferent axon endings in a neuroma. *Journal of Neurocytology*, *20*, 682–701. https://doi.org/10.1007/BF01187069

Gagné, M., Reilly, K. T., Hétu, S., & Mercier, C. (2009). Motor control over the phantom limb in above-elbow amputees and its relationship with phantom limb pain. *Neuroscience*, *162*(1), 78–86.

Garcia-Larrea, L. (2012). The posterior insular-opercular region and the search of a primary cortex for pain. *Neurophysiologie Clinique*. https://doi.org/10.1016/j.neucli.2012.06.001

Gill, J., Shah-Basak, P. P., & Hamilton, R. (2015). It's the thought that counts: Examining the task-dependent effects of transcranial direct current stimulation on executive function. *Brain Stimulation*, *8*(2), 253–259. https://doi.org/10.1016/j.brs.2014.10.018

Graziano, M. S. A., & Aflalo, T. N. (2007). Mapping behavioral repertoire onto the cortex. *Neuron*, *56*(2), 239–251. https://doi.org/10.1016/j.neuron.2007.09.013

Greve, D. N., & Fischl, B. (2009). Accurate and robust brain image alignment using

boundary-based registration. *NeuroImage*, *48*(1), 63–72. https://doi.org/10.1016/j.neuroimage.2009.06.060

Grüsser, S. M., Mühlnickel, W., Schaefer, M., Villringer, K., Christmann, C., Koeppe, C., & Flor, H. (2004). Remote activation of referred phantom sensation and cortical reorganization in human upper extremity amputees. *Experimental Brain Research*, *154*(1), 97–102. https://doi.org/10.1007/s00221-003-1649-4

Grüsser, S. M., Winter, C., Mühlnickel, W., Denke, C., Karl, A., Villringer, K., & Flor, H. (2001). The relationship of perceptual phenomena and cortical reorganization in upper extremity amputees. *Neuroscience*, *102*(2), 263–272. https://doi.org/10.1016/S0306-4522(00)00491-7

Hahamy, A., Macdonald, S. N., van den Heiligenberg, F. M. Z., Kieliba, P., Emir, U., Malach, R., … Makin, T. R. (2017). Representation of multiple body parts in the missing hand territory of congenital one-handers. *Current Biology*.

Harris, A. J. (1999). Cortical origin of pathological pain. *Lancet*. https://doi.org/10.1016/S0140-6736(99)05003-5

Hsu, T., Juan, C., & Tseng, P. (2016). Individual Differences and State-Dependent Responses in Transcranial Direct Current Stimulation. *Frontiers in Human Neuroscience*, *10*(December), 643. https://doi.org/10.3389/FNHUM.2016.00643

Iannetti, G. D., Zambreanu, L., Wise, R. G., Buchanan, T. J., Huggins, J. P., Smart, T. S., … Tracey, I. (2005). Pharmacological modulation of pain-related brain activity during normal and central sensitization states in humans. *Proceedings of the National Academy of Sciences*, *102*(50), 18195–18200. https://doi.org/10.1073/pnas.0506624102

Jain, N., Catania, K. C., & Kaas, J. H. (1998). A histologically visible representation of the fingers and palm in primate area 3b and its immutability following long-term deafferentations. *Cerebral Cortex*, *8*(3), 227–236. https://doi.org/10.1093/cercor/8.3.227

Jain, N., Florence, S. L., Qi, H. X., & Kaas, J. H. (2000). Growth of new brainstem connections in adult monkeys with massive sensory loss. *Proceedings of the National Academy of Sciences of the United States of America*, *97*(10), 5546–50. https://doi.org/10.1073/pnas.090572597

Jain, N., Qi, H.-X., Collins, C. E., & Kaas, J. H. (2008). Large-scale reorganization in the somatosensory cortex and thalamus after sensory loss in macaque monkeys. *The Journal of Neuroscience : The Official Journal of the Society for Neuroscience*, *28*(43), 11042–11060. https://doi.org/10.1523/JNEUROSCI.2334-08.2008

Jenkinson, M., Bannister, P., Brady, M., & Smith, S. M. (2002). Improved optimization for the robust and accurate linear registration and motion correction of brain images. *NeuroImage*, *17*(2), 825–841. https://doi.org/10.1016/S1053-8119(02)91132-8

Jenkinson, M., Beckmann, C. F., Behrens, T. E. J., Woolrich, M. W., & Smith, S. M. (2012). FSL. *NeuroImage*, *62*(2), 782–790. https://doi.org/10.1016/j.neuroimage.2011.09.015

Jenkinson, M., & Smith, S. M. (2001). A global optimization method for robust affine registration of brain images. *Medical Imaging Analysis*, *5*, 143–156.

Jutzeler, C. R., Curt, A., & Kramer, J. L. K. (2015). Relationship between chronic pain and brain reorganization after deafferentation: A systematic review of functional MRI findings. *NeuroImage: Clinical*, *9*, 599–606. https://doi.org/10.1016/j.nicl.2015.09.018

Jutzeler, C. R., Freund, P., Huber, E., Curt, A., & Kramer, J. L. K. (2015).

Neuropathic pain and functional reorganization in the primary sensorimotor cortex after spinal cord injury. *The Journal of Pain*, *16*(12), 1256–1267. https://doi.org/10.1016/j.jpain.2015.08.008

Kaas, J. H. (1993). The functional organization of somatosensory cortex in primates. *Annals of Anatomy*. https://doi.org/10.1016/S0940-9602(11)80212-8

Kaas, J., Nelson, R., Sur, M., Lin, C., & Merzenich, M. (1979). Multiple representations of the body within the primary somatosensory cortex of primates. *Science*, *204*(4392), 521–523. https://doi.org/10.1126/science.107591

Kambi, N., Halder, P., Rajan, R., Arora, V., Chand, P., Arora, M., & Jain, N. (2014). Large-scale reorganization of the somatosensory cortex following spinal cord injuries is due to brainstem plasticity. *Nature Communications*, *5*, 3602. https://doi.org/10.1038/ncomms4602

Kambi, N., Tandon, S., Mohammed, H., Lazar, L., & Jain, N. (2011). Reorganization of the Primary Motor Cortex of Adult Macaque Monkeys after Sensory Loss Resulting from Partial Spinal Cord Injuries. *Journal of Neuroscience*, *31*(10), 3696–3707. https://doi.org/10.1523/JNEUROSCI.5187-10.2011

Kandel, E. R., Schwartz, J. H., & Jessell, T. M. (2000). *Principles of Neural Science*. *Neurology* (Vol. 4). https://doi.org/10.1036/0838577016

Karl, A., Birbaumer, N., Lutzenberger, W., Cohen, L. G., & Flor, H. (2001). Reorganization of motor and somatosensory cortex in upper extremity amputees with phantom limb pain. *The Journal of Neuroscience : The Official Journal of the Society for Neuroscience*, *21*(10), 3609–18. https://doi.org/21/10/3609 [pii]

Katz, J., & Melzack, R. (1990). Pain "memories" in phantom limbs: review and clinical observations. *Pain*, *43*(3), 319–336. https://doi.org/10.1016/0304-3959(90)90029-D

Kikkert, S., Johansen-Berg, H., Tracey, I., & Makin, T. R. (n.d.). Reaffirming the link between chronic phantom limb pain and maintained missing hand representation. *Under Revisions*.

Kikkert, S., Kolasinski, J., Jbabdi, S., Tracey, I., Beckmann, C. F., Johansen-Berg, H., & Makin, T. R. (2016). Revealing the neural fingerprints of a missing hand. *eLife*, *5*, e15292. https://doi.org/10.7554/eLife.15292

Knecht, S., Henningsen, H., Elbert, T., Flor, H., Höhling, C., Pantev, C., & Taub, E. (1996). Reorganizational and perceptional changes after amputation. *Brain*, *119 (Pt 4*, 1213–1219. https://doi.org/10.1093/brain/119.4.1213

Knotkova, H., Cruciani, Tronnier, & Rasche. (2012). Current and future options for the management of phantom-limb pain. *Journal of Pain Research*, 39.

Kolasinski, J., Makin, T. R., Jbabdi, S., Clare, S., Stagg, C. J., & Johansen-Berg, H. (2016). Investigating the stability of fine-grain digit somatotopy in individual human participants. *Journal of Neuroscience*, *36*(4), 1113–1127.

Lang, N., Siebner, H. R., Ward, N. S., Lee, L., Nitsche, M. A., Paulus, W., … Frackowiak, R. S. (2005). How does transcranial DC stimulation of the primary motor cortex alter regional neuronal activity in the human brain? *European Journal of Neuroscience*, *22*(2), 495–504. https://doi.org/10.1111/j.1460-9568.2005.04233.x

Lefaucheur, J. (2016). Cortical neurostimulation for neuropathic pain: state of the art and perspectives. *Pain*, *157 Suppl*(2), S81-9. https://doi.org/10.1097/j.pain.0000000000000401

Lefaucheur, J.-P., Antal, A., Ahdab, R., Ciampi de Andrade, D., Fregni, F., Khedr, E. M., … Paulus, W. (2008). The use of repetitive transcranial magnetic stimulation (rTMS) and transcranial direct current stimulation (tDCS) to relieve pain. *Brain*

Stimulation, *1*(4), 337–44. https://doi.org/10.1016/j.brs.2008.07.003
Lefaucheur, J.-P., Antal, A., Ayache, S. S., Benninger, D. H., Brunelin, J., Cogiamanian, F., … Paulus, W. (2017). Evidence-based guidelines on the therapeutic use of transcranial direct current stimulation (tDCS). *Clinical Neurophysiology*, *128*(1), 56–92. https://doi.org/10.1016/j.clinph.2016.10.087
Lefaucheur, J. P., Drouot, X., Ménard-Lefaucheur, I., Keravel, Y., & Nguyen, J. P. (2006). Motor cortex rTMS restores defective intracortical inhibition in chronic neuropathic pain. *Neurology*, *67*(9), 1568–1574. https://doi.org/10.1212/01.wnl.0000242731.10074.3c
Lin, R. L., Douaud, G., Filippini, N., Okell, T. W., Stagg, C. J., & Tracey, I. (2017). Structural Connectivity Variances Underlie Functional and Behavioral Changes During Pain Relief Induced by Neuromodulation. *Scientific Reports*, *7*(December 2016), 41603. https://doi.org/10.1038/srep41603
London, B. M., & Miller, L. E. (2013). Responses of somatosensory area 2 neurons to actively and passively generated limb movements. *Journal of Neurophysiology*, *109*(6), 1505–13. https://doi.org/10.1152/jn.00372.2012
Lotze, M., Flor, H., Grodd, W., Larbig, W., & Birbaumer, N. (2001). Phantom movements and pain. An fMRI study in upper limb amputees. *Brain*, *124*(Pt 11), 2268–2277. https://doi.org/10.1093/brain/124.11.2268
MacIver, K., Lloyd, D. M., Kelly, S., Roberts, N., & Nurmikko, T. (2008). Phantom limb pain, cortical reorganization and the therapeutic effect of mental imagery. *Brain*, *131*(Pt 8), 2181–91. https://doi.org/10.1093/brain/awn124
MacLachlan, M., McDonald, D., & Waloch, J. (2004). Mirror treatment of lower limb phantom pain: a case study. *Disability and Rehabilitation*, *26*(14–15), 901–904. https://doi.org/10.1080/09638280410001708913
Makin, T. R., & Bensmaia, S. J. (2017). Stability of Sensory Topographies in Adult Cortex. *Trends in Cognitive Sciences*, *21*(3), 195–204. https://doi.org/10.1016/j.tics.2017.01.002
Makin, T. R., Cramer, A. O., Scholz, J., Hahamy, A., Henderson Slater, D., Tracey, I., & Johansen-Berg, H. (2013). Deprivation-related and use-dependent plasticity go hand in hand. *eLife*, *2*, 1–15. https://doi.org/10.7554/eLife.01273
Makin, T. R., Filippini, N., Duff, E. P., Henderson Slater, D., Tracey, I., & Johansen-Berg, H. (2015). Network-level reorganisation of functional connectivity following arm amputation. *NeuroImage*, *114*, 217–225. https://doi.org/10.1016/j.neuroimage.2015.02.067
Makin, T. R., Scholz, J., Filippini, N., Henderson Slater, D., Tracey, I., & Johansen-Berg, H. (2013). Phantom pain is associated with preserved structure and function in the former hand area. *Nature Communications*, *4*, 1570. https://doi.org/10.1038/ncomms2571
Makin, T. R., Scholz, J., Henderson Slater, D., Johansen-Berg, H., & Tracey, I. (2015). Reassessing cortical reorganization in the primary sensorimotor cortex following arm amputation. *Brain*, *138*(8), 2140–2146. https://doi.org/10.1093/brain/awv161
Mancini, F., Haggard, P., Iannetti, G. D., Longo, M. R., & Sereno, M. I. (2012). Fine-grained nociceptive maps in primary somatosensory cortex. *Journal of Neuroscience*, *32*(48), 17155–17162. https://doi.org/10.1523/JNEUROSCI.3059-12.2012
Mazzola, L., Isnard, J., & Mauguière, F. (2006). Somatosensory and pain responses to stimulation of the second somatosensory area (SII) in humans. A comparison with SI and insular responses. *Cerebral Cortex*, *16*(7), 960–968.

https://doi.org/10.1093/cercor/bhj038
Mazzola, L., Isnard, J., Peyron, R., Guénot, M., & Mauguière, F. (2009). Somatotopic organization of pain responses to direct electrical stimulation of the human insular cortex. *Pain*, *146*(1–2), 99–104. https://doi.org/10.1016/j.pain.2009.07.014
Mazzola, L., Isnard, J., Peyron, R., & Mauguire, F. (2012). Stimulation of the human cortex and the experience of pain: Wilder Penfield's observations revisited. *Brain*, *135*(2), 631–640. https://doi.org/10.1093/brain/awr265
McCabe, C. S., Haigh, R. C., Halligan, P. W., & Blake, D. R. (2005). Simulating sensory-motor incongruence in healthy volunteers: Implications for a cortical model of pain. *Rheumatology*, *44*(4), 509–516. https://doi.org/10.1093/rheumatology/keh529
Mercier, C., & Leonard, G. (2011). Interactions between pain and the motor cortex: Insights from research on phantom limb pain and complex regional pain syndrome. *Physiotherapy Canada*, *63*(3), 305–314. https://doi.org/10.3138/ptc.2010-08p
Mercier, C., Reilly, K. T., Vargas, C. D., Aballea, A., & Sirigu, A. (2006). Mapping phantom movement representations in the motor cortex of amputees. *Brain*, *129*(8), 2202–2210. https://doi.org/10.1093/brain/awl180
Merzenich, M. M., Kaas, J. H., Wall, J., Nelson, R. J., Sur, M., & Felleman, D. (1983). Topographic reorganization of somatosensory cortical areas 3b and 1 in adult monkeys following restricted deafferentation. *Neuroscience*, *8*(1), 33–55. https://doi.org/10.1016/0306-4522(83)90024-6
Merzenich, M. M., Nelson, R. J., Stryker, M. P., Cynader, M. S., Schoppmann, A., & Zook, J. M. (1984). Somatosensory cortical map changes following digit amputation in adult monkeys. *The Journal of Comparative Neurology*, *224*(4), 591–605.
Mezue, M., & Makin, T. R. (2016). Immutable body representations: lessons from phantoms in amputees. In *Body and the Self, Revisited*. MIT Press volume.
Moeller, S., Yacoub, E., Olman, C. A., Auerbach, E., Strupp, J., Harel, N., & Ugurbil, K. (2010). Multiband multislice GE-EPI at 7 tesla, with 16-fold acceleration using partial parallel imaging with application to high spatial and temporal whole-brain FMRI. *Magnetic Resonance in Medicine*, *63*(5), 1144–1153. https://doi.org/10.1002/mrm.22361
Mohan, A., & Vanneste, S. (2016). Adaptive and maladaptive neural compensatory consequences of sensory deprivation-From a phantom percept perspective. *Progress in Neurobiology*. https://doi.org/10.1016/j.pneurobio.2017.03.010
Moseley, G. L. (2006). Graded motor imagery for pathologic pain: A randomized controlled trial. *Neurology*, *67*(12), 2129–2134. https://doi.org/10.1212/01.wnl.0000249112.56935.32
Moseley, G. L., & Flor, H. (2012). Targeting cortical representations in the treatment of chronic pain: a review. *Neurorehabilitation and Neural Repair*, *26*(6), 646–52. https://doi.org/10.1177/1545968311433209
Moseley, G. L., Gallace, A., & Spence, C. (2012). Bodily illusions in health and disease: Physiological and clinical perspectives and the concept of a cortical "body matrix." *Neuroscience and Biobehavioral Reviews*. https://doi.org/10.1016/j.neubiorev.2011.03.013
Myers, A., & Hansen, C. (2006). Experimental psychology. *Experimental Psychology*. Retrieved from http://ovidsp.ovid.com/ovidweb.cgi?T=JS&PAGE=reference&D=psyc5&NEWS

=N&AN=2005-11404-000
Nitsche, M. A., & Paulus, W. (2000). Excitability changes induced in the human motor cortex by weak transcranial direct current stimulation. *The Journal of Physiology*, *527*(3), 633–639. https://doi.org/10.1111/j.1469-7793.2000.t01-1-00633.x
Nordin, M., Nystrom, B., Wallin, U., & Hagbarth, K. E. (1984). Ectopic sensory discharges and paresthesiae in patients with disorders of peripheral nerves, dorsal roots and dorsal columns. *Pain*, *20*(3), 231–245. https://doi.org/10.1016/0304-3959(84)90013-7
Nystrom, B., & Hagbarth, K. E. (1981). Microelectrode recordings from transected nerves in amputees with phantom limb pain. *Neuroscience Letters*, *27*(2), 211–216. https://doi.org/10.1016/0304-3940(81)90270-6
Orlov, T., Makin, T. R., & Zohary, E. (2010). Topographic representation of the human body in the occipitotemporal cortex. *Neuron*, *68*(3), 586–600. https://doi.org/10.1016/j.neuron.2010.09.032
Ortiz-Catalan, M., Guðmundsdóttir, R. A., Kristoffersen, M. B., Zepeda-Echavarria, A., Caine-Winterberger, K., Kulbacka-Ortiz, K., … Hermansson, L. (2016). Phantom motor execution facilitated by machine learning and augmented reality as treatment for Phantom Limb Pain. *The Lancet*, *388*(10062), 2885–289. https://doi.org/10.1016/S0140-6736(16)31598-7
Parazzini, M., Fiocchi, S., Rossi, E., Paglialonga, A., & Ravazzani, P. (2011). Transcranial Direct Current Stimulation: Estimation of the Electric Field and of the Current Density in an Anatomical Human Head Model. *IEEE Transactions on Biomedical Engineering*, *58*(6), 1773–1780. https://doi.org/10.1109/TBME.2011.2116019
Park, C., Chang, W. H., Ohn, S. H., Kim, S. T., Bang, O. Y., Pascual-Leone, A., & Kim, Y.-H. (2011). Longitudinal changes of resting-state functional connectivity during motor recovery after stroke. *Stroke; a Journal of Cerebral Circulation*, *42*(5), 1357–62. https://doi.org/10.1161/STROKEAHA.110.596155
Paulhus, D.L., Vazire, S. (2005). The Self-Report Method. *Handbook of Research Methods in Personality Psychology*, 224–239.
Penfield, W., & Boldrey, E. (1937). Somatic motor and sensory representation in the cerebral cortex of man as studied by electrical stimulation. *Brain*, *60*(4), 389–443. https://doi.org/10.1093/brain/60.4.389
Penfield, W., & Rasmussen, T. (1950). The Cerebral Cortex of Man. A Clinical Study of Localization of Function.pdf. *Academic Medicine*. https://doi.org/10.1097/00001888-195009000-00037
Philip, B. A., & Frey, S. H. (2014). Compensatory changes accompanying chronic forced use of the nondominant hand by unilateral amputees. *The Journal of Neuroscience*, *34*(10), 3622–31. https://doi.org/10.1523/JNEUROSCI.3770-13.2014
Polanía, R., Paulus, W., & Nitsche, M. A. (2012). Modulating cortico-striatal and thalamo-cortical functional connectivity with transcranial direct current stimulation. *Human Brain Mapping*, *33*(10), 2499–2508. https://doi.org/10.1002/hbm.21380
Pons, T. P., Garraghty, P. E., Ommaya, A. K., Kaas, J. H., Taub, E., & Mishkin, M. (1991). Massive cortical reorganization after sensory deafferentation in adult macaques. *Science (New York, N.Y.)*, *252*(5014), 1857–60.
Prestor, B. (2001). Microsurgical junctional DREZ coagulation for treatment of deafferentation pain syndromes. *Surgical Neurology*, *56*(4), 259–265.

https://doi.org/10.1016/S0090-3019(01)00600-0
Raffin, E., Giraux, P., & Reilly, K. T. (2012). The moving phantom: Motor execution or motor imagery? *Cortex*, *48*(6), 746–757. https://doi.org/10.1016/j.cortex.2011.02.003
Raffin, E., Mattout, J., Reilly, K. T., & Giraux, P. (2012). Disentangling motor execution from motor imagery with the phantom limb. *Brain*, *135*(2), 582–595. https://doi.org/10.1093/brain/awr337
Raffin, E., Richard, N., Giraux, P., & Reilly, K. T. (2016). Primary motor cortex changes after amputation correlate with phantom limb pain and the ability to move the phantom limb. *NeuroImage*, *130*, 134–144. https://doi.org/10.1016/j.neuroimage.2016.01.063
Raineteau, O., & Schwab, M. E. (2001). Plasticity of motor systems after incomplete spinal cord injury. *Nature Reviews Neuroscience*, *2*(4), 263–273. https://doi.org/10.1038/35067570
Ramachandran, V. S., & Hirstein, W. (1998). The perception of phantom limbs. The D. O. Hebb lecture. *Brain*, *121*(9), 1603–1630. https://doi.org/10.1093/brain/121.9.1603
Ramachandran, V. S., & Rogers-Ramachandran, D. (1996). Synaesthesia in phantom limbs induced with mirrors. *Proceedings of the Royal Society of London*, *263*(1369), 377–86. https://doi.org/10.1098/rspb.1996.0058
Ramachandran, V. S., Stewart, M., & Rogers-Ramachandran, D. C. (1992). Perceptual correlates of massive cortical reorganization. *Neuroreport*, *3*(7), 583–586. https://doi.org/10.1126/science.1439826
Reilly, K. T., Mercier, C., Schieber, M. H., & Sirigu, A. (2006). Persistent hand motor commands in the amputees' brain. *Brain*, *129*(8), 2211–2223. https://doi.org/10.1093/brain/awl154
Reilly, K. T., & Sirigu, A. (2008a). Neuroscientist The Motor Cortex and Its Role in Phantom Limb Phenomena Phantom Limb Phenomena. *The Neuroscientist*, *14*(November 2007), 195–202. https://doi.org/10.1177/1073858407309466
Reilly, K. T., & Sirigu, A. (2008b). The motor cortex and its role in phantom limb phenomena. *The Neuroscientist : A Review Journal Bringing Neurobiology, Neurology and Psychiatry*, *14*(2), 195–202. https://doi.org/10.1177/1073858407309466
Reis, J., Schambra, H. M., Cohen, L. G., Buch, E. R., Fritsch, B., Zarahn, E., … Krakauer, J. W. (2009). Noninvasive cortical stimulation enhances motor skill acquisition over multiple days through an effect on consolidation. *Proceedings of the National Academy of Sciences of the United States of America*, *106*(5), 1590–1595. https://doi.org/10.1073/pnas.0805413106
Rolke, R., Magerl, W., Campbell, K. A., Schalber, C., Caspari, S., Birklein, F., & Treede, R. D. (2006). Quantitative sensory testing: A comprehensive protocol for clinical trials. *European Journal of Pain*, *10*(1), 77–88. https://doi.org/10.1016/j.ejpain.2005.02.003
Rossi, S., Hallett, M., Rossini, P. M., Pascual-Leone, A., Avanzini, G., Bestmann, S., … Ziemann, U. (2009). Safety, ethical considerations, and application guidelines for the use of transcranial magnetic stimulation in clinical practice and research. *Clinical Neurophysiology*. https://doi.org/10.1016/j.clinph.2009.08.016
Rothgangel, S. A., Braun, M. S., Beurskens, J. A., Seitz, J. R., & Wade, T. D. (2011). The clinical aspects of mirror therapy in rehabilitation: a systematic review of the literature. *International Journal of Rehabilitation Research*, *34*(1), 1–13. https://doi.org/10.1097/MRR.0b013e3283441e98

Samii, M., Bear-Henney, S., Lüdemann, W., Tatagiba, M., & Blömer, U. (2001). Treatment of refractory pain after brachial plexus avulsion with dorsal root entry zone lesions. *Neurosurgery*, *48*(6), 1269–1277. https://doi.org/10.1227/00006123-200106000-00016

Sanchez-Panchuelo, R. M., Francis, S., Bowtell, R., & Schluppeck, D. (2010). Mapping human somatosensory cortex in individual subjects with 7T functional MRI. *Journal of Neurophysiology*, *103*(5), 2544–2556. https://doi.org/10.1152/jn.01017.2009

Schweinhardt, P., Kalk, N., Wartolowska, K., Chessell, I., Wordsworth, P., & Tracey, I. (2008). Investigation into the neural correlates of emotional augmentation of clinical pain. *NeuroImage*, *40*(2), 759–766. https://doi.org/10.1016/j.neuroimage.2007.12.016

Segerdahl, A. R., Mezue, M., Okell, T. W., Farrar, J. T., & Tracey, I. (2015). The dorsal posterior insula subserves a fundamental role in human pain. *Nature Neuroscience*, *18*(4), 499–500. https://doi.org/10.1038/nn.3969

Sereno, M. I., & Huang, R.-S. (2006). A human parietal face area contains aligned head-centered visual and tactile maps. *Nature Neuroscience*, *9*(10), 1337–43. https://doi.org/10.1038/nn1777

Serra, J., Duan, W. R., Locke, C., Solà, R., Liu, W., & Nothaft, W. (2015). Effects of a T-type calcium channel blocker, ABT-639, on spontaneous activity in C-nociceptors in patients with painful diabetic neuropathy: a randomized controlled trial. *Pain*, *156*(11), 2175–83. https://doi.org/10.1097/j.pain.0000000000000249

Silvanto, J., Muggleton, N., & Walsh, V. (2008). State-dependency in brain stimulation studies of perception and cognition. *Trends in Cognitive Sciences*, *12*(12), 447–454. https://doi.org/10.1016/j.tics.2008.09.004

Smirnakis, S. M., Brewer, A. A., Schmid, M. C., Tolias, A. S., Schüz, A., Augath, M., … Logothetis, N. K. (2005). Lack of long-term cortical reorganization after macaque retinal lesions. *Nature*, *435*(7040), 300–307. https://doi.org/10.1038/nature03495

Smith, S. M. (2002). Fast robust automated brain extraction. *Human Brain Mapping*, *17*(3), 143–155. https://doi.org/10.1002/hbm.10062

Smith, S. M., Jenkinson, M., Woolrich, M. W., Beckmann, C. F., Behrens, T. E. J., Johansen-Berg, H., … Matthews, P. M. (2004). Advances in functional and structural MR image analysis and implementation as FSL. *NeuroImage*, *23*(SUPPL. 1), 208–219. https://doi.org/10.1016/j.neuroimage.2004.07.051

Stagg, C. J., Lin, R. L., Mezue, M., Segerdahl, A., Kong, Y., Xie, J., & Tracey, I. (2013). Widespread Modulation of Cerebral Perfusion Induced during and after Transcranial Direct Current Stimulation Applied to the Left Dorsolateral Prefrontal Cortex. *Journal of Neuroscience*, *33*(28), 11425–11431. https://doi.org/10.1523/JNEUROSCI.3887-12.2013

Tan, D. W., Schiefer, M. A., Keith, M. W., Anderson, J. R., Tyler, J., & Tyler, D. J. (2014). A neural interface provides long-term stable natural touch perception. *Science Translational Medicine*, *6*(257), 257ra138-257ra138. https://doi.org/10.1126/scitranslmed.3008669

Teixeira, M. J., da Paz, M. G. da S., Bina, M. T., Santos, S. N., Raicher, I., Galhardoni, R., … de Andrade, D. C. (2015). Neuropathic pain after brachial plexus avulsion--central and peripheral mechanisms. *BMC Neurology*, *15*, 73. https://doi.org/10.1186/s12883-015-0329-x

Thieme, H., Morkisch, N., Rietz, C., Dohle, C., & Borgetto, B. (2016). The efficacy of movement representation techniques for treating limb pain - a systematic

review and meta-analysis. *The Journal of Pain*, *17*(2), 167–180. https://doi.org/10.1016/j.jpain.2015.10.015

Tracey, I. (2013). "Seeing" how our drugs work brings translational added value. *Anesthesiology*, *119*(6), 1247–8. https://doi.org/10.1097/ALN.0000000000000018

Ugurbil, K., Xu, J., Auerbach, E. J., Moeller, S., Vu, A. T., Duarte-Carvajalino, J. M., … Yacoub, E. (2013). Pushing spatial and temporal resolution for functional and diffusion MRI in the Human Connectome Project. *NeuroImage*, *80*, 80–104. https://doi.org/10.1016/j.neuroimage.2013.05.012

van den Heiligenberg, F. M. Z., Yeung, N., Brugger, P., Culham, J. C., & Makin, T. R. (2017). Adaptable Categorization of Hands and Tools in Prosthesis Users Adaptable Categorization of Hands and Tools in Prosthesis Users. *Psychological Science*, (January). https://doi.org/10.1177/0956797616685869

Vaso, A., Adahan, H.-M., Gjika, A., Zahaj, S., Zhurda, T., Vyshka, G., & Devor, M. (2014). Peripheral nervous system origin of phantom limb pain. *Pain*, *155*(7), 1384–1391. https://doi.org/10.1016/j.pain.2014.04.018

Vlaeyen, J. W., & Linton, S. J. (2000). Fear-avoidance and its consequences in chronic musculoskeletal pain: a state of the art. *Pain*, *85*(3), 317–32. https://doi.org/S0304395999002420 [pii]

von Hehn, C. A., Baron, R., & Woolf, C. J. (2012). Deconstructing the Neuropathic Pain Phenotype to Reveal Neural Mechanisms. *Neuron*. https://doi.org/10.1016/j.neuron.2012.02.008

VS., R. (1993). Behavioral and magnetoencephalographic correlates of plasticity in the adult human brain. *Proceedings of the National Academy of Sciences of the United States of America*, *90*(22 PG-10413-20), 10413–10420. https://doi.org/10.1073/pnas.90.22.10413

Wager, T. D., Atlas, L. Y., Lindquist, M. A., Roy, M., Woo, C.-W., & Kross, E. (2013). An fMRI-Based Neurologic Signature of Physical Pain. *New England Journal of Medicine*, *368*(15), 1388–1397. https://doi.org/10.1056/NEJMoa1204471

Wandell, B. A., Dumoulin, S. O., & Brewer, A. A. (2007). Visual field maps in human cortex. *Neuron.*, *56*(2), 366–383. https://doi.org/10.1016/j.neuron.2007.10.012

Wanigasekera, V., Mezue, M., Andersson, J., Kong, Y., & Tracey, I. (2016). Disambiguating Pharmacodynamic Efficacy from Implications for Analgesic Drug Development. *Anesthesiology*, *124*(1), 159–168. https://doi.org/10.1097/ALN.0000000000000924

Weeks, S. R., Anderson-Barnes, V. C., & Tsao, J. W. (2010). Phantom Limb Pain. *The Neurologist*, *16*(5), 277–286. https://doi.org/10.1097/NRL.0b013e3181edf128

Wiech, K., & Tracey, I. (2009). The influence of negative emotions on pain: Behavioral effects and neural mechanisms. *NeuroImage*. https://doi.org/10.1016/j.neuroimage.2009.05.059

Woods, A. J., Antal, A., Bikson, M., Boggio, P. S., Brunoni, A. R., Celnik, P., … Nitsche, M. A. (2016). A technical guide to tDCS, and related non-invasive brain stimulation tools. *Clinical Neurophysiology*, *127*(2), 1031–1048. https://doi.org/10.1016/j.clinph.2015.11.012

Woolf, C. J. (2011). Central sensitization: Implications for the diagnosis and treatment of pain. *Pain*. https://doi.org/10.1016/j.pain.2010.09.030

Woolrich, M. W., Behrens, T. E. J., Beckmann, C. F., Jenkinson, M., & Smith, S. M.

(2004). Multilevel linear modelling for FMRI group analysis using Bayesian inference. *NeuroImage*, *21*(4), 1732–1747. https://doi.org/10.1016/j.neuroimage.2003.12.023

Woolrich, M. W., Jbabdi, S., Patenaude, B., Chappell, M., Makni, S., Behrens, T. E. J., … Smith, S. M. (2009). Bayesian analysis of neuroimaging data in FSL. *NeuroImage*, *45*(1 Suppl), S173–S186. https://doi.org/10.1016/j.neuroimage.2008.10.055

Xu, J., Moeller, S., Auerbach, E. J., Strupp, J., Smith, S. M., Feinberg, D. A., … Uğurbil, K. (2013). Evaluation of slice accelerations using multiband echo planar imaging at 3T. *NeuroImage*, *83*, 991–1001. https://doi.org/10.1016/j.neuroimage.2013.07.055

Yanagisawa, T., Fukuma, R., Seymour, B., Hosomi, K., Kishima, H., Shimizu, T., … Saitoh, Y. (2016). Induced sensorimotor brain plasticity controls pain in phantom limb patients. *Nature Communications*, 13209. https://doi.org/10.1038/ncomms13209

Yousry, T. A., Schmid, U. D., Alkadhi, H., Schmidt, D., Peraud, A., Buettner, A., & Winkler, P. (1997). Localization of the motor hand area to a knob on the precentral gyrus. A new landmark. *Brain*, *120*(1), 141–157. https://doi.org/10.1093/brain/120.1.141

Zeharia, N., Hertz, U., Flash, T., & Amedi, A. (2015). New whole-body sensory-motor gradients revealed using phase-locked analysis and verified using multivoxel pattern analysis and functional connectivity. *Journal of Neuroscience*, *35*(7), 2845–2859. https://doi.org/10.1523/Jneurosci.4246-14.2015

Appendices

Supplementary Materials Chapter 2

Supplementary Tables and Figures

	High field scans					Standard field scans	
	Missing hand map	**Missing hand overlap**	**Intact hand map**	**Intact hand overlap**	**Bimanual digit map**	**Bimanual digit map**	**Missing hand overlap**
Above elbow	x	x	x	x	x	-	-
Below elbow	x	x	x	x	x	-	-
Brachial plexus	-	-	-	-	-	x	x
C1	x	x	x	x	x	x	x
C2	x	x	x	x	x	x	x
C3	x	x	x	x	x	x	x
C4	x	x	x	x	x	x	x
C5	x	x	-	-	-	-	-
C6	x	x	-	-	-	-	-
C7	x	x	-	-	-	-	-
C8	x	x	-	-	-	-	-
C9	x	x	-	-	-	-	-
C10	x	x	-	-	-	-	-
C11	x	x	-	-	-	-	-

Table A.2.1: Runs acquired for each participant. x = acquired; - = not acquired.

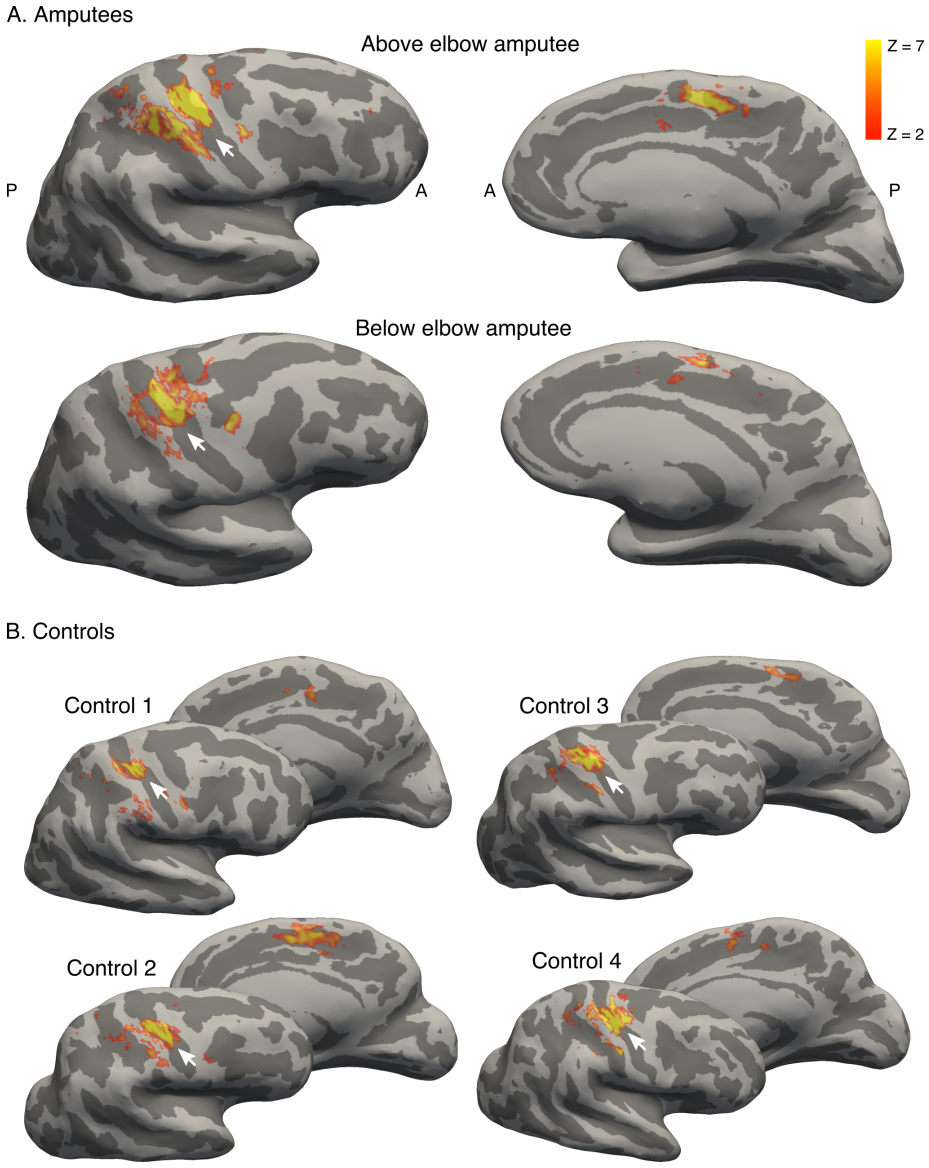


Figure A.2.1: Areas activated by phantom hand movement. Contrast between phantom (amputees; A) or left (controls; B) hand movements and baseline (rest) in the block design, projected on cortical surfaces of the contralateral hemisphere. Analysis was performed using a standard 2-level general linear model. Amputees and controls showed activation in primary somatosensory and motor cortex (S1 and M1, respectively; left panel), as well as in the supplementary motor area (SMA, right panel). Note that more inferior areas (e.g. secondary somatosensory cortex) were not covered by the partial field of view utilised for the ultra-high field acquisition. White arrows indicate the central sulcus. A = anterior; P = posterior. Displayed activations were thresholded at $Z > 2$. These results show that phantom hand movements activate a network of brain areas normally associated with hand movement.

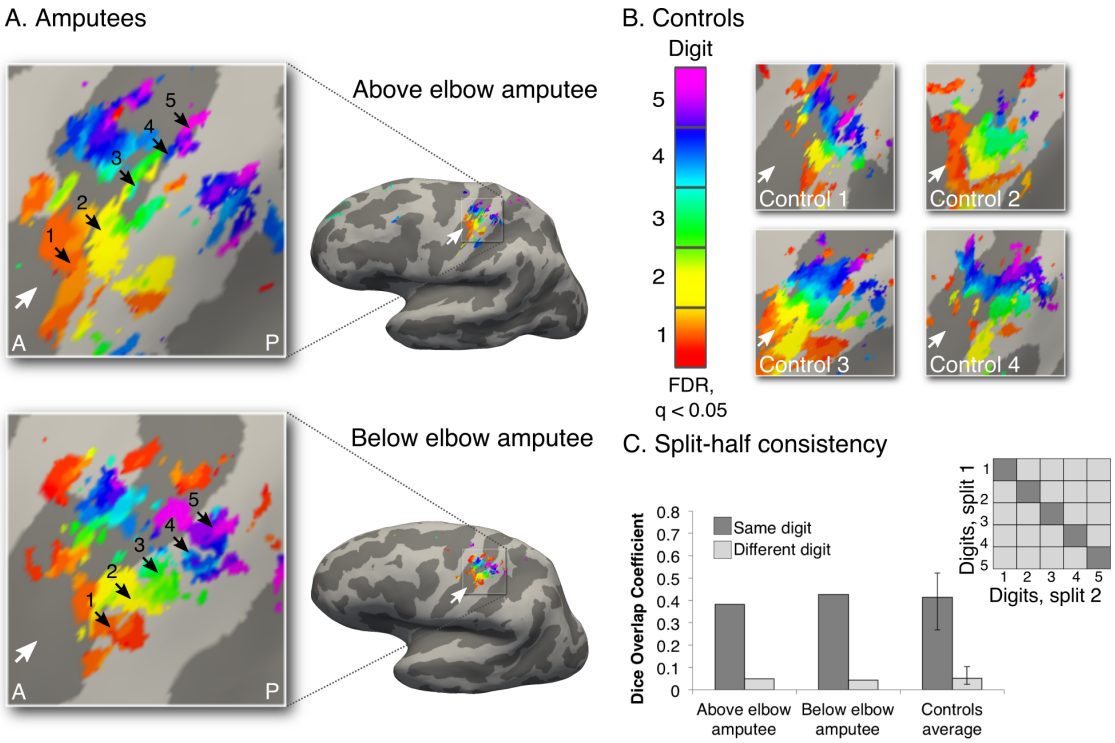


Figure A.2.2: Intact hand maps in amputees. In order to visualise standard topography in the amputees' somatosensory cortex, topographic mapping was also carried out for the intact hand. For this purpose, task demands were adjusted to optimally activate the somatosensory cortex. Participants were provided with tactile feedback via a MRI-compatible button-box (manufactured in house), placed on the participant's torso for the duration of the scan. Participants pressed the button box with the relevant digit using a travelling wave paradigm (Figure 2.1). Since this task did not involve any difficulty for the amputees as it only consisted of moving digits of the intact hand, all participants were paced to perform button press movements with individual digits at a set (1Hz) frequency, as indicated by the flashing of the corresponding circle at the specified rate. A forward and backward sequence was employed in separate runs. Each of the forward and backward runs was repeated twice, for a total duration of 25min and 40s. All other procedures and analysis were as described in the main analysis for the missing hand digit maps (Figure 2.2). The black arrows indicate preferences for digits 1-5: thumb (red); index (yellow); middle (green); ring (blue) and little finger (purple) for the intact hand in amputees (A) and two handed controls (B). White arrows indicate the central sulcus. A = anterior; P = posterior. Multiple comparisons were adjusted using false discovery rate (FDR). (C) Intra-individual split-half consistency was assessed using the Dice overlap coefficient for the digit maps. "Same"-digit selective clusters (dark) showed significantly greater consistency than "different"-digit clusters (light) in amputees and controls. Error bars

indicate 95% confidence intervals. Note that the organisation, extent and consistency of the digit maps qualitatively resembled the left (missing) hand maps (obtained using self-paced digit flexion and extension) found in both controls and amputees (Figure 2.2).

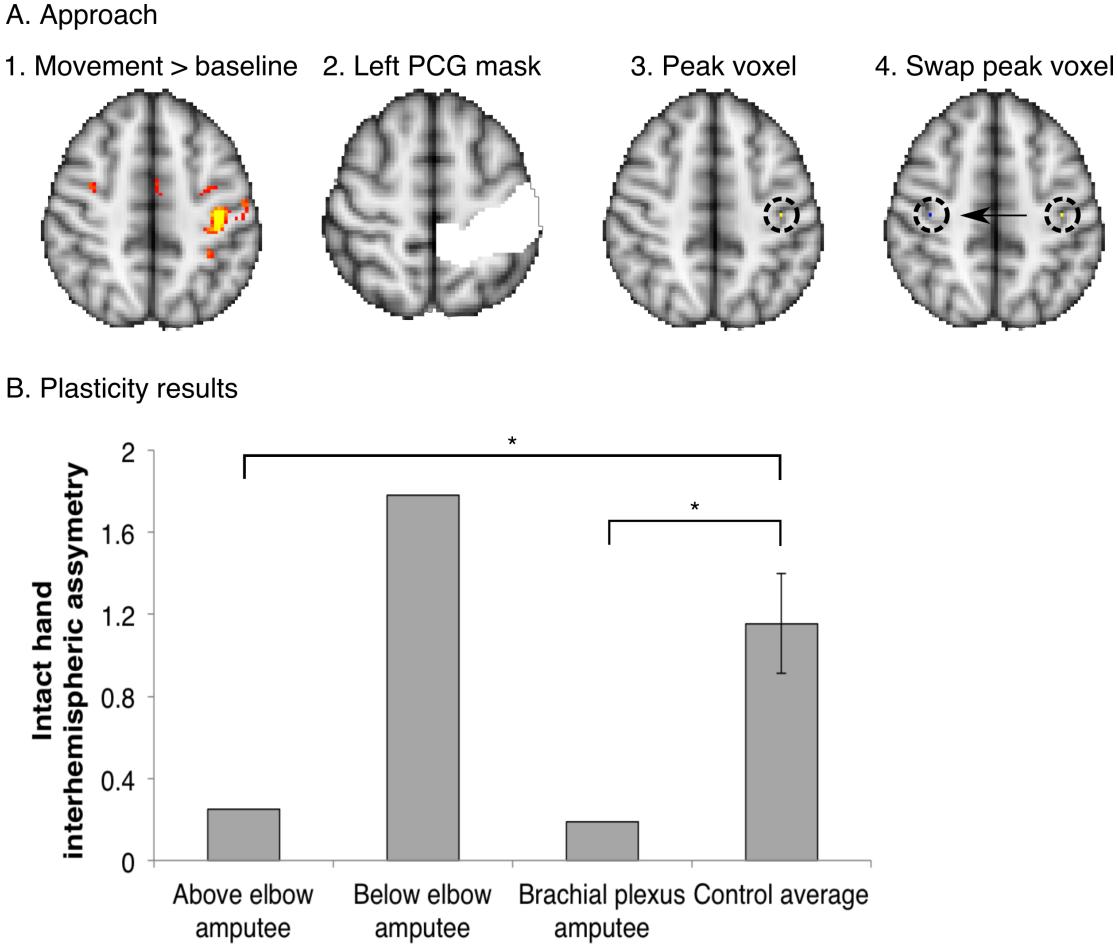


Figure A.2.3: Over-representation of the intact hand in the missing hand territory. To investigate whether the observed missing hand maps (Figure 2.2, Figure 2.5) were preserved despite reorganisation of displaced inputs (as reported previously (Makin, Cramer, et al., 2013)), we quantified intact hand representation in the territory of the missing hand in the amputees participating in the current study. For this purpose, we employed an independent dataset (described in Chapters 4 and 5), acquired using standard field neuroimaging (acquisition parameters were identical to those described in the materials and methods section, with the exception of the number of acquisition volumes). (A) Participants were cued to perform movements with their intact hand (simultaneous flexion and extension of all five digits), or dominant hand in controls (n = 15), as part of a block-design protocol, used to identify body-part representations (see (Makin, Cramer, et al., 2013) for details of a similar protocol). This movement condition was contrasted against a baseline (rest) period and standardised (z) beta values during intact/dominant hand movements were extracted from the peak voxel within a postcentral gyrus (PCG) mask in the contralateral hemisphere. To identify the estimated position of the missing hand territory, this peak voxel was mirror flipped on the axial plane, and the standardised beta value for intact hand activity was extracted

from this ROI in the ipsilateral hemisphere. (B) To assess asymmetry in intact hand activity across the two hemisphere, the following inter-hemispheric asymmetry index was calculated for each of the three amputees and 15 controls individually: (contralateral hemisphere – ipsilateral hemisphere) / (contralateral hemisphere + ipsilateral hemisphere). Higher values of this index indicate that the activity pattern for the intact hand was greater in the contralateral, compared to the ipsilateral sensorimotor hand area, as found in the control participants. Lower values in this index represent less asymmetry, resulting from (relatively) higher activity in the ipsilateral hand area during intact hand movements. Error bars indicate 95% confidence intervals. The above elbow and brachial plexus amputees showed significantly lower asymmetry than controls (one-tailed Crawford and Howell t-test (Corballis, 2009); $t(14) = -1.84$, $p = 0.04$; and $t(14) = -1.96$, $p = 0.04$ respectively). The below elbow amputee showed a high asymmetry value, similar to controls (one-tailed Crawford and Howell t-test (Corballis, 2009); $t(14) = 1.26$, $p = 0.11$). This indicates that two of the tested amputees show over-representation of their intact hand in the missing hand territory, as previously reported (Makin, Cramer, et al., 2013). These results suggest that the missing hand maps can be preserved while reorganisation of displaced inputs from the intact hand has taken place.

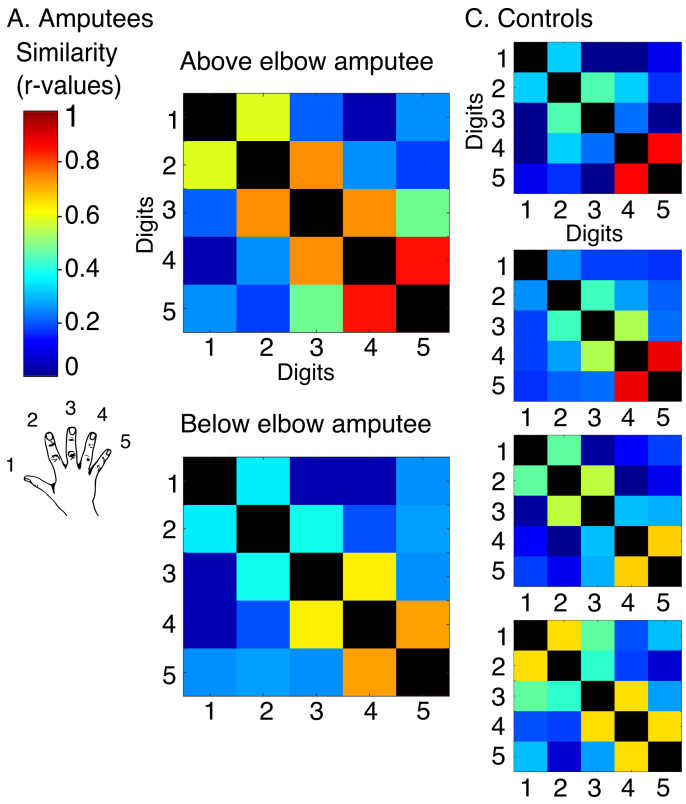


Figure A.2.4: Intact hand inter-digit overlap in amputees. In order to visualise standard topography in the amputees' somatosensory cortex, inter-digit representational similarity was assessed for multivoxel patterns underlying the right (intact) hand maps shown in Figure A.2.2 in amputees (intact hand, A) and controls (dominant hand, B). To estimate inter-digit representational similarity for the intact hand, the same blocked design as described in the materials and methods section missing hand inter-digit overlap was used. Tactile feedback (from the button box) was incorporated into the task to optimally activate the somatosensory cortex. Participants were instructed to perform single digit button presses (using an MRI-compatible button-box manufactured in house) with their right intact (amputees) or right dominant (controls) hand at a 1Hz frequency. To cue the participant which digit should be moved, the circle corresponding to this digit flashed at the specified 1Hz rate. Digits 1-5: thumb; index; middle; ring and little finger.

Supplementary Materials Chapter 4

Supplementary Materials & Methods

A.4.1 Scanning procedures

Baseline body localiser

To assess the neural encoding of phantom/non-dominant hand movements at baseline in amputees and controls, a baseline body localiser scan was acquired in the first experimental session, i.e. prior to any tDCS stimulation. Scanning procedures, MRI data acquisition and preprocessing was similar to that of the body localiser scans acquired post tDCS (see main text Chapter 4).

Baseline resting state

To assess functional connectivity in amputees and controls, a resting state scan was obtained at baseline in the first experimental session, i.e. prior to any tDCS application. Participants were instructed to lie still, stay awake, keep their eyes open, stare at the screen and let their mind wonder while a fixation cross was displayed on the screen.

A.4.2 MRI data acquisition and analysis

Movement quality during stimulation

Quality of phantom hand movements made during the stimulation period was assessed offline in a subset of 11 amputees, using video recordings. The bimanual runs, in which amputees were instructed to use their intact hand to mirror the precise degree and speed of movement of the phantom hand, were inspected and scored by a

blinded experimenter. Specially, we focused on the phantom hand movements during the hand opening/closing and ring finger flexion movements. These movements were chosen to represent a relatively easy and a more difficult phantom movement (respectively).

To rate the quality of movement, the hand movements were rated from 1 (full movement) to 4 (barely any movement) was used. For the hand opening/closing movement this ranging was specified by: 1- opening/closing past 90°; 2, fingers opening to 90°; 3, fingers flexed 45°; 4, fingers flexed less than 45° (i.e., a twitch). For the ring finger flexing: 1, ring finger flexed past 90°; 2, ring finger flexed up to 90°; 3, ring finger flexed 45°; 4, finger flexed less than 45°. A movement score was calculated for each stimulation session by dividing the total count of movements made by the rated quality of the movements. No significant differences in movement scores were found between conditions (phantom hand opening/closing: $X^2_{(3)} = 2.68$, $p = 0.443$; phantom ring finger flexion: $X^2_{(3)} = 1.04$, $p = 0.792$). We therefore suggest that differences between stimulation sessions as found in behavioural and fMRI results, were not caused by differences in movement during stimulation.

Baseline body localiser

Preprocessing and image registration of the baseline body localisers was similar to that applied for the post-tDCS body localiser scans. As for the post-tDCS body localisers, first-level (time-series) parameter estimates were computed using a voxel-based general linear model (GLM), as implemented in FEAT. Each condition in the block design was convolved with a double-gamma HRF function, and its temporal derivative was used to model the activation time course. One main contrast was

defined between different task movement conditions: phantom (or non-dominant) hand versus feet.

Scrubbing was applied to remove residual motion effects: All fMRI data were assessed for excessive motion using the motion estimate outputs from MCFLIRT. Volumes with estimated absolute mean displacement greater than 1mm (half of the functional voxel size) were scrubbed (amputees: scrubbing applied in 29% of all scans, maximum percentage of volumes scrubbed in a given session: 1%; controls: scrubbing applied in 7% of all scans, maximum percentage of volumes scrubbed in a given session: 1%).

Group level analysis was carried out using FMRIB's Local Analysis of Mixed Effects (Woolrich et al., 2004). A whole brain average map was created for the amputees' phantom hand versus feet movement contrast. Whole brain differences between the amputees and control group were tested for the phantom (or non-dominant) hand versus feet movement contrast. Z statistic images were thresholded using clusters determined by $Z > 2.3$ and a family- wise-error-corrected cluster significance threshold of $P < 0.05$ was applied to the suprathreshold clusters.

Baseline resting state

Functional images for the resting state scan was acquired using the same T2*-weighted multiband sequence as was used for the body localiser scan (see main text), with the exception of 230 acquired volumes. Similar preprocessing and registration to that for body localiser scans was applied for the resting state scans.

Individual time series were extracted using a missing hand ROI that was defined based on control's average non-dominant hand activation (see main methods for further details on ROI definition). These missing hand cortex time series were then used as individual 'seeds' to model the activation time course for a further first-level FEAT analysis (with white matter and cerebrospinal fluid time series as nuisance regressors). Head motion parameters were included as nuisance regressors in individual scans. All fMRI data was further assessed for excessive motion using motion estimate outputs from MCFLIRT. Volumes with estimated absolute mean displacement greater than 1mm (half of the functional voxel size) were scrubbed to remove residual motion effects (amputees: scrubbing applied in 7% of all scans, maximum percentage of volumes scrubbed in a given session: 1%; controls: scrubbing applied in 7% of all scans, maximum percentage of volumes scrubbed in a given session: <1%).

We conducted an ROI analysis to examine the resting state functional connectivity between the missing hand cortex and right and left insula. Averaged percent signal change was extracted from all voxels underlying anatomical left and right insular ROIs.

Supplementary Results

A.4.3 Phantom hand activity and resting state functional connectivity at baseline in amputees

Phantom hand movements activity in amputees

As visualised in Figure A.4.2, phantom hand movements in amputees recruited brain areas that are normally associated with hand movement. Importantly, as shown previously (Makin, Scholz, et al., 2013; see also Chapter 3), amputees activated the primary sensorimotor missing hand cortex during phantom hand movements. Amputees and two-handed control participants did not differentially activate their contralateral primary sensorimotor cortex during phantom/non-dominant hand movements at baseline. However, amputees showed increased excitability in bilateral insula (see Figure A.4.4A), in particular in bilateral mid- and posterior insula, compared to controls.

Amputees have increased functional connectivity between missing hand cortex and bilateral insula

Amputees showed increased functional connectivity at rest between the primary sensorimotor missing hand cortex and the ipsilateral ($t_{(28)}$ = -2.75, p = 0.01) and contralateral ($t_{(28)}$ = -3.82, p = 0.001) insula at baseline, compared to two-handed control participants (see Figure A.4.4B).

As the insula has been suggested to adhere to right/left lateralisation, the same functional resting state analysis was conducted prior to the flipping of the brains. We found that amputees show increased functional connectivity at rest between the

primary sensorimotor missing hand cortex with the right ($t_{(28)}$ = -2.99 p = 0.006) and left insula ($t_{(28)}$ = -3.81, p = 0.001), compared to controls.

Supplementary Tables and Figures

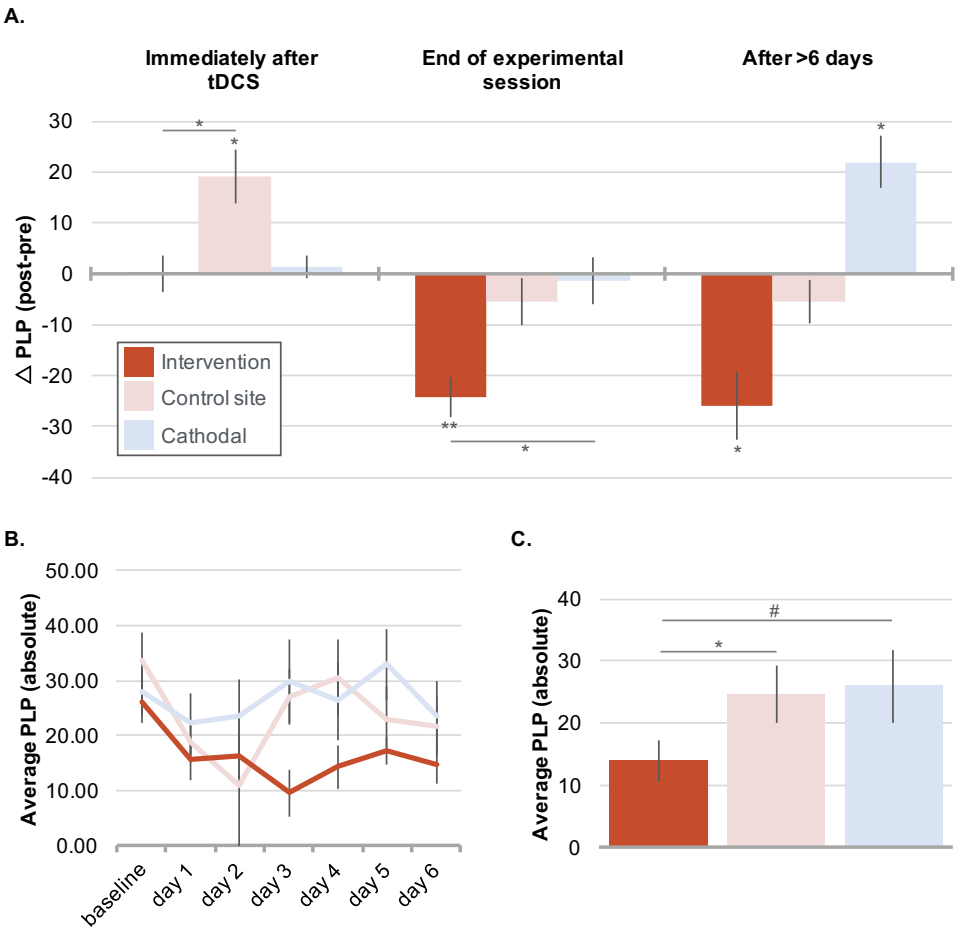


Figure A.4.1: Phantom limb pain effects in the control site and cathodal stimulation condition. (A) PLP effects achieved by the different stimulation conditions, as asses in the experimental sessions. To account for inter-subject variability, post-tDCS PLP ratings were contrasted with their respective baselines. As such, positive values on the y-axis indicate PLP increases and negative values indicate PLP relief. The intervention condition is shown in dark red, for comparison. The control site condition is depicted in pink and the cathodal condition in blue. (A, left) While PLP was significantly increased in the control site condition (as for sham, see Figure 4.1) immediately after stimulation offset, no such PLP change was observed for the intervention and cathodal conditions. There was a significant difference in PLP change between the intervention and control site condition. (A, middle) At the end of the experimental session, no PLP change was observed in the control site and cathodal stimulation conditions. In the intervention condition, however, PLP was significantly relieved. The PLP change was significantly different between the intervention and cathodal stimulation conditions. A trend towards a difference in PLP change was found

between the intervention and control site condition. (A, right) In the following session (at least one week after the previous experimental session), there was no longer a change in PLP in the control site condition, but significant PLP relief was observed for the intervention condition. PLP was significantly increased in the cathodal stimulation condition. (B&C) A second measure of longer-term tDCS effects on PLP was obtained using text messages, asking amputees to rate their average PLP on a daily basis. Note that no difference scores were calculated for this measure and as such, the y-axis reflects absolute PLP ratings. (C) PLP ratings over the course of 6 days post stimulation. (D) The results in (C) tested as a main effect. In the week after stimulation, PLP was significantly lower in the intervention condition, compared to both the control site and cathodal stimulation conditions. All annotations are as in Figure 4.1.

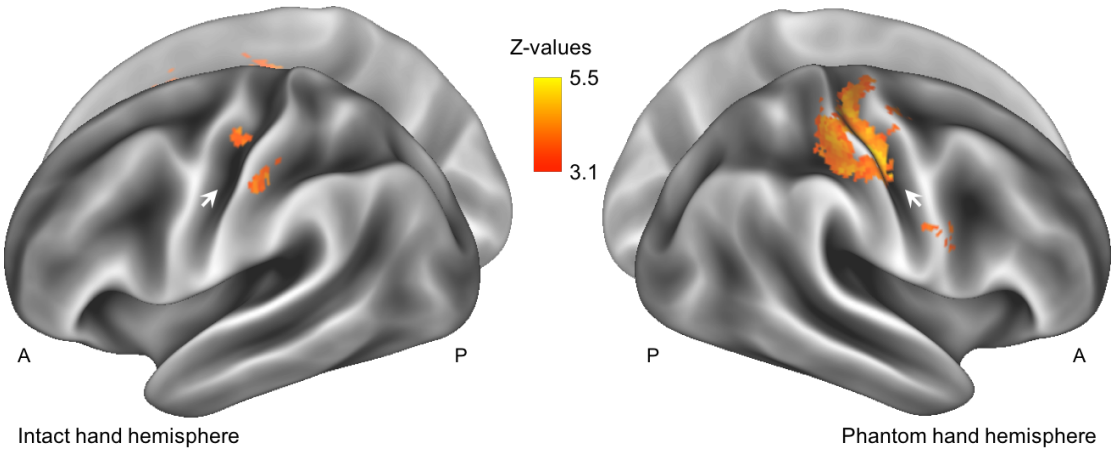


Figure A.4.2: Areas activated by phantom hand movement. Contrast between phantom hand movements and baseline (rest) in the first baseline body localiser scan. Amputees activated the primary somatosensory and motor hand cortex (S1 and M1, respectively) contralateral to the missing hand. These results show that phantom hand movements activate brain areas normally associated with hand movement. White arrows indicate the central sulcus. A = anterior; P = posterior.

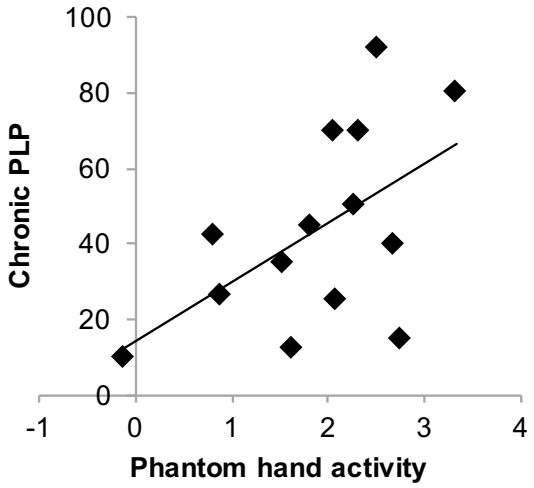


Figure A.4.3: Chronic phantom limb pain relates to maintained cortical phantom hand representation. Amputees suffering worse chronic phantom limb pain activated the phantom hand cortex more strongly during phantom hand movement ($r = 0.55$, $p = 0.04$). Phantom hand movement activity was extracted from the first baseline measurement.

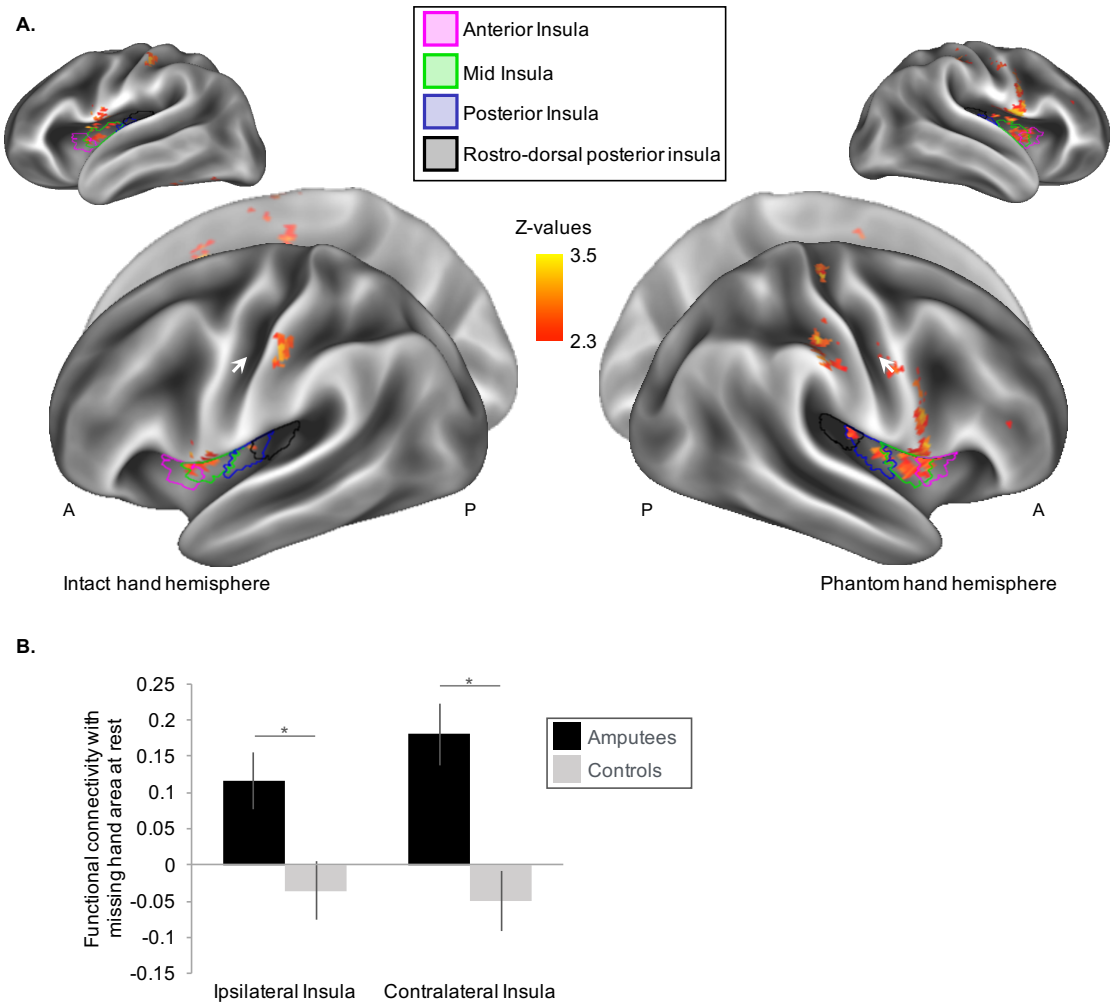


Figure A.4.4: Hyperactivity and hyperconnectivity in amputees' insular cortex at baseline. Functional connectivity at rest and task-related activity during phantom hand were compared between amputees and controls. (A) Amputees show increased BOLD response (hereafter excitability) in bilateral insula during phantom hand movements, compared to two-handed controls, when moving their non-dominant hand. White arrows indicate the central sulcus. A = anterior; P = posterior. (B) Functional connectivity at rest was examined by means of a 'seed' of the primary sensorimotor missing hand cortex. We conducted an ROI analysis to examine the resting state functional connectivity between the missing hand cortex and right and left insula. Averaged percent signal change was extracted from all voxels underlying anatomical left and right insular ROIs. Amputees had increased functional connectivity (hereafter hyperconnectivity) between the primary sensorimotor missing hand cortex and bilateral insula, compared to two-handed controls.

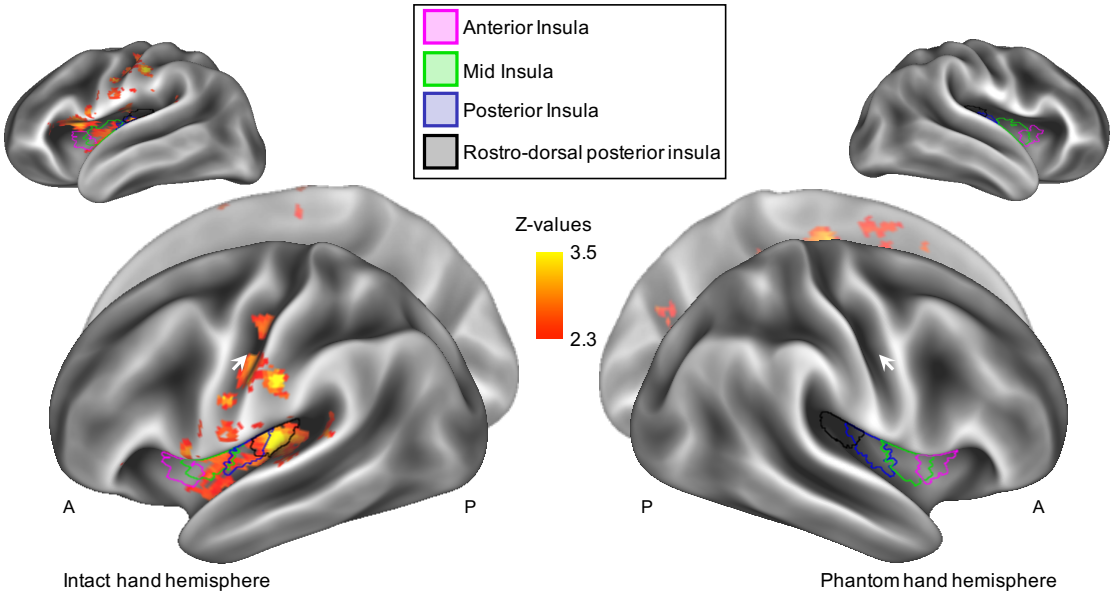


Figure A.4.5: Phantom pain relief is associated with increased insular recruitment during intervention. To assess the neural correlates of PLP relief, we carried out a whole brain regression analysis of phantom hand movement activity during intervention stimulation, using pain relief as measured at the end of the experimental session as a regressor. We found that increased activity in the ipsilateral insula, S2, and other areas was predictive of subsequent PLP relief. White arrows indicate the central sulcus. A = anterior; P = posterior.

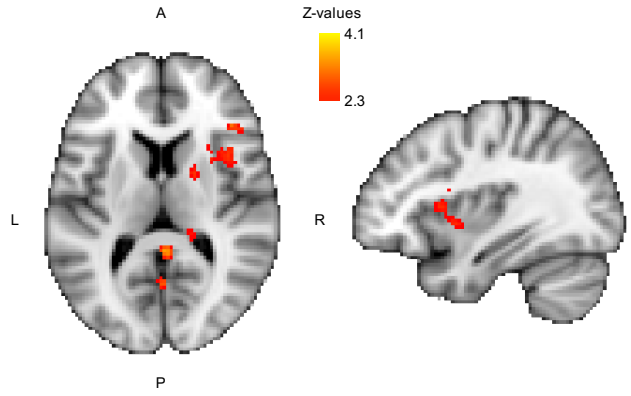


Figure A.4.6: Increased right insular recruitment during stimulation predicts a subsequent downregulation of sensorimotor phantom hand activity post stimulation. To assess the neural correlates of sensorimotor downregulation in brain regions that adhere to right/left lateralisation, as opposed to ipsilateral/contralateral lateralisation, we repeated the analysis described in Figure 4.3 in brains that were not flipped (i.e. the primary sensorimotor missing hand cortex was not aligned). In short, we conducted a regression analysis using the phantom hand movement activity levels underlying the cluster shown in Figure 4.2A as a whole brain regressor of phantom hand movement activity during intervention. Increased right insular recruitment during task-concurrent intervention stimulation was predictive of a subsequent downregulation of activity in the primary sensorimotor missing hand cortex. A = anterior; P = posterior; L = left; R = right.

Supplementary Materials Chapter 5

Supplementary Results, Tables and Figures

As in the main results section of Chapter 5, here we focus on the normalised measure for phantom hand movements, i.e. phantom minus intact hand response times. To confirm that the results were not driven by intact hand response times, results were also examined for phantom hand response times and intact hand response times alone. These results are summarised in Table A.5.1. All results reported below were similar for phantom hand response times only, unless stated otherwise.

A.5.1 Bimanual test performance as a measure for task consistency

Besides showing inter-session consistency by means of the ICC measure, test consistency for phantom hand movements was confirmed by demonstrating a strong correlation in response times between bimanual and phantom hand movements (phantom minus intact hand: $r = 0.77$, $p = 0.001$; phantom hand: $r = 0.81$, $p < 0.001$). No such correlation was found between bimanual and intact hand movements ($r = 0.11$, $p = 0.71$). Amputees were significantly slower in performing the bimanual task, both compared to the phantom and intact hands ($t_{(13)} = 6.06$, $p < 0.001$ and $t_{(13)} = 3.32$, $p = 0.005$, respectively).

A.5.2 Movement execution difficulty

Movement difficulty ratings showed a similar pattern of results as those of the response times. Inter-session consistency for phantom hand movement difficulty was considered fair, as indicated by an ICC value of 0.52 with 95% CI = 0.25-0.79 ($F_{(12,36)}$

= 5.36, $p < 0.001$) (Fleiss et al., 2003). Average difficulty ratings were used for further analysis.

Results obtained using difficulty ratings reflected deteriorated phantom hand motor control (Figure A.5.1). Amputees' perceived phantom hand movements as more difficult compared to the control group ($U = 0$, $p < 0.001$). When considering phantom hand and intact hand movement difficulty separately, amputees' phantom hand movements were perceived as more difficult, both compared to the intact hand ($Z = -3.18$, $p = 0.001$) and compared to controls ($U = 24.50$, $p < 0.001$). No difference in difficulty was found between dominant and non-dominant hand movements in controls ($Z = -1.14$, $p = 0.26$).

There was a trend towards a relationship between phantom hand movement difficulty and chronic PLP. Amputees experiencing worse chronic PLP found it more difficult to perform phantom hand movements ($r = 0.50$, $p = 0.08$). No relationship existed between phantom hand movement difficulty and chronic phantom sensation experience ($r_s = -0.39$, $p = 0.19$). Furthermore, no significant correlation was found between phantom hand movement difficulty in the individual sessions and transient PLP (average $r_s = 0.07$, $p = 0.81$).

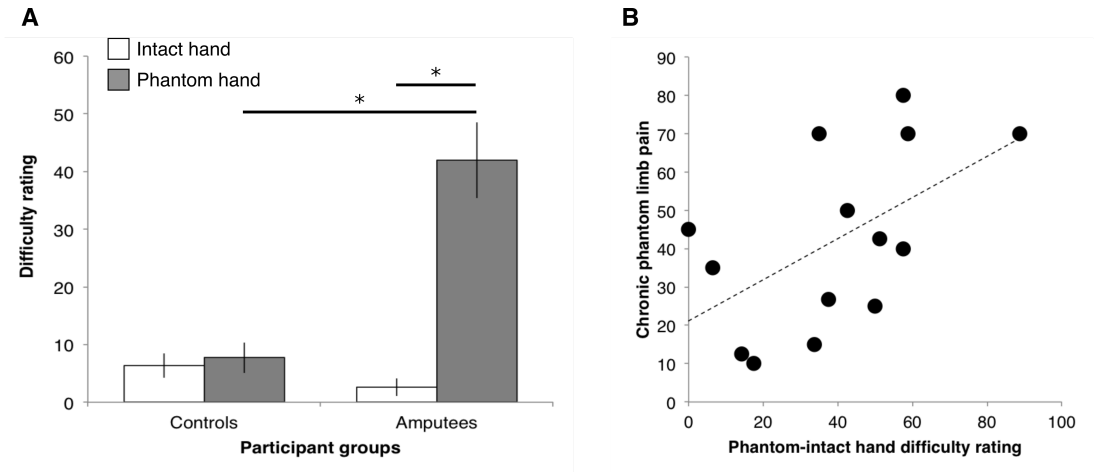


Figure A.5.1: Phantom hand movement difficulty is deteriorated and relates to chronic phantom limb pain. (A) Amputees found it more difficulty to perform the task with their phantom hand, both compared to their intact hand and to movement difficulty of the non-dominant hand of controls. (B) There was a trend towards a relationship between phantom hand movement difficulty and chronic phantom limb pain ($r = 0.50$, $p = 0.08$). Asterisks denote $p < 0.001$. Response time is shown in seconds. Error bars indicate the s.e.m.

A.5.3 Movement imagery as a surrogate measure for phantom limb pain

Overall, the movement imagery task resulted in a similar, though less robust, pattern of results as the movement execution task. No significant difference in phantom hand movement imagery response times was found across the four sessions (repeated measures ANOVA; $F_{(3,33)} = 0.20$, $p = 0.90$). The ICC measure revealed fair inter-session consistency for phantom hand movement imagery response times (ICC = 0.45 with 95% CI = 0.16-9.75, $F_{(11,33)} = 4.2$, $p = 0.001$) (Fleiss et al., 2003). Average response times across sessions were used for further analysis.

Phantom hand movement imagery and phantom hand movement execution response time were correlated (phantom minus intact hand: $r = 0.58$, $p = 0.03$; phantom hand: $r = 0.51$, $p = 0.06$). This was not true for the intact hand ($r = 0.40$, $p = 0.16$).

Results from the movement imagery task were dissimilar to those of the movement execution task (Figure A.5.2A). No difference in response time was found between amputees and controls for phantom hand movement imagery (i.e. phantom minus intact hand; U = 73, p = 0.16). Amputees took longer to perform the movement imagery task compared to controls, both with their phantom and intact hand (U = 32, p = 0.001 and U = 52, p = 0.02, respectively). While controls were equally fast with the two hands in performing the movement imagery task (Z = -1.36, p = 0.17), amputees were slower when performing the movement imagery task with their phantom hand compared to their intact hand ($t_{(13)}$= 2.59, p = 0.02).

No relationship was found between the normalised measure for phantom hand movement imagery response time and chronic PLP (Figure A.5.2B; r = 0.22, p = 0.46). A trend towards a relationship with chronic PLP was however found when considering phantom hand movement imagery response time separately (r = 0.52, p = 0.06). There was no significant correlation between phantom hand movement imagery and chronic phantom sensation (r_s = 0.10, p = 0.73). Furthermore, there was no correlation between the normalised measure for phantom hand movement imagery and transient PLP in the individual sessions (average r_s= 0.12, p = 0.68). A trend towards a relationship with transient PLP was however found when considering phantom hand movement imagery response times separately (average r_s = 0.52, p = 0.06). This is consistent with previous findings, showing a positive, though non-significant relationship between phantom hand movement imagery and chronic PLP (Raffin, Giraux, et al., 2012).

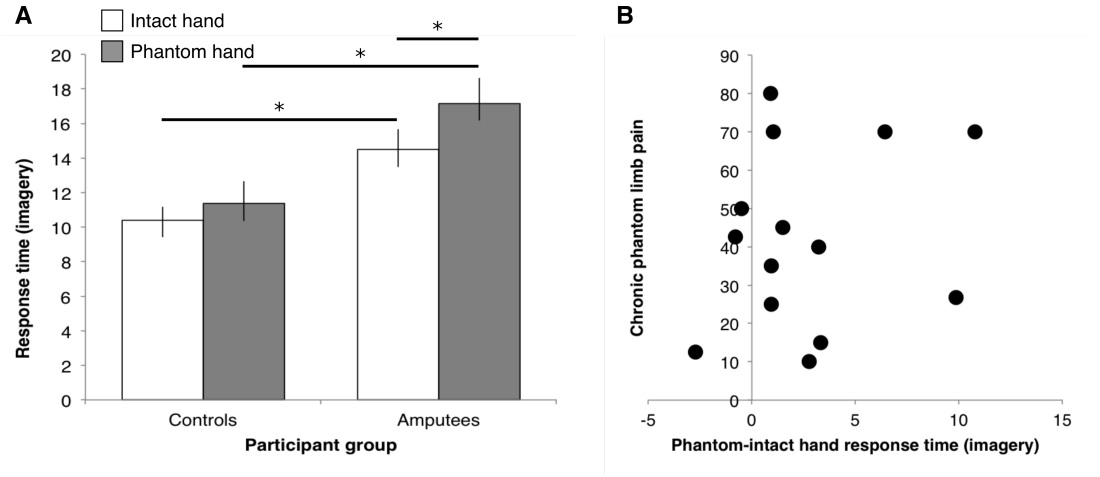


Figure A.5.2: Phantom hand motor imagery is altered in amputees, but this does not correlate with chronic phantom limb pain. (A) Amputees were slower at performing the imagined finger-tapping task, compared to controls. It took amputees longer to perform motor imagery with their phantom hand, compared to their intact hand. (B) There was no significant relationship between phantom hand motor imagery and chronic phantom limb pain (r_s= 0.12, p = 0.68). Asterisks denote $p < 0.05$. Response time is shown in seconds. Error bars indicate the s.e.m.

A.5.4 Chronic phantom limb pain may positively scale with activity in the cortical phantom hand area

A positive correlation was found between chronic PLP and activity in the cortical phantom hand area in the first and second sessions (one-tailed r = 0.55, p = 0.02 and r = 0.48, p = 0.04 respectively). Amputees experiencing worse chronic PLP showed stronger activity in the cortical phantom hand area during flexion and extension of all phantom fingers (Figure A.5.3 for results of the first session). No significant relationship with chronic PLP was found for the third and fourth scanning sessions (one-tailed r = 0.18, p = 0.26 and r = 0.20, p = 0.25 respectively), or for the averaged cortical phantom hand activity (across sessions; r = 0.30, p = 0.28).

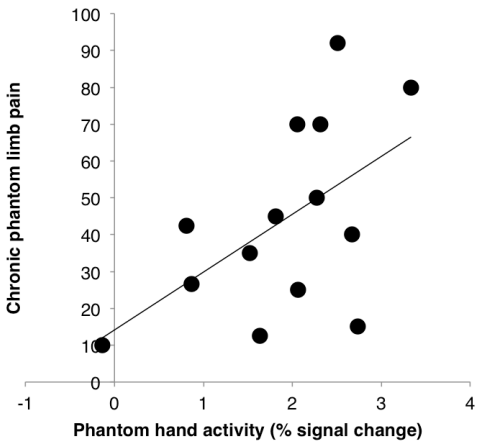


Figure A.5.3: Chronic phantom limb pain associates with the cortical sensorimotor phantom hand representation. There was a significant relationship between chronic phantom limb pain and activity in the cortical phantom hand area in the first session ($r = 0.55$, $p = 0.02$). Amputees who activated the cortical phantom hand area more during flexion and extension of all phantom fingers experienced worse chronic phantom limb pain.

A.5.5 Representation of controls' hands and amputees' intact hand

No correlation was found between intact hand response time in the finger-tapping task and activity in the cortical sensorimotor intact hand area during flexion and extension of all fingers of the intact hand ($r = 0.36$, $p = 0.20$). Furthermore, no relationship was found between the cortical sensorimotor hand representations and finger-tapping response times in controls (non-dominant minus dominant hand response time & non-dominant hand representation: $r = -0.27$, $p = 0.32$; non-dominant hand response time & non-dominant hand representation: $r_s = 0.20$, $p = 0.48$; dominant hand response time & dominant hand representation: $r = -0.27$, $p = 0.34$).

	Inter-session relationships			Correlations with phantom limb phenomena			Correlations with activity in cortical sensorimotor hand area	
	Average Pearson	ICC		Chronic PLP	Chronic non-painful PLS	Transient PLP	Phantom hand area	Intact hand area
		ICC-value	ICC-CI					
Response times								
Execution								
Phantom-intact hand	0.68**	0.64	0.37-0.86	0.57*	[a]0.08	[a]0.30	0.70**	-
Phantom hand	0.62*	0.60	0.33-0.84	0.62*	[a]0.06	[a]0.38	0.61*	-
Intact hand	0.78**	0.80	0.60-0.93	0.15	-	-	-	0.36
Imagination								
Phantom-intact hand	[a]0.35	0.45	0.16-0.75	0.22	[a]0.10	[a]0.12	-	-
Phantom hand	0.60*	0.58	0.30-0.83	0.52	[a]-0.10	[a]0.52	-	-
Intact hand	0.70**	0.67	0.41-0.87	0.45	-	-	-	-
Difficulty ratings								
Execution								
Phantom-intact hand	0.55*	0.52	0.25-0.79	0.50	[a]-0.39	[a]0.07	-	-
Phantom hand	[a]0.55*	0.54	0.27-0.80	0.49	[a]-0.45	[a]0.06	-	-
Intact hand	[a]0.70**	0.79	0.60-0.92	[a]-0.42	-	-	-	-

Table A.5.1: Statistics for phantom and intact hand measures separately. Intraclass correlation (ICC) values range from 0 to 1: we designate ICC values <0.4 as poor, 0.4 to 0.59 as fair, 0.6 to 0.74 as good, and >0.75 as excellent (Fleiss et al., 2003). ICC values designated as poor or fair are printed in red. ICC values designed as good or excellent are printed in green. CI = 95% confidence interval. PLP = phantom limb pain. PLS = phantom limb sensation. Asterisks indicate significance, with: * = p <0.05, ** = p < 0.01, *** = p < 0.001. [a] = normality assumption was violated and non-parametric equivalent was used (Spearman).